AD 0800377

AMC PAMPHLET

AMCP 706-283

ENGINEERING DESIGN HANDBOOK

BALLISTIC MISSILE SERIES

AERODYNAMICS

Approved for public release -
Distribution is Unlimited

HEADQUARTERS, U. S. ARMY MATERIEL COMMAND   **APRIL 1965**

HEADQUARTERS
UNITED STATES ARMY MATERIEL COMMAND
WASHINGTON, D.C. 20315

30 April 1965

AMCP 706-283, <u>Aerodynamics</u>, forming part of the Ballistic Missile Series of the Army Materiel Command Engineering Design Handbook Series, is published for the information and guidance of all concerned.

(AMCRD)

FOR THE COMMANDER:

SELWYN D. SMITH, JR.
Major General, USA
Chief of Staff

OFFICIAL:

STANLEY J. SAWICKI
Colonel, GS
Chief, Administrative Office

DISTRIBUTION: Special

PREFACE

The Engineering Design Handbook Series of the Army Materiel Command is a coordinated series of handbooks containing basic information and fundamental data useful in the design and development of Army materiel and systems. The handbooks are authoritative reference books of practical information and quantitative facts helpful in the design and development of Army materiel so that it will meet the tactical and the technical needs of the Armed Forces.

This handbook, *Aerodynamics*, is one of a series on ballistic missiles. It presents design information peculiar to ballistic missile flight, i.e., information outside the scope of basic subsonic and supersonic aerodynamics which may be termed "conventional aerodynamics." Accordingly, this handbook treats the problems unique to ballistic flight, namely, high-speed, high temperature and high altitude effects. Empirical as well as theoretical data are presented in the tables and graphs which accompany the text material. As of the cut-off date for publication, the data and theory are believed to be current, representing the latest thinking and observations in the areas of atmospheric and geophysical parameters, typical ballistic trajectories, physical properties of air particularly at elevated temperatures, pressure distributions over bodies at high speeds as required for determining aerodynamic loads and heating effects, aerodynamic heating and cooling methods, hypersonic aerodynamic forces and stability considerations, and techniques and problems of aerodynamic experimentation. Appropriate engineering approximations have been introduced, where applicable, to simplify the complex theory and make the text adaptable to the solution of practical problems.

The original manuscript for this handbook was supplied by Vitro Laboratories for the Engineering Handbook Office of Duke University, prime contractor to the Army Research Office-Durham.

Elements of the U.S. Army Materiel Command having need for handbooks may submit requisitions or official requests directly to Publications and Reproduction Agency, Letterkenny Army Depot, Chambersburg, Pennsylvania 17201. Contractors should submit such requistitions or requests to their contracting officers.

Comments and suggestions on this handbook are welcome and should be addressed to Army Research Office-Durham, Box CM, Duke Station, Durham, North Carolina 27706.

TABLE OF CONTENTS

CHAPTER 1

AERODYNAMICS IN BALLISTIC MISSILE DESIGN

CHAPTER 2

ATMOSPHERIC AND GEOPHYSICAL PROPERTIES

TABLE OF CONTENTS (cont'd)

TABLE OF CONTENTS (cont'd)

CHAPTER 7

HYPERSONIC AERODYNAMIC FORCES

CHAPTER 8

AERODYNAMIC TESTING

LIST OF ILLUSTRATIONS

LIST OF ILLUSTRATIONS (cont'd)

LIST OF ILLUSTRATIONS (cont'd)

LIST OF TABLES

CHAPTER 1*

AERODYNAMICS IN BALLISTIC MISSILE DESIGN

1-1 AERODYNAMIC PROBLEM AREAS

The design and specification of a ballistic missile of one or more stages require areodynamic information somewhat wider in scope than that usually required for totally-guided missiles. This is due mainly to enlarged operational conditions. Of great importance for ballistic missiles, for instance, are the thermal effects engendered by high velocities, particularly during re-entry into the higher density regime of the atmosphere. Furthermore, ballistic missiles encounter significant variations in atmospheric conditions as they traverse wide altitude ranges. In addition, aerodynamic factors which influence the precision of aiming and launching become important since trajectories cannot readily be altered after ballistic flight has begun.

Aerodynamic phenomena bear on numerous facets of missile design and operation:

(1) Overall performance and flight mechanics are influenced by resultant aerodynamic forces.

(2) Stability and control depend upon aerodynamic moments and stability derivatives.

(3) Structural design in the low temperature range depends upon steady and time-dependent aerodynamic loads.

(4) Material selection and structural design in the high temperature range depend upon a knowledge of aerodynamic heat inputs and losses, as well as cooling techniques. Factors of this type dominate the re-entry capabilities of high performance missiles. In fact, trajectories may be programmed to alleviate high temperature effects.

(5) The effectiveness of detection, discrimination, tracking and interception of high speed missiles, as well as communication to or from the missile, bear strongly on the physical state of high temperature gases in the immediate vicinity of the vehicle and in its wake. In particular, electron concentrations and radia-

tion properties are significant in this regard.

(6) Aerodynamic experimentation and testing, and the establishment of model-scaling procedures in connection with a given design are important problem areas in themselves.

(7) The magnitude of the dispersion of the missile at impact may be influenced by various aerodynamic disturbances. These disturbances may be introduced by meteorological conditions, as well as by the aerodynamic consequences of structural inaccuracies.

(8) Aeroelastic phenomena such as flutter depend upon steady and time-dependent aerodynamic loads, and upon aerodynamic derivatives which act as forcing and damping functions.

The process of designing, building and using a missile is a "closed-loop" system in which information is constantly fed back and forth between various phases of the system, engendering corrections, modifications, and compromises in each phase. Thus requirements set by other than aerodynamic factors, such as structural design or handling, may alter the ideal aerodynamic configuration. An important role of aerodynamics is to aid in the evaluation of the effects of these changes.

Furthermore, meteorological information is required for the determination of aerodynamic phenomena. Aside from the usual atmospheric characteristics, features such as winds, gusts and high altitude properties may be of importance. Moreover, phenomena such as bombardment by meteoric or electrically charged particles may influence the condition of aerodynamic surfaces and consequently the aerodynamic ballistics.

1-2 OBJECTIVES OF AERODYNAMICS HANDBOOK

Significant amounts of information in the areas previously cited lie within the scope of basic subsonic and supersonic aerodynamics, and are not peculiar to ballistic missile flight. With some liberty, these aspects may be termed "conventional aerodynamics." On the other hand, high-speed, high-temperature and high-altitude effects are essentially

---

* This volume was written by M. H. Bloom. S. V. Nardo aided with the chapter on aerodynamic testing, and P. M. Sforza assisted in arrangement and editing. All are from Polytechnic Institute of Brooklyn. C. D. Fitz, then of Vitro Laboratories, presented constructive suggestions.

unique to ballistic flight. As a result they receive major emphasis in this chapter.

Atmospheric and geophysical parameters are discussed in Chapter 2; typical ballistic trajectories in Chapter 3; physical properties of air, particularly at elevated temperatures, in Chapter 4; pressure distributions over bodies at high speeds, as required for determining aerodynamic loads and aerodynamic heating effects, in Chapter 5; aerodynamic heating and some cooling methods in Chapter 6; hypersonic aerodynamic forces and stability considerations in Chapter 7; and techniques and problems of aerodynamic experimentation in Chapter 8.

Basic references on aerodynamics and tabulations in general use are listed at the end of this chapter.

REFERENCES

Introductory References

1. H. Glauert, *Elements of Aerofoil and Airscrew Theory*, Cambridge University Press, 1948.
2. A. M. Kuethe and J. D. Schetzer, *Foundations of Aerodynamics*, Second Ed., John Wiley & Sons, N. Y., 1959.
3. A. H. Shapiro, *Compressible Fluid Flow*, Ronald Press, Inc., N. Y., 1954.
4. R. W. Truitt, *Hypersonic Aerodynamics*, Ronald Press, Inc., N. Y., 1959.
5. H. Liepmann and A. Roshko, *Elements of Gasdynamics*, John Wiley & Sons, N. Y., 1957.

Advanced Treatments

6. A. Ferri, *Elements of Aerodynamics of Supersonic Flows*, MacMillan Co., N. Y., 1949.
7. W. Hayes and R. Probstein, *Hypersonic Flow Theory*, Academic Press, N. Y., 1959.
8. K. Oswatitsch, *Gas Dynamics* (English version by G. Kuerti), Academic Press, N. Y., 1956.
9. H. Schlichting, *Boundary Layer Theory*, McGraw-Hill, Inc., N. Y., 1955.
10. *Series on High-Speed Aerodynamics and Jet Propulsion*, Princeton University Press, Princeton, N. J. (Twelve volumes)
11. S. Goldstein, Ed., *Modern Developments in Fluid Dynamics*, Oxford University Press, 1938.
12. L. Howarth, Ed., *Modern Developments in Fluid Dynamics*, Oxford University Press, 1953.
13. R. L. Bisplinghoff, H. Ashley and R. L. Halfman, *Aeroelasticity*, Addison-Wesley Publishing Co., Cambridge, Mass., 1955.
14. G. N. Patterson, *Molecular Flow of Gases*, John Wiley & Sons, N. Y., 1956.
15. F. M. Devienne, Ed., *Rarefied Gas Dynamics*, Proceedings of First Symposium held at Nice, France, B. H. Blackwell, England, 1959.

References Specialized to Deal with Missile Problems

16. E. A. Bonney, *Aerodynamics*, D. Van Nostrand, Princeton, N. J., 1956. (Monograph in Guided Missile Design Series)
17. B. Etkin, *Dynamics of Flight*, John Wiley & Sons, N. Y., 1959.
18. *Guided Missiles*, Air Force Manual, McGraw-Hill, Inc., N. Y., 1958.
19. J. B. Rosser, R. R. Newton and G. L. Gross,

Mathematical Theory of Rocket Flight, McGraw-Hill, Inc., N. Y., 1947.
20. L. Davis, J. W. Follin and L. Blitzer, *Exterior Ballistics of Rockets*, D. Van Nostrand, Princeton, N. J., 1958.
21. R. B. Dow, *Fundamentals of Advanced Missiles*, John Wiley & Sons, N. Y., 1958.

Compilations and Tabulations of Functions and Data

22. Ames Research Staff, *Equations, Tables and Charts for Compressible Flow*, National Advisory Committee for Aeronautics Technical Report 1135, 1953.
23. Lewis Laboratory Computing Staff, *Tables of Various Mach Number Functions for Specific Heat Ratios from 1.28 to 1.38*, National Advisory Committee for Aeronautics Technical Note 3981, 1957.
24. *Handbook of Supersonic Aerodynamics*, NAVORD Report 1488, 1950.
25. S. Feldman, *Hypersonic Gas Dynamic Charts for Equilibrium Air*, AVCO Research Laboratory, Everett, Mass., 1957.
26. *Handbook of Geophysics*, First Ed., Air Force Cambridge Research Center, GRD, ARDC, 1957.
27. R. A. Minzer, K. S. W. Champion and H. L. Pond, *ARDC Model Atmosphere, 1959*, Air Force Cambridge Research Center Technical Report 59-267, 1959.
28. W. E. Moeckel and K. C. Weston, *Composition and Theormodynamic Properties of Air in Chemical Equilibrium*, National Advisory Committee for Aeronautics Technical Note 4265, 1958.
29. I. Korobkin and S. M. Hastings, *Mollier Chart for Air in Dissociated Equilibrium at Temperatures of 2000°K to 15000°K*, NAVORD Report 4446, U. S. Naval Ordnance Laboratory, 23 May 1957.
30. R. A. Hord, *Approximate Composition and Thermodynamic Properties of Nonionized Nitrogen-Oxygen Mixtures*, National Aeronautics and Space Administration Technical Note D-2, 1959.
31. C. F. Hansen, *Approximations for the Thermodynamic and Transport Properties of High-Temperature Air*, National Advisory Committee for Aeronautics Technical Note 4150, 1958. (Super-

seded by National Aeronautics and Space Administration Technical Report R-50).

32. C. F. Hansen and S. P. Heims, *A Review of the Thermodynamic, Transport and Chemical Reaction Rate Properties of High-Temperature Air*, National Advisory Committee for Aeronautics Technical Note 4359, 1958.

33. R. E. English and W. W. Wachtl, *Charts of Thermodynamic Properties of Air and Combustion Products from 300°R to 3500°R*, National Advisory Committee for Aeronautics Technical Note 2071, 1950.

34. S. M. Scala and C. W. Baulknight, "Transport and Thermodynamic Properties ... [of Air]," ARS Journ. **29**, 39 (1959).

35. W. Chinitz, C. L. Eisen and R. A. Gross, "Aerothermodynamic and Electrical Properties of Some Gas Mixtures to Mach 20," ARS Journ. **29**, 573 (1959).

36. E. Bauer and M. Zlotnick, "Transport Coefficients of Air to 8000°K," ARS Journ. **29**, 721 (1959).

37. J. Keck, B. Kivel and T. Wentink, *Emissivity of High Temperature Air*, AVCO Research Laboratory, Everett, Mass., Research Report 8, 1957.

38. B. Kivel and K. Bailey, *Tables of Radiation from High Temperature Air*, AVCO Research Laboratory, Everett, Mass., Research Report 21, 1957.

39. C. W. Besserer, *Missile Engineering Handbook*, D. Van Nostrand, Princeton, N. J., 1958.

40. S. F. Hoerner, *Fluid-Dynamic Drag*, Published by the author, 48 Busteed Dr., Midland Park, N. J., 1958.

41. R. B. Morrison, Ed., *Design Data for Aeronautics and Astronautics*, John Wiley & Sons, N. Y., 1962.

CHAPTER 2

ATMOSPHERIC AND GEOPHYSICAL PROPERTIES

2-1 INTRODUCTION

The aerodynamic characteristics and dynamic behavior of a vehicle in the vicinity of a planet such as the earth, depend upon the nature of the atmosphere and upon geophysical parameters such as the planet's gravitational field.

Standards for the principal atmospheric and geophysical properties of the earth have been set up by the Air Research and Development Command (ARDC), the U. S. Air Force[1,2] and more recently by the U.S. Committee on Extension to the Standard Atmosphere (COESA)[20] after extensive study of existing information. Reviews are made annually as new information is acquired. These Standards provide a unified basis for reference and are recommended for initial design.

In actuality, deviations from standard conditions occur due to such factors as geographic location, seasonal changes, time of day and weather. Their effect may be significant for purposes of final design and detailed performance. However, their importance depends upon the magnitude of their effect on vehicle parameters, the required reliability of the vehicle and the probability that deviations from standard will occur.

At altitudes below 46 km (150,000 ft) atmospheric data are obtained quite accurately with the use of balloons. At higher altitudes, data are obtained by means of rockets, satellites and remote observations. Theoretical analyses are used to correlate the data and provide extrapolations to extremely high altitudes (700 km).

The 1959 ARDC Standard takes into account density data obtained by rocket-borne ionization gages in the 110 to 220 km range. It also considers the more uncertain densities inferred from the change in period of satellites having perigee (minimum) altitudes of 170 to 650 km. Below 20 km, the 1959 Standard agrees with prior Standards such as that of NACA[3]. Below 53 km this Standard agrees with the 1956 ARDC model. Between 90 and 150 km the values of density are about one-half the 1956 values. At 200 km, the density is about 5 times the prior Standard, and at 600 km the 1959 value is about 20 times the 1956 Standard.

The U.S. Standard Atmosphere is based on more recent data acquired in such additional diverse experiments as rocket grenade launchings, falling sphere density measurements, etc. Below 20 km the 1962 U.S. Standard Atmosphere agrees with the 1959 ARDC Atmosphere and the International Civil Aviation Organization (ICAO) Atmosphere. Up to 80 km the 1959 Standard is still in agreement with the 1962 Standard. Above 80 km the differences between the two are depicted graphically in Figs. 2-1(Q) and 2-1(R).

Probable errors in pressure and density are estimated to be less than 10 percent at altitudes below 60 km (200,000 ft), and to increase to perhaps 200–300 percent at 200 km[4].

2-2 PROPERTIES OF THE EARTH'S ATMOSPHERE

For the purposes of this handbook, the properties of the earth's atmosphere as developed for the 1962 U.S. Standard Atmosphere and, secondarily, the 1959 ARDC Standard Atmosphere will be adopted. Table 2-1 presents a list of the notations used in both Standards[2,20]. Sea-level values are given in Table 2-2 in both metric and English units. Values of the physical constants used in deriving the Standard are shown in Table 2-3. Pertinent conversion factors are given in Table 2-4. Table 2-5 lists the numerous altitude-dependent atmospheric properties which are examined in the 1962 Standard. The variation of these properties with altitude is illustrated in Figure 2-1 (scaled in metric units).

2-2.1. Acceleration of Gravity

The variation of acceleration of gravity g with actual geometric altitude Z is classically expressed by the equation:

$$\frac{g}{g_0} = \left(\frac{r}{r + Z}\right)^2 \qquad (2-1)$$

where g_0 is a standard value at zero altitude (Table 2-2), and r is an effective radius of the earth adjusted to provide for its rotation and nonspherical shape (Table 2-3). This relation may be applied to other planets if suitable values of g_0 and r are employed.
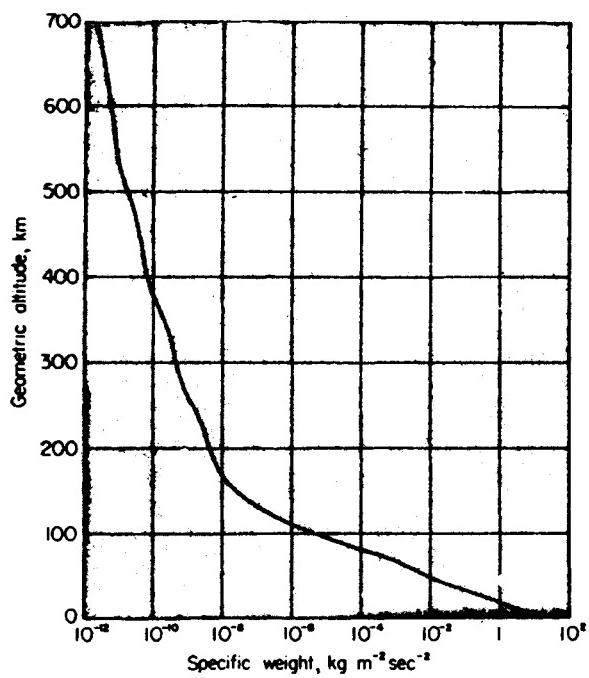
(A) Specific Weight vs. Altitude
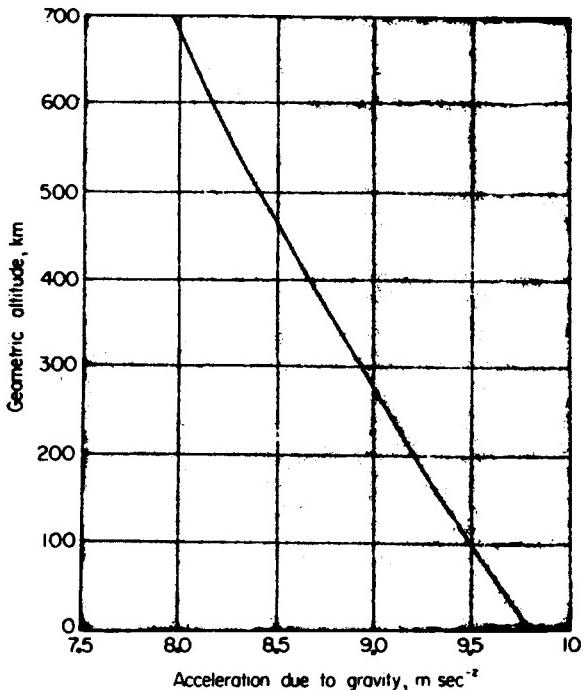
(B) Acceleration of Gravity vs. Altitude
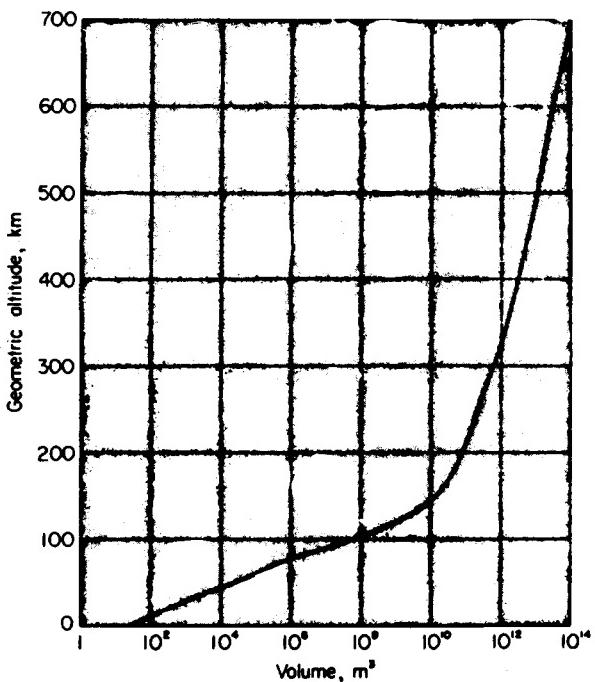
(C) Mole Volume vs. Altitude
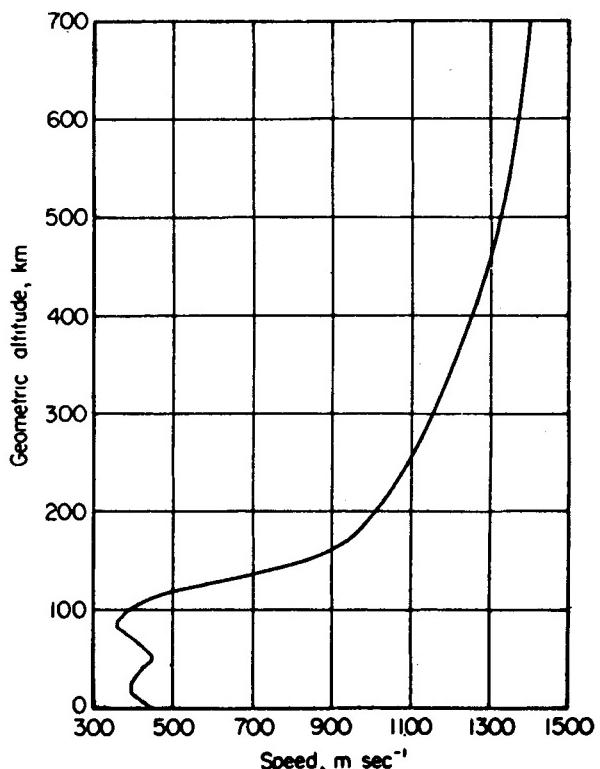
(D) Mean Particle Speed vs. Altitude

Figure 2-1. Altitude-Dependent Atmospheric Properties in Metric Units[20]
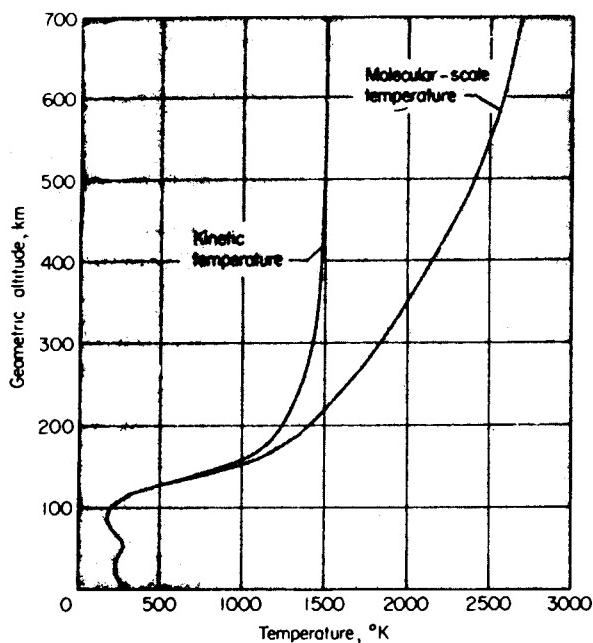
(E) *Kinetic Temperature and Molecular-Scale Temperature vs. Altitude*
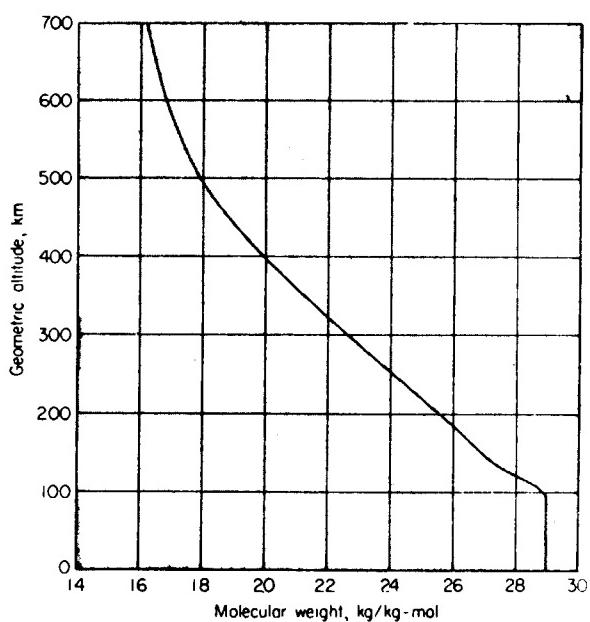
(F) *Mean Molecular Weight vs. Altitude*
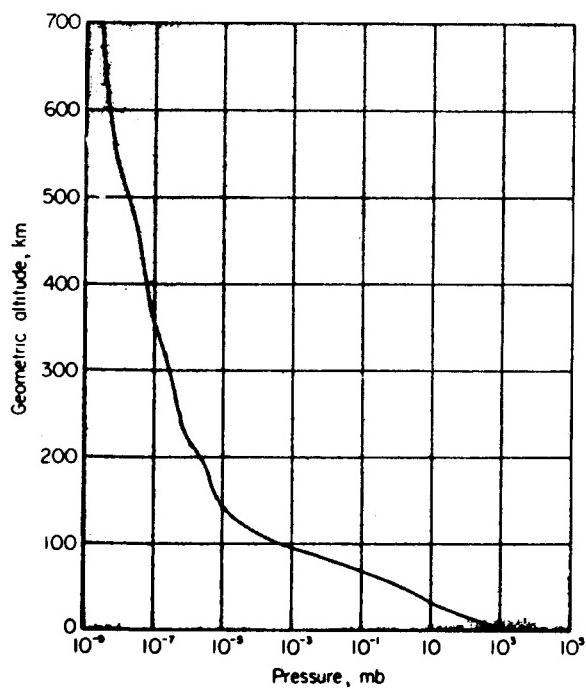
(G) *Pressure vs. Altitude*
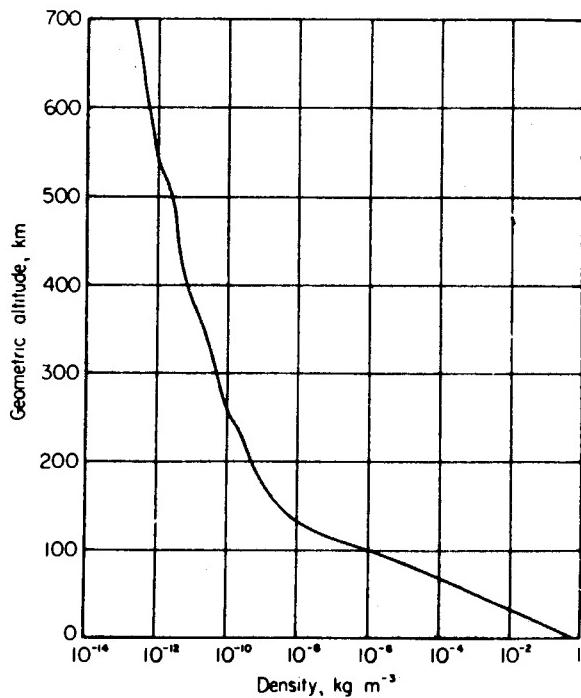
(H) *Mass Density vs. Altitude*

Figure 2-1. Altitude-Dependent Atmospheric Properties in Metric Units[20] (continued)

2-3
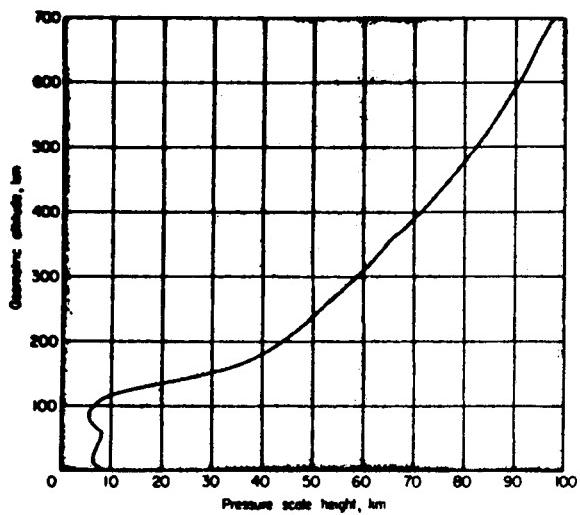
(I) Scale Height vs. Altitude
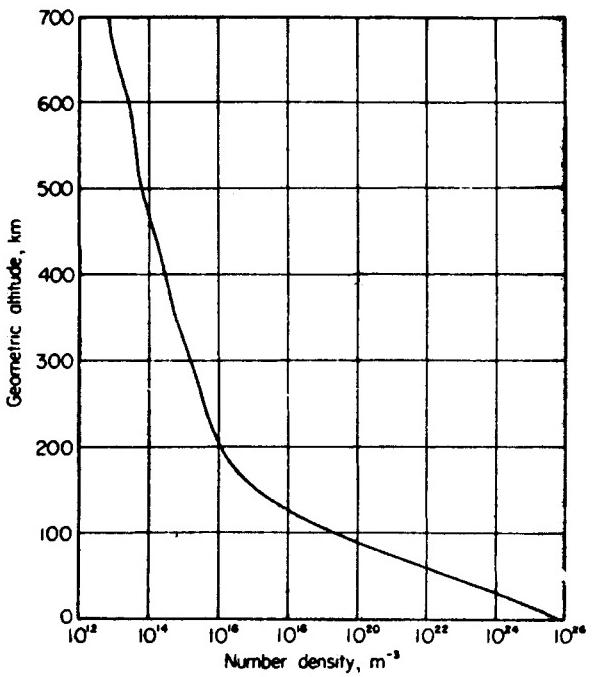
(J) Number Density vs. Altitude
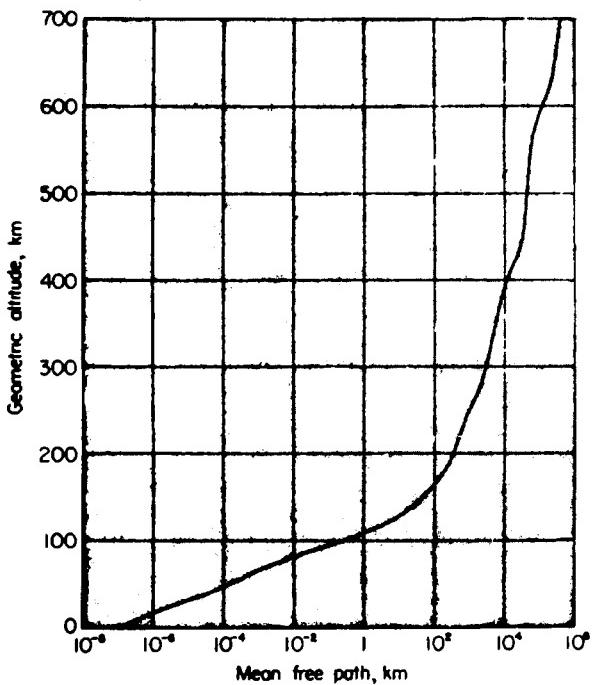
(K) Mean Free Path vs. Altitude
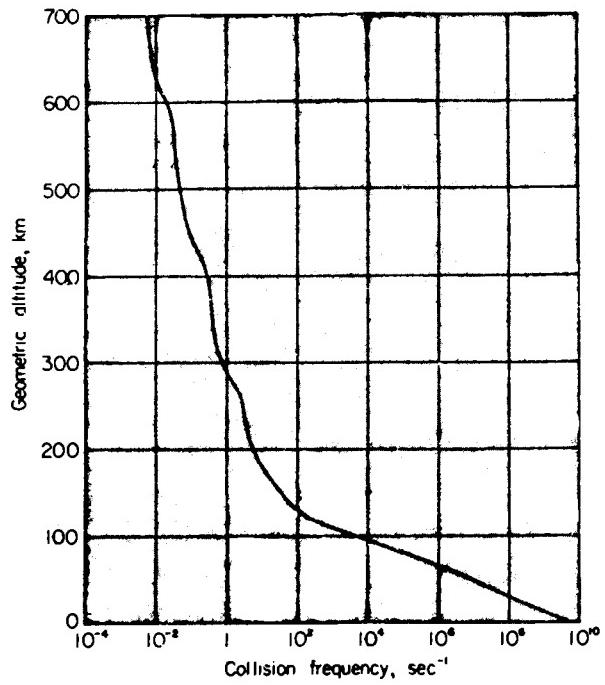
(L) Collision Frequency vs. Altitude

Figure 2-1. Altitude-Dependent Atmospheric Properties in Metric Units [20] (continued)
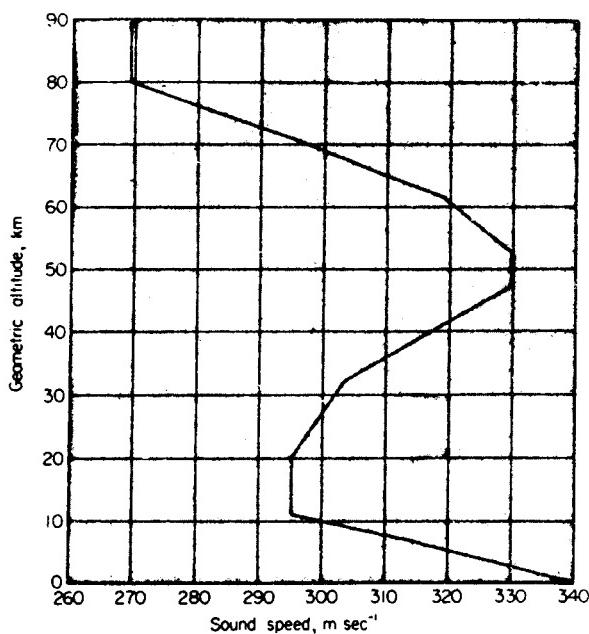
(M) Speed of Sound vs. Altitude
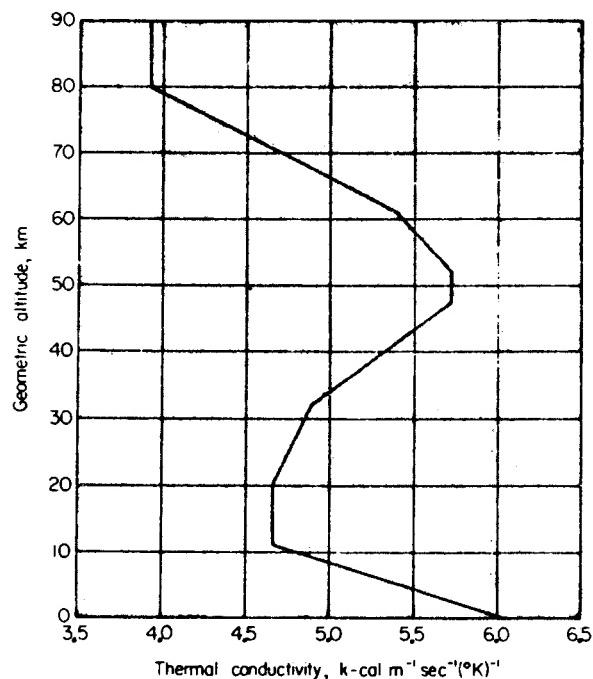
(N) Coefficient of Thermal Conductivity vs. Altitude
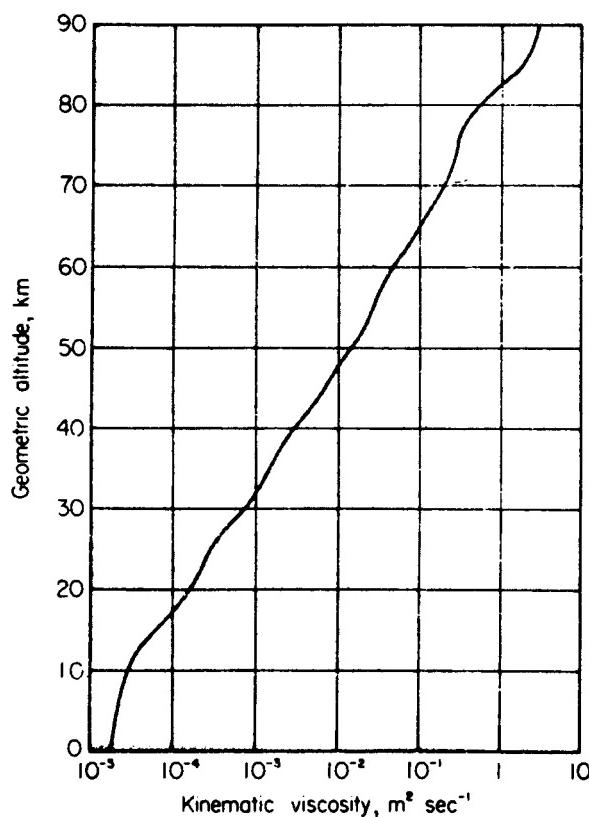
(O) Kinematic Viscosity vs. Altitude
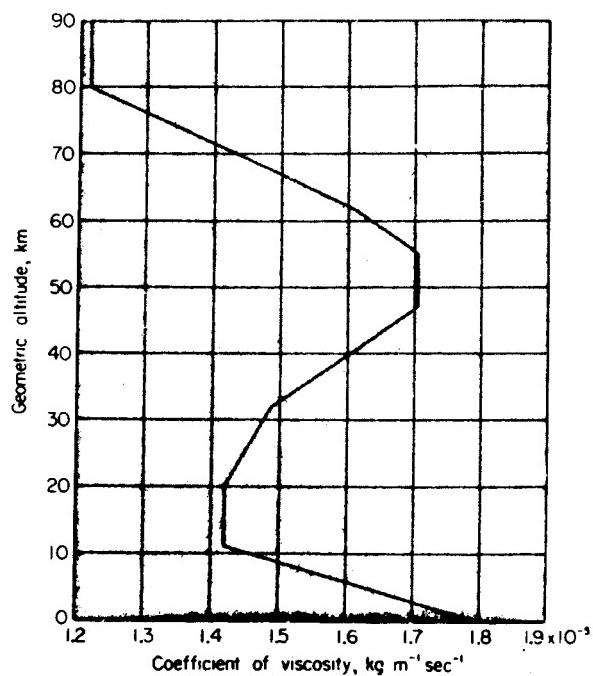
(P) Coefficient of Viscosity vs. Altitude

Figure 2-1. Altitude-Dependent Atmospheric Properties in Metric Units[20] (continued)
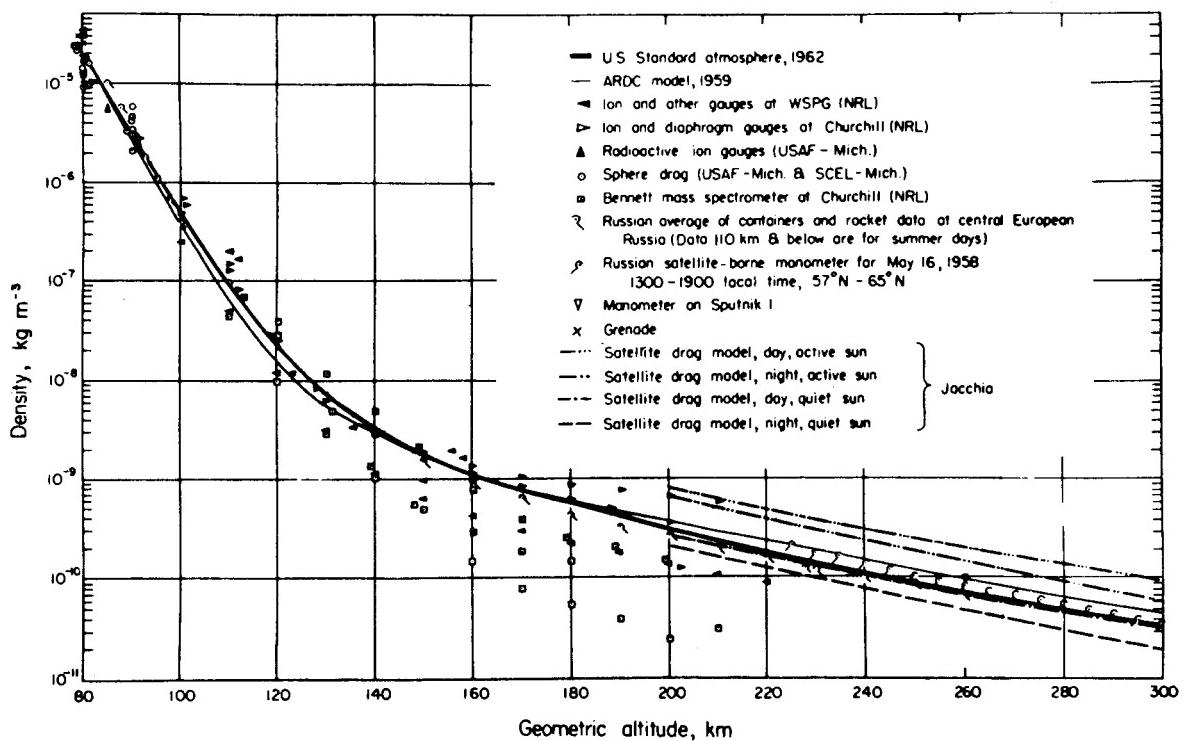
(Q) *Density of U. S. Standard Atmosphere, 1962 Compared with ARDC Model Atmosphere, 1959 and with Available Data*
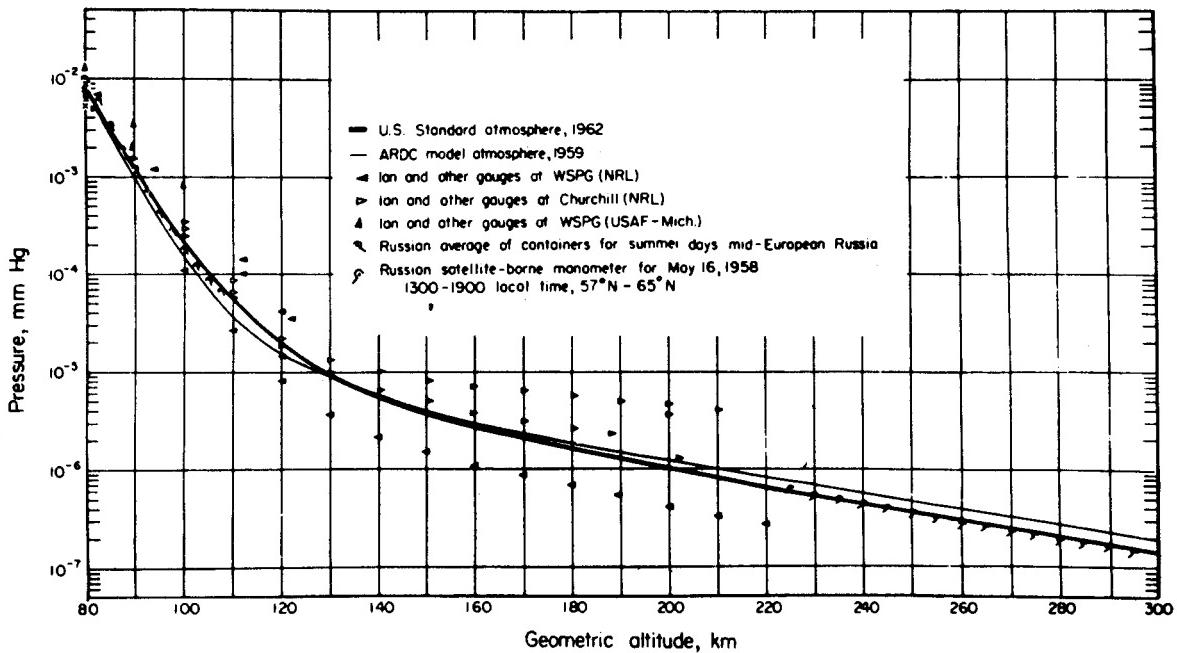
(R) *Pressures of U. S. Standard Atmosphere, 1962 Compared with ARDC Model Atmosphere, 1959 and with Available Data*

Figure 2-1. Altitude-Dependent Atmospheric Properties in Metric Units[20] (continued)

2-2.2. Modified Geopotential Altitude

The modified geopotential altitude H^* is simply a transformed altitude scale with the units of length, defined to facilitate the solution of the basic equation of static equilibrium of fluids in the atmosphere by absorbing the effect of variations in g. It is defined by the differential relation

$$g_0 \, dH^* = g(Z) \, dZ \qquad (2\text{-}2)$$

which, when combined with Eq. 2-1 and integrated, yields

$$\frac{H^*}{r} = \frac{Z}{r + Z} \qquad (2\text{-}3)$$

The equation of static equilibrium of a fluid, sometimes termed the "barometric equation," is

$$dP = -\rho g \, dZ \qquad (2\text{-}4)$$

Substitution of Eq. 2-2 into Eq. 2-4 produces an equation resembling that which holds for $g = g_0 =$ constant, namely

$$dP = -\rho g_0 \, dH^* \qquad (2\text{-}5)$$

TABLE 2-1.

LIST OF SYMBOLS AND ABBREVIATIONS USED IN STANDARD ATMOSPHERE TABLES*

a	Acceleration	lbf	Pound (force)
a	Radius of the earth at the equator	M	Mean molecular weight of air
b	Subscript indicating base or reference level	m	Meter
BTU	British Thermal Unit	m′	Standard geopotential meter
°C	Degrees, in thermodynamic Celsius scale	m	Mass
C_s	Speed of sound	mb	Millibar
cal	Calorie	mks	Meter-kilogram-second system of units
cm	Centimeter	N	Avogadro's number
E	Energy	n	Number density
°F	Degrees, in thermodynamic Fahrenheit scale	n_i	Loschmid's number
f	Ellipsoid flattening	nt	Newton
F	Force	o	Subscript indicating sea-level value
fps	Foot-pound-second system of units	P	Pressure
ft	Foot	pdl	Poundal
ft′	Standard geopotential foot	°R	Degrees, in thermodynamic Rankine scale
G	Dimensional constant in geometric-geopotential relationship	R^*	Universal gas constant
g	Acceleration of gravity, effective value	r	Effective radius of earth
g_s	Acceleration of gravity at the equator	S	Sutherland's constant
gm	Gram	sec	Second
gm-mol	Gram mole	T	Temperature in absolute thermodynamic scales
H	Altitude in geopotential measure	T_i	Ice point temperature in absolute thermodynamic scales
Hg	Mercury		
H_s	Scale height	T_M	Molecular-scale temperature in absolute thermodynamic scales
H'_s	Geopotential scale height		
H^*	Modified geopotential altitude	t	time
i	Subscript indicating ice point value	t	Temperature in nonabsolute thermodynamic scales
in.	Inch	thsd ft	Thousands of feet
i. n. mi	International nautical mile	t_i	Ice point temperature in nonabsolute thermodynamic scales
°K	Degrees, in thermodynamic Kelvin scale		
k	Thermal conductivity	$\bar{V}$	Particle speed (arithmetic average)
kg-cal	Kilogram-calorie	v	Mole volume of air under existing conditions of T and P
kg	Kilogram (mass)		
kgf	Kilogram (force)	Z	Altitude in geometric measure
kg-mol	Kilogram-mole	β	Constant used in Sutherland's viscosity equation
km	Kilometer		
km′	Standard geopotential kilometer	γ	Ratio of specific heats (C_p/C_v)
kwhr	Kilowatt hour	η	Kinematic viscosity
L	Mean free path	μ	Coefficient of viscosity
L_M	Molecular-scale-temperature gradient	ν	Collision frequency
ℓ	Length	ρ	Mass density
lb	Pound (mass)	σ	Effective collision diameter of a mean air molecule
		ψ	Latitude of the earth
		ω	Specific weight

* For numerical values of physical constants see Table 2–3.

TABLE 2-2. SEA-LEVEL VALUES OF ATMOSPHERIC PROPERTIES[20]

Symbol	Metric units (mks)	English units (ft-lb-sec)
P_0	1.013250×10^5 newtons m^{-2}	2116.22 lbf ft^{-2}
ρ_0	1.2250 kg m^{-3}	0.076474 lb ft^{-3}
t_0	15° C	59.0° F
g_0	9.80665 m sec^{-2}	32.1741 ft sec^{-2}
S	110.4° K	198.72° R
T_i	273.15° K	491.67° R
β	1.458×10^{-6} kg sec^{-1}m^{-1}(°K)$^{-1/2}$	7.3025×10^{-7} lb ft^{-1}sec^{-1}(°R)$^{-1/2}$
γ	1.40 (dimensionless)	1.40 (dimensionless)
σ	3.65×10^{-10} m	1.1975×10^{-9} ft
N	6.02257×10^{26} (kg-mol)$^{-1}$	2.73179×10^{26} (lb-mol)$^{-1}$
R^*	8.31432 joules (°K)$^{-1}$ mol^{-1}	1545.31 ft lb (lb-mol)$^{-1}$ (°R)$^{-1}$

Differences between H^* and Z are generally rather small except at very high altitudes.

2-2.3. Geopotential Altitude

The geopotential altitude H is numerically equal to H^*, but is expressed in units of energy per unit mass, or velocity squared, rather than in units of simple length. It is given by the relation

$$H = (g_0/G)H^* \qquad (2\text{-}6)$$

where g_0 is defined in Table 2-3 and G has the value 9.80665 m^2 sec^{-2} m'^{-1} in the metric system and 32.1741 ft^2 sec^{-2} ft$'^{-1}$ in the English system of units. The units of H are geopotential-meters m', where m' is 9.80665 (m/sec)^2. Physically, the geo-

potential meter expresses the fact that if 1 kg of mass is raised through one m', its potential energy is increased by 9.80665 joules (see Table 2-4 for conversions to English units).

2-2.4. Molecular-Scale Temperature

The molecular-scale temperature T_M is defined so as to simplify the equation of state of a perfect gas, which is assumed to apply throughout the atmosphere, by weighting the effects of changes in average molecular weight at the higher altitudes. T_M may be related uniquely to the density, pressure or speed of sound without specification of the molecular weight. The density and sound speed are quantities often measured experimentally in high altitude tests.

TABLE 2-3. NUMERICAL VALUES USED IN 1962 U. S. STANDARD ATMOSPHERE[20]

Symbol	Metric units (mks)	English units (ft-lb-sec)
$C_{s,0}$	340.294 m sec^{-1}	1116.45 ft sec^{-1}
*g_0	9.80665 m sec^{-2}	32.1741 ft sec^{-2}
$H_{P,0}$	8434.5 m	27,672 ft
k_0	6.0530×10^{-6} kg-cal m^{-1} sec^{-1}(°K)$^{-1}$	4.0674×10^{-6} BTU ft^{-1} sec^{-1}(°R)$^{-1}$
L_0	6.6328×10^{-8} m	2.1761×10^{-7} ft
M_0	28.9644 (dimensionless)	28.9644 (dimensionless)
n_0	2.5471×10^{25} m^{-3}	7.2127×10^{23} ft^{-3}
*P_0	1.013250×10^5 newtons m^{-2}	2116.22 lbf ft^{-2}
•T_0	288.15° K	518.67° R
$\overline{V}_0$	458.94 m sec^{-1}	1505.7 ft sec^{-1}
η_0	1.4607×10^{-5} m^2 sec^{-1}	1.5723×10^{-4} ft^2 sec^{-1}
μ_0	1.7894×10^{-5} kg m^{-1} sec^{-1}	1.2024×10^{-5} lb ft^{-1} sec^{-1}
ν_0	6.9193×10^9 sec^{-1}	6.9193×10^9 sec^{-1}
*ρ_0	1.2250 kg m^{-3}	0.076474 lb ft^{-3}
*σ_0	3.65×10^{-10} m	11.975×10^{-10} ft
ω_0	12.013 kg m^{-3} sec^{-2}	2.4605 lb ft^{-3} sec^{-2}

*These values are adopted for purposes of computation.   The remaining values are derived from the adopted values.

TABLE 2-4. CONVERSION FACTORS[20]

(A) Metric to English Conversions of Units of Length, Mass and Geopotential

A. Defined relations (the constants are adopted as being exact):

1 foot	$= 0.3048$ meter
1 i.n. mi	$= 1,852$ meters
1 pound	$= 0.45359237$ kilogram
1 standard geopotential foot	$= 0.3048$ standard geopotential meter

B. Derived relations:

1 meter	$= 3.2808399\ldots$ feet
1 meter	$= 5.3995680\ldots \times 10^{-4}$ i.n. mi
1 kilogram	$= 2.2046226\ldots$ pounds
1 i.n. mi	$= 6,076.1155\ldots$ feet
1 foot	$= 1.6457883\ldots \times 10^{-4}$ i.n. mi
1 standard geopotential meter	$= 3.2808399\ldots$ standard geopotential feet

(B) Metric to English and Absolute to Non-Absolute Conversions of Temperature Units

A. Defined:

$t(°C)$	$= T(°K) - T_i(°K)$, where $T_i(°K) = 273.15(°K)$
$T(°R)$	$= 1.8 T(°K)$
$t(°F) - t_i(°F)$	$= T(°R) - T_i(°R)$, where $t_i(°F) = 32(°F)$

B. Derived relations:

$t_i(°C)$	$= 0(°C)$
$T_i(°R)$	$= 491.670(°R)$
$t(°C)$	$= [T(°R) - T_i(°R)]/1.8 = [t(°F) - t_i(°F)]/1.8$
$T(°R)$	$= 1.8[t(°C) + 273.15(°C)] = t(°F) - t_i(°F) + 491.670(°R)$
$t(°F) - 32(°F)$	$= 1.8 t(°C) = 1.8[T(°K) - 273.15(°K)]$

(C) Absolute Systems of Units to Absolute-Force, Gravitational System of Units, Metric-English

A. Defined:

1 force unit $= 1$ mass unit $\times g_0$

B. Derived relations:

1 kgf $= 9.80665$ kg m sec^{-2}

1 kg $= \dfrac{1}{9.80665}$ kgf sec^2 m$^{-1} = 0.10197162$ kgf sec^2 m^{-1}

1 lbf $= 0.45359237$ kgf

1 lbf $= 32.174049$ lb ft sec^{-2}

1 lb $= 0.031080950$ lbf sec^2 ft^{-1}
$= 0.031080950$ slug

1 slug $= 32.174049$ lb

The molecular-scale temperature is defined by the relation

$$\frac{T_M}{M_0} = \frac{T}{M} \qquad (2\text{-}7)$$

where M_0 is a standard molecular weight defined in Table 2-3.

The equation of state is expressed as follows:

(D) Thermal to Mechanical Units, Metric-English

A. Defined relations:[*]

1 kg-cal $= \dfrac{1}{860}$ kw-hr (exact)

1 kg-cal $= \dfrac{1.8}{0.45359237}$ BTU $= 3.9683207$ BTU

1 joule $= 1$ watt-sec

B. Derived relations:

1 kw-hr $= 3.6 \times 10^6$ watt sec $= 3.6 \times 10^6$ joules

1 kg-cal $= \dfrac{3.6 \times 10^6}{860}$ joules $= 4,186.0465$ joules

$\qquad = 4,186.0465$ kg m^2 sec^{-2}

1 kg-cal $= \dfrac{3.6 \times 10^6}{860 \times 9.80665}$ m kgf $= 426.85795$ m kgf

1 kg-cal $= \dfrac{3.6 \times 10^6}{860 \times 9.80665 \times 0.45359237 \times 0.3048}$ ft lbf

$\qquad = 3087.4696$ ft lbf

1 BTU $= \dfrac{0.45359237}{1.8}$ kg-cal $= 0.25199576$ kg-cal

1 BTU $= \dfrac{3.6 \times 10^6}{860 \times 0.3048 \times 9.80665 \times 1.8}$ ft lbf

$\qquad = 778.02922$ ft lbf

1 BTU $= \dfrac{3.6 \times 10^6}{860 \times (0.3048)^2 \times 1.8}$ lb ft^2 sec^{-2}

$\qquad = 25032.349$ lb ft^2 sec^{-2}

[*]The calorie used here is the International Steam Table calorie and the joule is the mean international joule.

$$P/\rho = (R^*/M)T$$

$$= (R^*/M_0)T_M \quad \frac{P}{\rho} = \frac{R^*T}{M} = \frac{R^*T_M}{M_0} \qquad (2\text{-}8)$$

Thus T_M is seen to be directly proportional to p/ρ which will be seen to be proportional to the square of the sound speed C_s.

If it is assumed that T_M is a function of H^* which can be estimated or measured, Eqs. 2-5 and 2-8 can be combined to yield the expression

$$ln\left(\frac{P}{P_0}\right) = \frac{\rho_0 g_0}{P_0} \int_0^{H^*} \frac{T_0}{T_M} dH^*$$

$$= \frac{M_0 g_0}{R^* T_0} \int_0^{H^*} \frac{T_0}{T_M} dH^* \qquad (2\text{-}9)$$

where

$$\frac{\rho}{\rho_0} = \left(\frac{P}{P_0}\right)\left(\frac{T_M}{T_0}\right)^{-1} \qquad (2.10)$$

In the 1959 ARDC Standard, the ratio T_M/T_0 is the basic function which is assumed as a function

TABLE 2-4. CONVERSION FACTORS[20] (continued)

(E) Defining Properties of the Standard Atmosphere

Altitude, H, km	Molecular-scale temperature, T_M, °K	Gradient, L'_M, °K/km	Molecular weight, M	Kinetic temperature, T, °K
0.000	288.15		28.9644	288.15
		−6.5		
11.000	216.65		28.9644	216.65
		0.0		
20.000	216.65		28.9644	216.65
		+1.0		
32.000	228.65		28.9644	228.65
		+2.8		
47.000	270.65		28.9644	270.65
		0.0		
52.000	270.65		28.9644	270.65
		−2.0		
61.000	252.65		28.9644	252.65
		−4.0		
79.000	180.65		28.9644	180.65
		0.0		
88.743	180.65		28.9644	180.65

Altitude, Z, km	Molecular-scale temperature, T_M, °K	Gradient, L_M, °K/km	Molecular weight, M	Kinetic temperature, T, °K
90	180.65		28.9644	180.65
		+3		
100	210.65		28.88	210.02
		+5		
110	260.65		28.56	257.00
		+10		
120	360.65		28.07	349.49
		+20		
150	960.65		26.92	892.79
		+15		
160	1,110.65		26.66	1,022.2
		+10		
170	1,210.65		26.40	1,103.4
		+7		
190	1,350.65		25.85	1,205.4
		+5		
230	1,550.65		24.70	1,322.3
		+4		
300	1,830.65		22.66	1,432.1
		+3.3		
400	2,160.65		19.94	1,487.4
		+2.6		
500	2,420.65		17.94	1,499.2
		+1.7		
600	2,590.65		16.84	1,506.1
		+1.1		
700	2,700.65		16.17	1,507.6

of H^* in order to match test data. All other parameter variations follow as outlined above.

2-2.5. Scale Height

Scale heights are indicative of the magnitude of vertical pressure gradients in the atmosphere and may be defined in geometric units (H_s, meters) and in modified geopotential units (H^*_s, meters) as follows:

$$H_s = \left(\frac{R^* T_0}{g_0 M_0}\right)\left(\frac{T_M}{T_0}\right)\left(\frac{g_0}{g}\right)$$
$$= H^*_s\left(\frac{g_0}{g}\right) = H_s\left(\frac{G}{g_0}\right)\left(\frac{g_0}{g}\right) \quad (2\text{-}11)$$

where

$$\frac{1}{H_s} = -\frac{d}{dZ}(\ln P) \quad \text{and} \quad \frac{1}{H^*_s} = -\frac{d}{dH^*}(\ln P) \quad (2\text{-}12)$$

2-2.6. Speed of Sound

The speed of sound C_s is a scalar parameter defined here formally as follows:

$$C_s = \left(\gamma\frac{P}{\rho}\right)^{1/2} = \left(\frac{\gamma R^*}{M_0}\right)^{1/2} T_M^{1/2} \quad (2\text{-}13)$$

where γ is the isentropic exponent or, in perfect gases, the ratio of specific heats. Actually γ is a function of the state and molecular structure of the gas. Here it is assumed that $\gamma = 1.4$ (exactly for altitudes below 90 km). Above this altitude, information on the sound speed is given by neither the 1962 U.S. nor the 1959 ARDC Standards.

The value of C_s is not necessarily the actual speed with which sound is transmitted over long distances, although in usual cases of high density gas and moderate wave frequency, the actual long range propagation speed coincides with the value of C_s. In fact, the definition used here [Equation 2-13] stems from this classical case. However, a real disturbance traveling an appreciable distance from its generator is attenuated or damped to a degree which increases with increasing wave frequency and with decreasing density of the medium. In moving fluids, particularly those in which chemical reactions are occurring, still other factors influence the actual propagation of disturbances. For this reason the parameter C loses its significance at very high altitudes and is replaced for reference purposes by the mean speed of the gas particles, a quantity closely related to the formal definition of C_s. It is noted that even in the formal definition of C_s given by Ref. 13, the value of γ is no longer considered

TABLE 2-5.

ALTITUDE-DEPENDENT ATMOSPHERIC PROPERTIES

Kinetic temperature	Scale height
Molecular-scale temperature	Number density
Mean molecular weight	Mean free path
Pressure	Collision frequency
Mass-density	Speed of sound
Specific weight	Thermal conductivity
Acceleration of gravity	Kinematic viscosity
Mole volume	Viscosity coefficient (absolute)

constant at extreme altitudes due to the changing physical and chemical structure of the atmosphere.

2-2.7. Air Particle Speed

The mean air particle speed $\bar{V}$ is the arithmetic average of the distribution of speeds of all air particles within a unit volume, assuming that all air particles in the mixture have an average mass associated with the mean molecular weight. The quantity has statistical meaning only if a sufficiently large number of particles is present so that their velocities follow a "Maxwellian" statistical distribution[5] and provided that variations in P and ρ are negligible within the volume. The following definition, derived from the classical kinetic theory of gases[5], is introduced:

$$\bar{V} = \left(\frac{8}{\pi}\frac{P}{\rho}\right)^{1/2} = \left(\frac{8}{\pi}\frac{R^*}{M_0}\right)^{1/2} T_M^{1/2} \qquad (2-14)$$

This yields

$$\frac{\bar{V}}{\bar{V}_0} = \frac{C_s}{C_{s_0}} = \left(\frac{T_M}{T_0}\right)^{1/2} \qquad (2-15)$$

where

$$\frac{\bar{V}_0}{C_{s_0}} = \left(\frac{8}{\pi\gamma}\right)^{1/2} = 1.35$$

Although the physical meaning of $\bar{V}$ also decreases at extremely high altitudes, it is utilized on the basis of its formal definition.

2-2.8. Specific Weight

The specific weight ω is defined as follows:

$$\omega = \rho g \qquad (2-16)$$

This simply Newton's second law referred to a unit volume, where the mass density is assumed to be defined and the force (weight) derived.

2-2.9. Molecular Weight

The molecular weight M of a compound is defined from a chemical standpoint as a dimension-

less number whose magnitude is 16 times the ratio of the average mass of a molecule of the compound to the average mass of an oxygen atom. It is assumed that the oxygen and the compound have their natural distribution of isotopes and that the average is to be construed as the arithmetic mean.

A unit such as the *gram-mole* is defined as the quantity of mass in grams which is numerically equal to the molecular weight of the substance. That is, 1 gram-mole = M gm. The *molar concentration* is defined as the number of moles of a component (in metric units, gram-mole), per unit volume of gas mixture. A *mole-fraction* is defined as the number of moles of a component per mole of mixture.

Standard air is assumed to be *dry*. Its standard sea-level molar composition is shown in Table 2-6. This composition is assumed to be constant below 90 km. Therefore the following standard molecular weight for the air mixture applies in this regime: $M_0 = 28.966$. For higher altitudes the mean molecular weight variation shown in Fig. 2-1(F) is assumed as a standard, based upon experimental evidence.

2-2.10. Mole Volume

The mole volume v is defined by the relation

$$v = M/\rho \quad \text{(volume/mole)}$$

$$= \frac{R^*T}{P} \quad \text{for perfect gases} \qquad (2-17)$$

TABLE 2-6.

SEA LEVEL ATMOSPHERIC COMPOSITION FOR A DRY ATMOSPHERE*

Constituent Gas	Mol. Fraction (Percent)	Molecular Weight (0 = 16.000)
Nitrogen (N_2)	78.09	28.016
Oxygen (O_2)	20.95	32.0000
Argon (A)	0.93	39.944
Carbon dioxide (CO_2)	0.03	44.010
Neon (Ne)	1.8×10^{-3}	20.183
Helium (He)	5.24×10^{-4}	4.003
Krypton (Kr)	1.0×10^{-4}	83.7
Hydrogen (H_2)	5.0×10^{-5}	2.0160
Xenon (Xe)	8.0×10^{-6}	131.3
Ozone (O_3)	1.0×10^{-6}	48.0000
Radon (Rn)	6.0×10^{-18}	222.0

* These values are taken as standard and do not necessarily indicate the exact condition of the atmosphere. Ozone and Radon particularly are known to vary at sea level and above, but these variations would not appreciably affect the value of M_0.

At given values of P and T, the mole volume is the same for all perfect gases.

2-2.11. Number Density

The number density n of a gas denotes the number of gas particles per unit volume, neglecting electrons or other sub-atomic particles. Since Avogadro's number N, defined as the number of particles in one mole of gas, is a universal constant, it follows that

$$n = \frac{N}{V} \quad \text{particles/vol} \qquad (2\text{-}18)$$

where $N = 6.024 \times 10^{26}$ particles/kg-mole of gas

2-2.12. Collision Frequency

By classical methods of the kinetic theory of gases[5] an estimate may be made of the frequency ν with which a given gas particle will collide successively with other particles. In the simplest case, all participating particles are characterized by the same dimension, a diameter σ, which expresses the effective extent of a particle's force field. Moreover, the gas is considered to behave as a perfect gas with σ small compared to distances between particles. The result is the following expression for the collision frequency:

$$\nu = \sqrt{2}\,\pi n\sigma^2 \overline{V} \qquad (2\text{-}19)$$

$$= \text{collisions/sec, or particles colliding with a given particle/sec}$$

Although care must be used in ascribing too much significance to the dimension σ, because of the actual field-like nature of a particle's range of influence, the expression for ν is carried over formally to the standard air mixture. For this purpose an average effective collision diameter is defined as follows:

$$\sigma = 3.65 \times 10^{-10} \text{ meters} = 1.199 \times 10^{-9} \text{ ft} \quad (2\text{-}20)$$

2-2.13. Mean Free Path

A mean free path length L which would be traversed by a particle traveling with mean speed $\overline{V}$ and participating in ν collisions per second, is given by the expression

$$L = \frac{\overline{V}}{\nu} = (\sqrt{2}\,n\pi\sigma^2)^{-1} \qquad (2\text{-}21)$$

2-2.14. Temperature (Real Kinetic)

The temperature T is a quantity related to the kinetic energy per unit mass of the random motion (as distinct from ordered mass motion) of gas mole-

cules and atoms comprising the atmosphere at a given altitude. Usually the random translational degrees of freedom furnish the kinetic energy by which the temperature is defined. For a homogeneous gas with a "Maxwellian" particle velocity distribution the previously given expression for the mean random speed[14] yields a relation between the random kinetic energy and the temperature, namely,

$$\tfrac{1}{2}M\overline{V}^2 = \frac{4}{\pi}R^*T \qquad (2\text{-}22)$$

or in terms of the mean square speed $\overline{V}^2$,

$$\tfrac{1}{2}M\overline{V}^2 = \tfrac{3}{2}R^*T \qquad (2.23)$$

The kinetic temperature T is not necessarily the temperature which would be acquired by a body at rest within the gas or moving through it, since the ultimate temperature of a body depends upon a balance between various modes of energy transfer.

2-2.15. Viscosity

The absolute viscosity μ and the kinematic viscosity $\eta = \mu/\rho$ are obtained by use of the Sutherland equation, which is based on the kinetic theory of gases and is adjusted empirically, as follows:

$$\mu = \frac{\beta T^{3/2}}{T + S} \qquad (2\text{-}24)$$

where

$\beta = 1.458 \times 10^{-6}$ kg/sec·m·$\sqrt{°\text{K}}$ and

$S = 110.4°\text{K}$.

The use of this relation should be limited to altitudes below 40 km.

2-2.16. Thermal Conductivity

A modified Sutherland type of relation is used for the thermal conductivity k, namely,

$$k = \frac{\beta_1 T^{3/2}}{T + S_1 \times 10^{-12/T}} \text{ kg-cal/m·sec °K} \qquad (2\text{-}25)$$

where

$\beta_1 = 6.235 \times 10^{-7}$

$S_1 = 245.4°\text{K}$

and the relation is also limited to altitudes below 40 km.

2-2.17. Simplified Exponential Approximation of Density Variation

Both the pressure and density vary approximately exponentially with altitude in the atmos-

phere, each decreasing by a factor of about 10 roughly every 50,000 ft. In trajectory analyses it has been found useful to approximate the 1956 ARDC Standard density as follows[6,7] for altitudes below 150 km (490, 000 ft.):

$$\frac{\rho}{\rho_r} = \exp\left(-\beta_r z\right)$$

where ρ_r is a reference density evaluated to achieve the best fit of the actual density in the altitude range of prime interest, and β_r is a local decay factor. A fit of the 1956 Standard is shown in Figs. 2-2 and 2-3 where the following values have been used:

$$\rho_r = 0.0027 \text{ slugs/ft}^3$$

$$\frac{1}{\beta_r} = 23,500 \text{ ft}$$

$$\beta_r(r + Z) = 900$$

A series of local values of β_r estimated[8] in the 70 to 169 km range (230,000 to 540,000 ft) are also shown marked on Fig. 2-2. To obtain these values, values of ρ_r were selected at the altitudes indicated, and corresponding values of $1/\beta_r$ varying between 18,500 and 29,800 ft were derived for the intervals delineated.

2-2.18. Extreme Deviations from Standard Conditions

Deviations from standard temperatures are found to approach practical extremes under the following general circumstances:[1] arctic winter, arctic summer and tropical day. Values of these temperature deviations, compared with the ARDC Standard for altitudes up to 100,000 ft, are shown in Figs. 2-4 and 2-5.

The corresponding pressures and densities are found by solution of the hydrostatic equations for perfect gases, as previously discussed in this handbook, assuming an invariant atmospheric composition. Values of these extreme conditions are tabulated in Ref. 1 and are also discussed in Refs. 9 and 10.
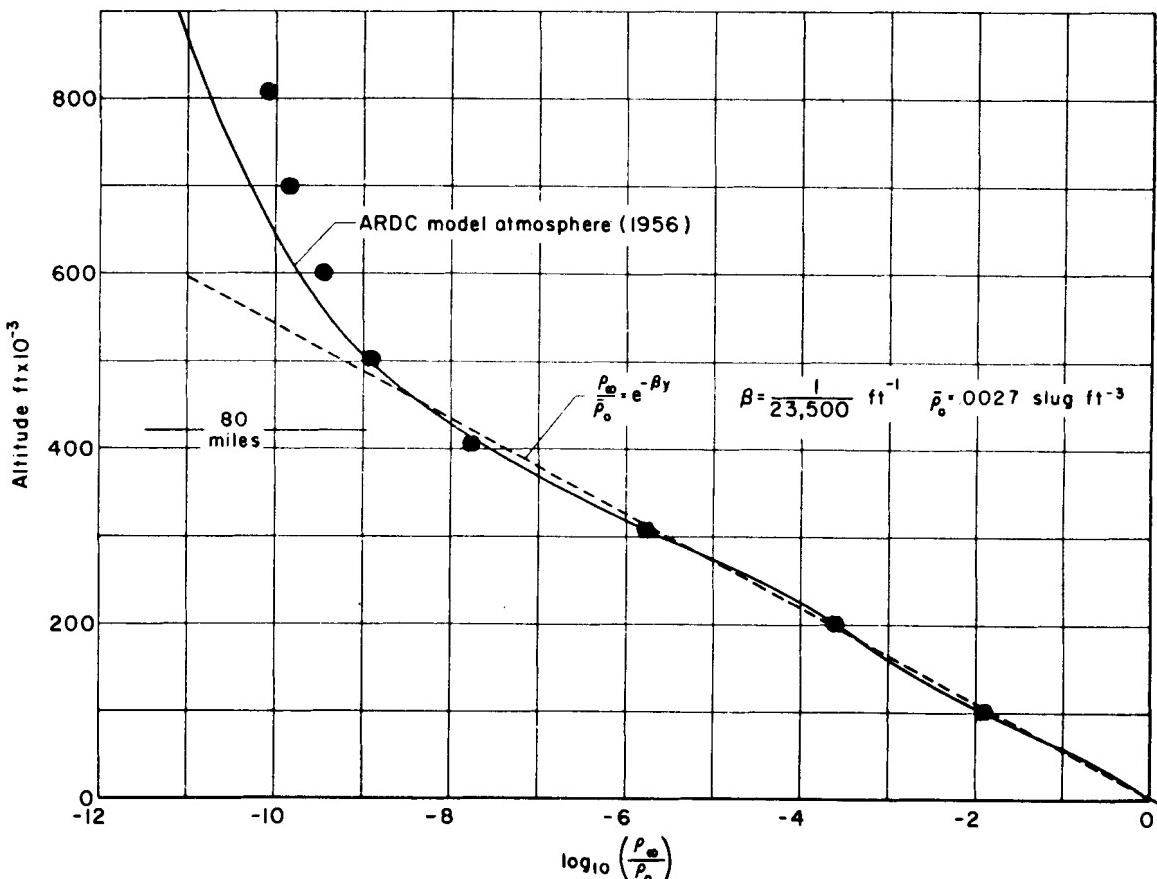
Figure 2-2. Comparison of Exponential Approximation with ARDC Model of Earth Atmosphere (1956). (Solid circles indicate 1962 U. S. Standard values.)
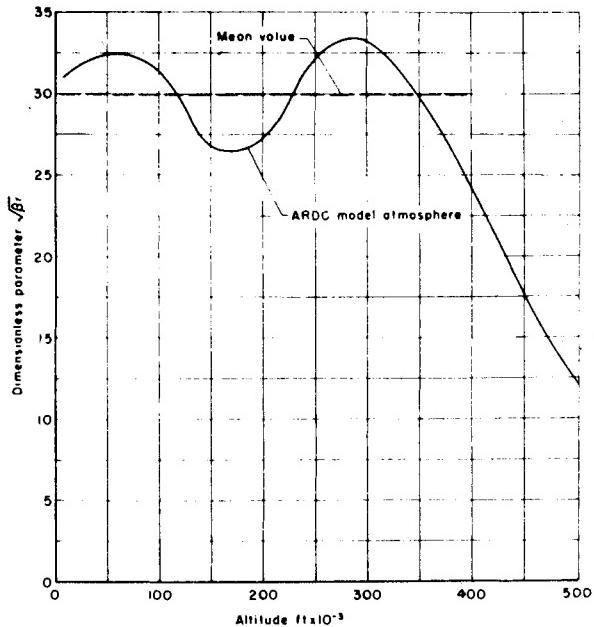
Figure 2-3. Dimensionless Parameter $\sqrt{\beta_r}$ for ARDC Model of Earth Atmosphere[20]

2-2.19. Atmospheric Shells

A number of classifications of altitude ranges in the atmosphere have been proposed. Several are indicated in Figures 2-6(A) and (B).[11]

2-3 PROPERTIES OF THE ATMOSPHERE IMPORTANT FOR ELECTROMAGNETIC WAVE TRANSMISSION

2-3.1. Index of Refraction (D)

The index of refraction of air for radio waves is defined as the ratio of the propagation velocity in real air to the propagation velocity which would be attained in a vacuum, that is, the speed of light. This index is essentially independent of frequency, except possibly for wavelengths of less than one cm, and is also independent of polarization. It is primarily a function of the air temperature, pressure and moisture content[12] as indicated by the following empirical formula:

$$(D - 1) \times 10^6 = \frac{79P}{T} - \frac{11A}{T} - \frac{3.8 \times 10^5 A}{T^2}$$

where

P = barometric pressure (millibars)

T = temperature (°K)

A = water vapor pressure (millibars)

For many purposes it is sufficiently accurate to assume that D decreases linearly with altitude.

Figure 2-4. Temperature-Height Profiles of Extreme and ARDC Model Atmospheres to 100,000 ft
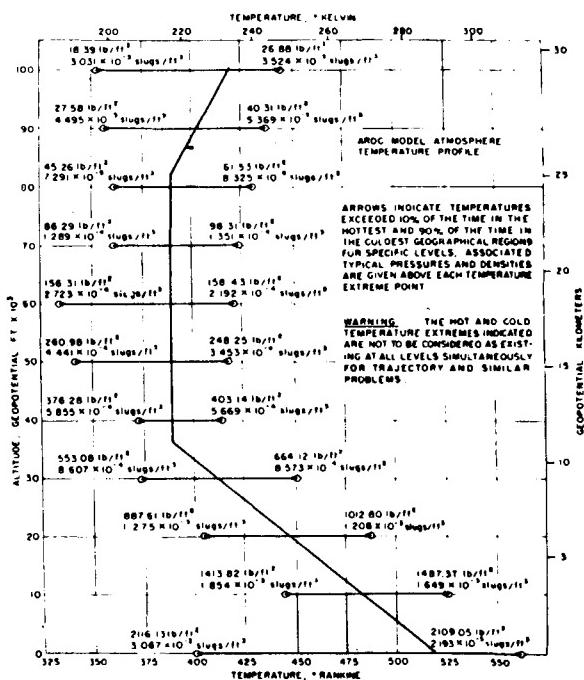
Figure 2-5. Hot and Cold Temperature Extremes and ARDC Model Atmosphere Temperature-Height Profile to 100,000 ft
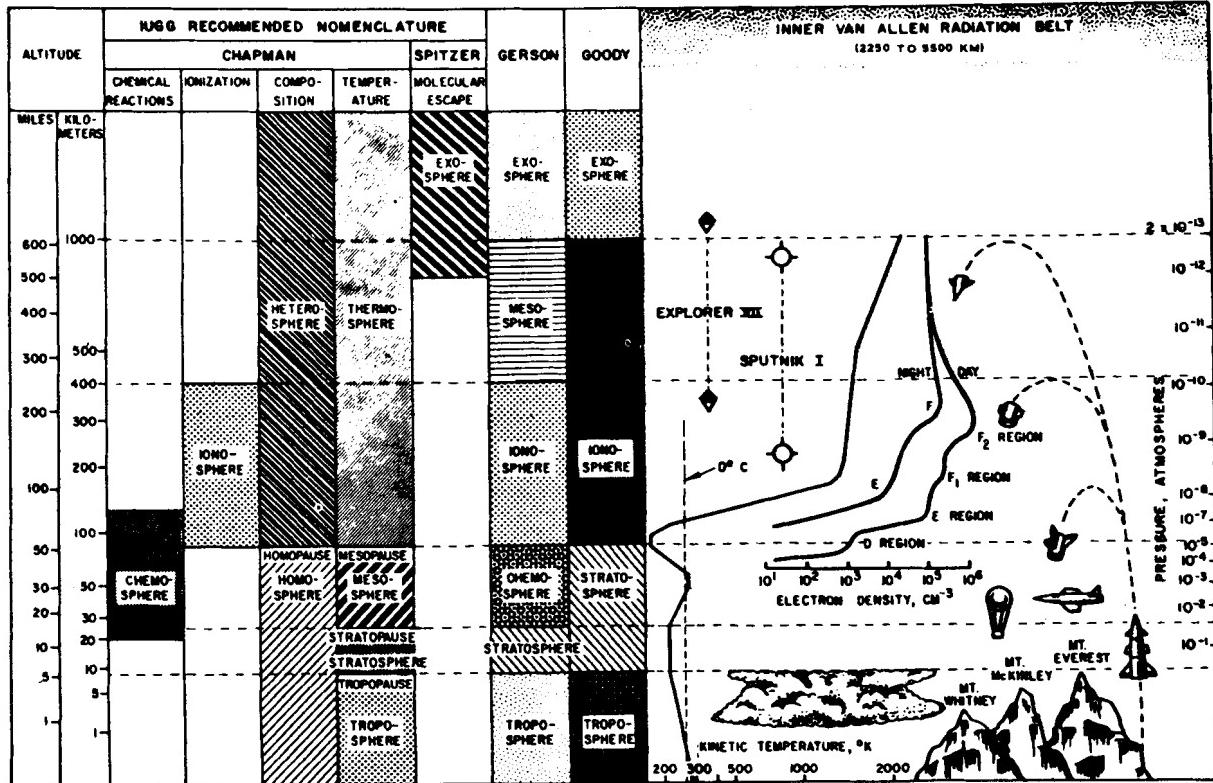
(A) *Schematic Representation of Proposed Atmospheric Nomenclature*

Figure 2-6. Systems of Nomenclature[1]

2-3.2. Electrical Conductivity (σ)

The current in a gaseous medium can be shown to be given by

$$I = Nqv = Nq^2 \frac{(G - iwm)}{(w^2 m^2 + G^2)} E_m e^{iwt}$$

where

I = current (amps)

N = number of electrons/cm^3

q = electric unit charge (esu in cgs electrostatic units)

v = velocity of a charged particle (cm/sec)

G = average frictional constant

i = $\sqrt{-1}$

w = angular frequency of electric field (radian/sec)

m = mass of charged particle (gm)

E_m = amplitude of applied electric field (stat-volts/cm)

t = time (sec)

Only the current due to electrons need be considered because of the large mass of other particles.

The conductivity is then a complex number given as follows:

$$\sigma = \sigma_r - i\sigma_i = \frac{Nq^2 \tau}{m} \left(\frac{1 - iw\tau}{1 + w^2 \tau^2} \right)$$

with

$$\sigma_r = \frac{Nq^2 \tau}{m(1 + w^2 \tau^2)} \quad \text{and} \quad \sigma_i = w\tau\sigma_r$$

where

$\tau \equiv m/G$, á characteristic time, for practical purposes the mean free time between electron collisions.

Thus it is seen that the population of electrons N in the air, primarily in the ionosphere, is a quantity which is significant for wave transmission.

2-3.3. Electron Density in the Atmosphere (N)

The levels of maximum electron density at middle latitudes[13] are given in Table 2-7 and Fig. 2-7. Figure 2-8(B) illustrates the estimated electron distribution in the Van Allen belts located at altitudes of several earth radii.[14]

2-15

It is of interest to note that the electron density and resulting conductive properties of air at very high temperatures have become of interest because of the high temperatuers generated in regions very near the surfaces of high-speed aircraft. Since the transmission of electromagnetic waves through this hot gas blanket may be necessary, the properties which govern the transmission characteristics, pri-marily N and τ, must be obtained for the thermo-dynamic state of the hot gas blanket. Once these properties are evaluated, the conductivities and other characteristics may be estimated as for any other transmitting medium. This also holds true for transmission through flaming exhaust gases. A further discussion of these problems will be given in a later paragraph.

NAME	DESCRIPTION
TEMPERATURE	
TROPOSPHERE	The region nearest the surface, having a more or less uniform decrease of tempera-ture with altitude. The nominal rate of temperature decrease is 6.5°K/km, but in-versions are common. The troposphere, the domain of weather, is in convective equilibrium with the sun-warmed surface of the earth. The tropopause, which occurs at altitudes between 6 and 18 kilometers (higher and colder over the equator), is the domain of high winds and highest cirrus clouds.
STRATOSPHERE	The region next above the troposphere and having a nominally constant temperature. The stratosphere is thicker over the poles, thinner or even nonexistent over the equator. Maximum of atmospheric ozone found near stratopause. Rare nacreous clouds also found near stratopause. Stratopause is at about 25 kilometers in middle latitudes. Stratospheric temperatures are in the order of arctic winter temperatures.
MESOSPHERE	The region of the first temperature maximum. The mesosphere lies above the stra-tosphere and below the major temperature minimum, which is found near 80 kilo-meters altitude and constitutes the mesopause. A relatively warm region between two cold regions; the region of disappearance of most meteors. The mesopause is found at altitudes of from 70 to 85 kilometers. Mesosphere is in radiative equilibrium between ultraviolet ozone heating by the upper fringe of ozone region and the infrared ozone and carbon dioxide cooling by radiation to space.
THERMOSPHERE	The region of rising temperature above the major temperature minimum around 80 kilometers altitude. No upper altitude limit. The domain of the aurorae. Tempera-ture rise at base of thermosphere attributed to too infrequent collisions among mole-cules to maintain thermodynamic equilibrium. The potentially enormous infrared radiative cooling by carbon dioxide is not actually realized owing to inadequate colli-sions.
COMPOSITION	
HOMOSPHERE	The region of substantially uniform composition, in the sense of constant mean molecular weight, from the surface upwards. The homopause is found at altitudes between 80 and 100 kilometers. The composition changes here primarily because of dissociation of oxygen. Mean molecular weight decreases accordingly. The ozono-sphere, having its peak concentration near stratopause altitude, does not change the mean molecular weight of the atmosphere significantly.
HETEROSPHERE	The region of significantly varying composition above the homosphere and extending indefinitely outwards. The "molecular weight" of air diminishes from 29 at about 90 kilometers to 16 at about 500 kilometers. Well above the level of oxygen dissocia-tion, nitrogen begins to dissociate and diffusive separation (lighter atoms and mole-cules rising to the top) sets in.
IONIZATION	
IONOSPHERE	The region of sufficiently large electron density to affect radio communication. How-ever, only about one molecule in 1000 in the F_2 region to one in 100,000,000 in the D region is ionized. The bottom of the ionosphere, the D region, is found at about 80 kilometers during the day. At night the D region disappears and the bottom of the ionosphere rises to 100 kilometers. The top of the ionosphere is not well defined but has often been taken as about 400 kilometers. The recent extension upward to 1000 km based on satellite and rocket data is shown.
CHEMICAL REACTIONS	
CHEMOSPHERE	The region where chemical activity (primarily photochemical) is predominant. The chemosphere is found within the altitude limits of about 20 to 110 kilometers.
MOLECULAR ESCAPE	
EXOSPHERE	The region wherein molecular escape from the earth's atmosphere is significant. The base of the exosphere, the critical level, is thought to be at an altitude above 300 kilometers, possibly as high as 1000 kilometers. Satellite data indicating higher densities at these altitudes favor higher exosphere levels. Lighter atoms and mole-cules can escape at lower altitudes than heavier ones. The earth's magnetic field ef-fectively prevents the escape of charged particles, however.

(B) Salient Features of Various Atmospheric Regions

Figure 2-6. Systems of Nomenclature[1] *(continued)*
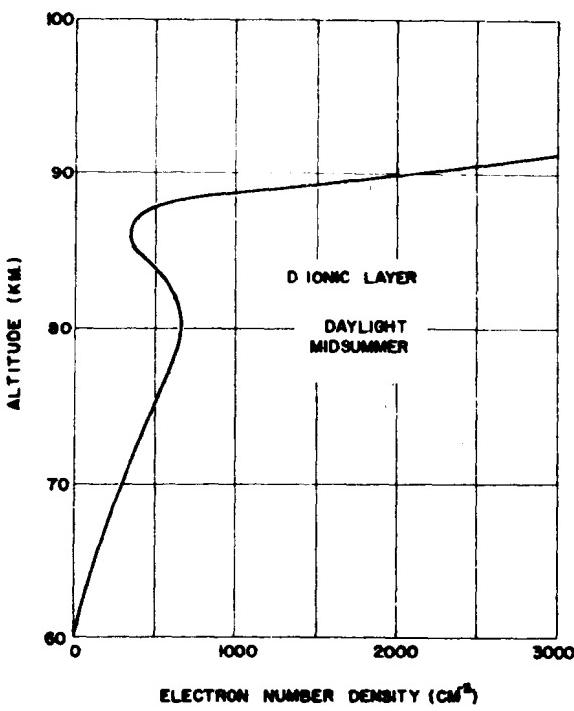
Figure 2-7. Average Variation of Electron Density with Altitude in the D Ionic Layer During a Summer Day[1]

TABLE 2-7.

LEVELS OF MAXIMUM ELECTRON DENSITY AT MIDDLE LATITUDES[10]

Region	Level (km)	Range (km)	Approximate N (electrons per cm³)	
			(Day)	(Night)
D	60	60–100	1.5×10^4	—
E	100	70–120	1.5×10^5	1×10^4
E_s	120	75–130	3.0×10^6	—
F_1	200	160–220	2.5×10^5	—
F_2	300	250–500	1.5×10^6	2.5×10^5
G	500	400–700	2.0×10^0	—

2-4 WINDS

2-4.1. Introduction

Although the presence of winds and gusts in the atmosphere must be considered in formulating the structural loads on a missile in flight, these factors are even more important for determining the characteristics of flight control systems and dispersion in ballistic flight. For ballistic vehicles, control
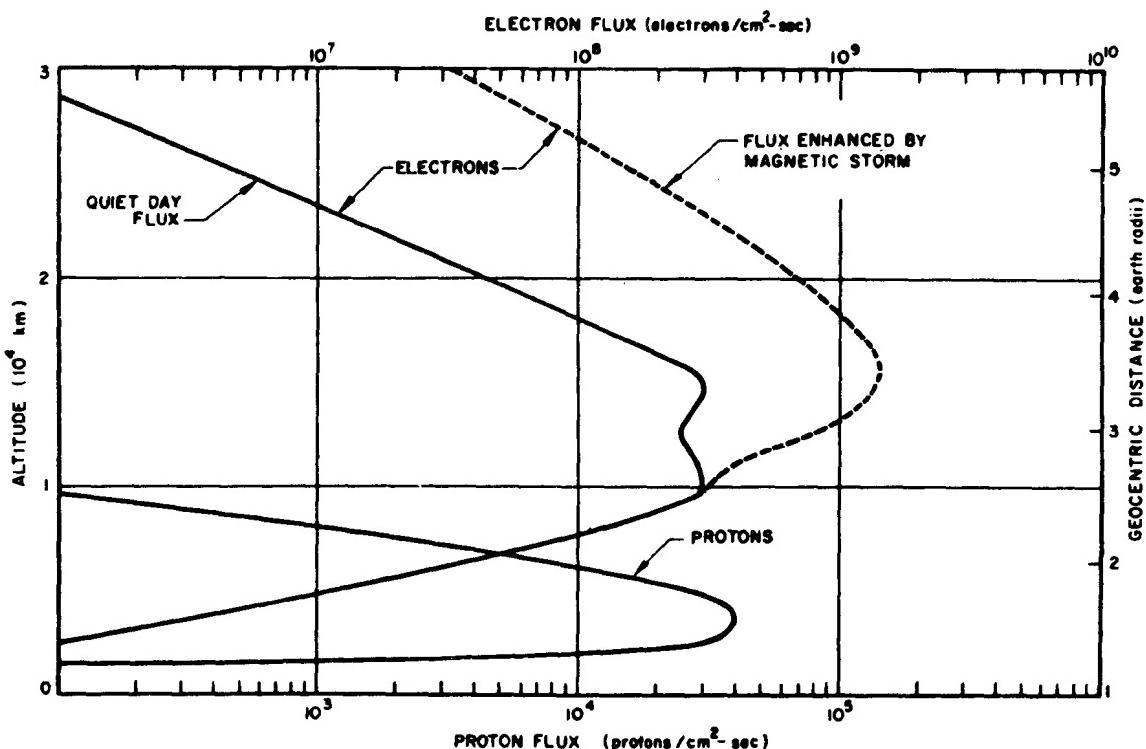
(A) Particle Flux versus Altitude in the Equatorial Plane

Figure 2-8. Particle Flux in Van Allen Radiation Belt[21]

2-17
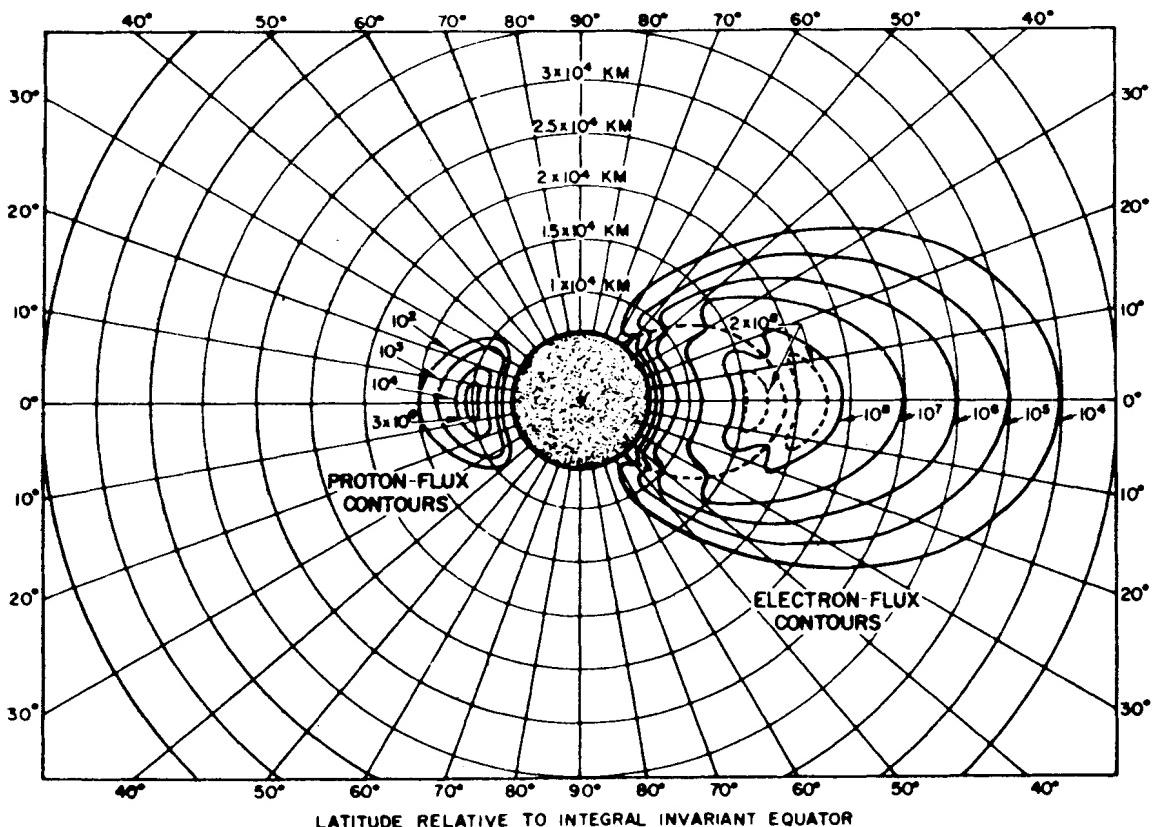
(B) Quiet Day Flux Contours of Electrons with Energies Greater than 20 kev in Electrons/cm²-sec (Proton Flux Contours are shown for reference. Accuracy is only to several orders of magnitude. Data shown is as of 1961. New information is continually being evolved and should be consulted for quantitative utility.)

Figure 2-8. Particle Flux in Van Allen Radiation Belt[21] (continued)

systems are particularly important for establishing accurately the terminal properties of the boost stages. Launching inaccuracies cannot be corrected in the ballistic flight. Therefore, design atmospheres for wind magnitude profiles and the rate of change of wind magnitude with altitude, that is, "wind shear" distributions, must be established in connection with a given missile design.

Figures 2-9(A) and 2-9(B) illustrate synthetic wind speed profiles for winter conditions in the northeastern and northwestern parts of the United States.

The main factors which are influenced by winds, and which are important for determining control system features and ultimate dispersion of ballistic stages, are: maneuver loads due to winds, possible dispersion due to winds and the effect of wind shear on a system in which control of the longitudinal Mach number involves employment of on-board aerodynamic sensors.

Wind effects are relatively unimportant during the high speed flight of heavy, nonmaneuvering ballistic stages such as modern re-entry nose cones of long range missiles. However they may be significant for new maneuverable re-entry concepts and for ballistic interceptors which employ lift (glide) after thrust is terminated. These subjects are discussed in detail in References 13, 15, 16 and 17.

2-4.2. Loads Due to Winds on a Maneuvering Missile

A ballistic missile is controlled during its boost and aiming stages. A completely guided missile is controlled during the time it closes in on the target as well. The control load problem is the same provided the missile is commanded to follow a programmed attitude (angle of attack) over a period of time. The presence of winds during this period induces an additional angle of attack over the no-wind angle. This results in an additional aerodynamic
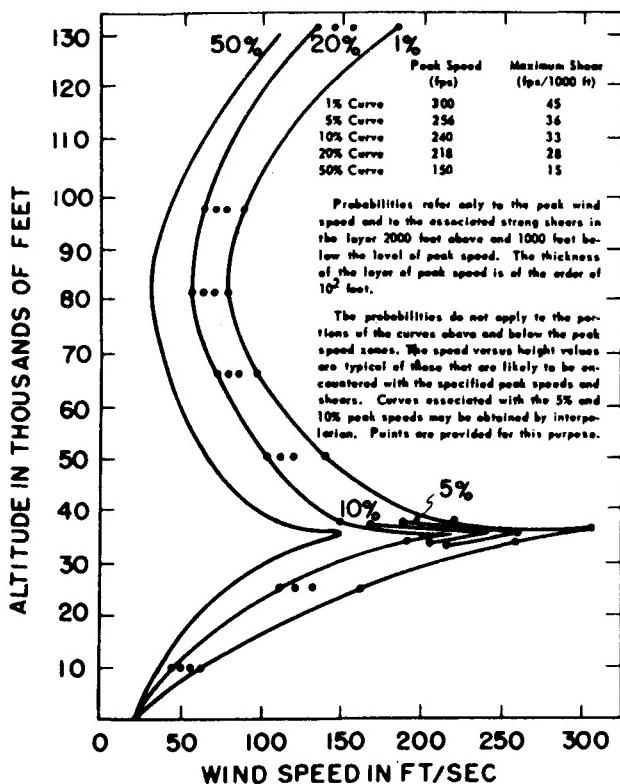
Figure 2-9(A). Synthetic Wind Speed Profiles Exceeded 1%, 5%, 10%, 20% and 50% of the Winter for the Windiest Area (Northeastern Part) of the United States[1]
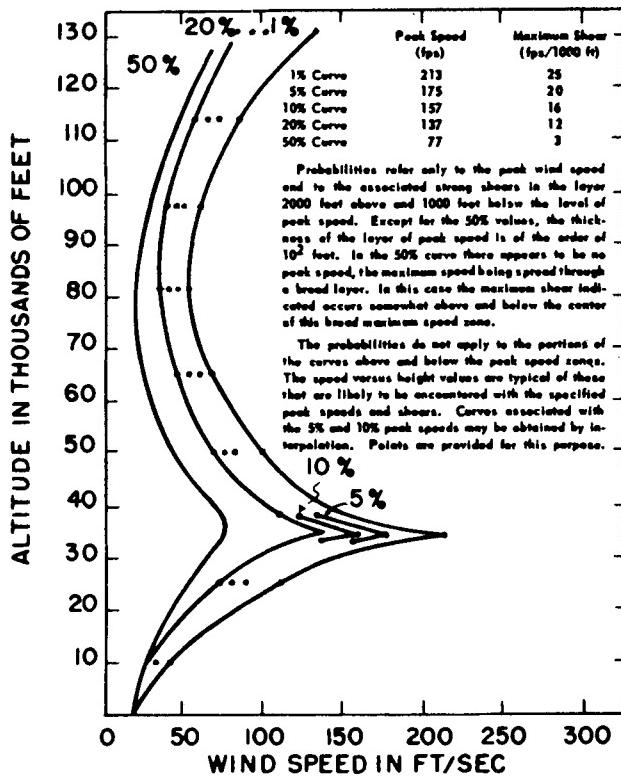
Figure 2-9(B). Synthetic Wind Speed Profiles Exceeded 1%, 5%, 10%, 20% and 50% of the Winter for the Calmest Area (Northwestern Part) of the United States[1]

maneuver load dependent on both wind velocity and shear, which the control system must handle.

If a missile is aerodynamically stable, the wind load increment will set up a moment which causes the missile to decrease its angle of attack and thereby

Figure 2-10. Rate of Heat Gain by Solar and Nocturnal Radiation[18]

reduce the load increment. However if the missile is changing altitude, the nature of the wind shear and the missile's time rate of change of altitude may be such that the missile response to wind loads does not lead to a load reduction. For the Navaho SM-64A missile, a guided robot plane with ramjet engines, solid-fuel launching boosters and 5000-mi range, a large portion of the lateral and longitudinal maneuver loads during boost and terminal dive-in were directly attributable to winds. Critical trajectory conditions existed in the 25,000 to 45,000 ft altitude band, a region of severe wind velocities and wind shears. In this band, during boost, winds contributed nearly all the lateral load requirement ($\pm 90{,}000$ lb) and the largest dispersion in longitudinal maneuver loads ($\pm 30{,}000$ lb).

2-4.3. Wind Dispersions

Winds contribute strongly to aerodynamic and flight control system dispersions; the critical condition for dive dispersions is that of maximum wind velocity during the entire dive. Mach number fluc-

tuations due to changing winds may engender large control load requirements in systems which are commanded by means of Mach number sensing devices. This is true particularly if the detected Mach number is too low.

2-4.4. Control of Horizontal Flight

If part of a controlled trajectory is horizontal, if the control system is actuated by a Mach number sensing device and if speed corrections are made by climbing or diving, the control system will be strongly sensitive to wind shear which results in changes in relative velocity. Consequently, if the missile acceleration capabilities are insufficient to decrease the indicated error signal, the missile system may become destabilized.

2-5 RADIATION FROM SOLAR SYSTEM AND SURROUNDING ATMOSPHERE

The heat flux q in Btu/ft^2 sec due to direct solar irradiation, due to nocturnal irradiation from below the missile (mainly caused by the earth) and that due to nocturnal irradiation from above (mainly caused by the gaseous atmosphere) are shown in Fig. 2-10.

REFERENCES

1. *Handbook of Geophysics*, Air Force Cambridge Research Center, GRD, ARDC, Revised Edition, 1961.

2. R. A. Minzer, K. S. W. Champion and H. L. Pond, *ARDC Model Atmosphere, 1959*, Air Force Cambridge Research Center Technical Report 59-267, 1959.

3. *Standard Atmosphere (ICAO and NACA)— Tables and Data for Altitudes to 65,800 ft.*, National Advisory Committee for Aeronautics Report 1235, 1955.

4. L. V. Baldwin and P. L. Blackshear, *Preliminary Survey of Propulsion Using Chemical Energy Stored in the Upper Atmosphere*, National Advisory Committee for Aeronautics Technical Note 4267, 1958.

5. E. H. Kennard, *Kinetic Theory of Gases*, McGraw-Hill, Inc., N. Y., 1938.

6. H. J. Allen and A. J. Eggers, Jr., *A Study of the Motion and Aerodynamic Heating of Missiles Entering the Earth's Atmosphere at High Supersonic Speeds*, National Advisory Committee for Aeronautics Technical Note 4047, 1957.

7. D. R. Chapman, *An Approximate Analytical Method for Studying Entry into Planetary Atmospheres*, National Advisory Committee for Aeronautics Technical Note 4276, 1958.

8. K. A. Ehricke, *Space Flight, Vol. I, Environment and Celestial Mechanics*, D. Van Nostrand, N. Y., 1960.

9. *Atmospheric Properties-Extreme Cold and Hot Standard for Aeronautical Design*, ANA Bulletin No. 421, September 24, 1953.

10. MIL-STD-210A, *Climatic Extremes for Military Equipment*, 2 August 1957.

11. N. C. Gerson, *The Atmosphere*, Air Force Cambridge Research Center Technical Note 55-216, 1955.

12. A. S. Locke et al, *Guidance*, D. Van Nostrand, N. Y., 1955. pp. 95, 120-122.

13. J. Kaplan, G. F. Schilling and H. K. Kallman, *Methods and Results of Upper Atmosphere Research*, Geophysical Research Paper No. 43, Air Force Cambridge Research Center Technical Report 55-224, 1955.

14. J. A. Van Allen, *Radiation Measurements in the Vicinity of the Earth and Moon*, IGY Bulletin No, 30. December 1959.

15. N. Sissenwine, *Windspeed Profile, Windshear, and Gusts for Design of Guidance Systems for Vertical Rising Air Vehicles*, Air Force Surveys in Geophysics No. 57, Air Force Cambridge Research Center Technical Note 54-22, 1954.

16. D. M. Badger and L. A. Nelson, *A Study of General Gust Criteria for Airborne Missile Operations*, Northrop Aircraft Inc., NAI 54-754, Structural Research Report SRR-71, November 26, 1954, AD 56317.

17. *Wind Criteria for SM-64A Missile Flight Control System Design*, Prepared by Aerodynamics Section, North American Aviation, Inc., Missile Development Division, Contract AF-33(600)-28469, 9 September 1957, AD 147904. (Navaho program)

18. H. A. Johnson, M. W. Rubesin, F. M. Sauer, E. G. Slack and L. Possner, *A Design Manual for Determining the Thermal Characteristics of High Speed Aircraft*, Army Air Forces Technical Report 5632, Air Material Command, Dayton, Ohio, September 10, 1947. (Appended Bibliography contained in AAF Technical Report 5633.)

19. R. B. Morrison, Ed., *Design Data for Aeronautics and Astronautics*, John Wiley & Sons, N. Y., 1962.

20. *U. S. Standard Atmosphere, 1962*, Prepared by COESA under sponsorship of National Aeronautics and Space Administration, U. S. Air Force and U. S. Weather Bureau, Government Printing Office, December 1962.

21. Francis S. Johnson, *Satellite Environment Handbook*, Stanford University Press, 1961.

CHAPTER 3

TYPICAL BALLISTIC TRAJECTORIES

3-1 INTRODUCTION

Although a detailed discussion of trajectories is given in AMCP 706-284 (C), Engineering Design Handbook, Ballistic Missile Series, *Trajectories* (U), a number of interesting trajectory characteristics which can be represented in relatively simple fashion are restated here for convenience. A ready reference for this simplified presentation is Reference 1 which is based in part on the discussions of References 2 and 3.

3-2 BALLISTIC FLIGHT AND RE-ENTRY

The powered flight of launching usually terminates above the effective atmosphere. At the power-off or burnout point, the vehicle's flight is characterized by a velocity V_i and an inclination angle Θ_i between the velocity vector and local horizontal. Subsequent flight outside the atmosphere occurs in an elliptic trajectory with the earth's center as one focus. Thus the vehicle again approaches the atmosphere with velocity $V_e = V_i$ and an angle $\Theta_e = \Theta_i$.

For minimum expenditure of energy to achieve a given range (Φ = range ÷ earth's radius) the injection and re-entry velocities are given by

$$V_i = V_e = V_s \left[\frac{2 \sin (\Phi/2)}{1 + \sin (\Phi/2)} \right]^{1/2};$$

$$0 \leq \Phi \leq \Pi, \qquad (3-1)$$

Φ measured in radians

where V_s is the orbiting speed near the earth's surface, equal to $\sqrt{g r_0}$ or 25,930 ft/sec,

$$g = 32.2 \text{ ft/sec}^2, \text{ and}$$
$$n_0 = \text{earth's radius in feet.}$$

The corresponding launching and re-entry angles are

$$\Theta_i = \Theta_e = \frac{\Pi - \Phi}{4} \qquad (3-2)$$

For a 6000 mile range $V_i \sim 23{,}000$ ft/sec and $\Theta_i \sim 23°$, whereas for a 2000 mile range $V_i \sim 16{,}000$ ft/sec and $\Theta_i \sim 38°$.

In the analysis of vehicle re-entry it is convenient to approximate the vertical variation of atmospheric density by the simple relation

$$\rho/\rho_0 = e^{-\beta y} \qquad (3-3)$$

where

$$\rho_0 = 0.0034 \text{ slugs/ft}^3$$
$$1/\beta = 22{,}000 \text{ ft}$$
$$y = \text{altitude in ft.}$$

With this relation and neglecting lift, variations in the drag coefficient C_D, and gravity forces as compared to aerodynamic forces, one obtains the following expression for velocity history during flight within the atmosphere:

$$\frac{V}{V_i} = \exp \left[\frac{-\rho g}{2 \beta B \sin \Theta_i} \right] \qquad (3-4)$$

where

B is the ballistic coefficient, $W/C_D A$
W is the vehicle weight,
A is the area upon which C_D is based, and
ρ is the local density.

The value of C_D for many blunt bodies at high speed approximates that of a sphere or a value on the order of 0.9. For satellite configurations and weights, values of B are on the order of 10 lb/ft^2. For a representative body such as an iron sphere 3.6 in. diameter, $B = 100$ lb/ft^2; for a 3-ft diameter iron sphere, $B = 1000$ lb/ft^2.

The deceleration of the vehicle measured in units of g can be shown to be equal to the ratio of drag to weight. This in turn can be expressed by $\rho V^2/2B$.

Examination of deceleration characteristics (Figure 3-1) shows the following:

a. Peak deceleration occurs when $V = 0.61 \, V_i$ regardless of B.

b. Deceleration is negligibly small at altitudes above 250,000 ft (less than 1 g from $B > 10$) unless one considers satellite flight over long periods of time. This indicates that rarefied gas effects are relatively unimportant insofar as aerodynamic forces of ballistic vehicles are concerned.
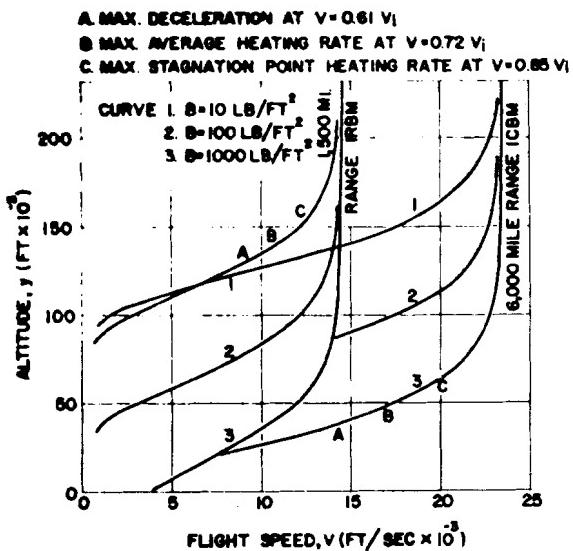
Figure 3-1. Altitude and Velocity for Maximum Deceleration and Heating of Ballistic Missiles

c. Maximum deceleration of 58 g occurs for a minimum energy range of 4700 mi. regardless of B.

It can be shown that within reasonable engineering accuracy the heat transfer rate to the stagnation point of a blunt body is proportional to $\sqrt{\rho}V^3$, whereas the overage heating rate of the entire surface of blunt or sharp vehicles is roughly proportional to ρV^3. For a ballistic missile, the maxima of these rates occur at $V/V_i = 0.85$ (stagnation point) and $V/V_i = 0.72$ (average heating).

3-3 LIFTING RE-ENTRY (GLIDE)

Basic characteristics of re-entry for unpowered vehicles whose lift (force component normal to the flight path) cannot be neglected may be deduced in a simplified manner by the use of a reasonable set of approximations, namely:

a. Sum of lift and centrifugal force is equal to the vehicle weight.
b. Angle between flight path and local horizontal is small.
c. Centrifugal force is approximately WV^2/gr_0.
d. Lift-to-drag ratio L/D is constant.

The above assumptions are poorest near impact.

Skip vehicles, which enter and leave the atmosphere again one or more times, are not considered here. Despite the fact that these vehicles are efficient in the conversion of velocity to range, they have a number of disadvantages related to repeated and large decelerations and heating cycles.

The glide velocity history as a function of the partial range Ψ (angular displacement from launch site swept out by radius vector joining vehicle and earth's center) is given by

$$\left(\frac{V}{V_s}\right)^2 = 1 - \exp\left[\frac{-2(\Phi - \Psi)}{L/D}\right] \qquad (3\text{-}5)$$

or, as a function of altitude,

$$\left(\frac{V}{V_s}\right)^2 = \frac{1 + \rho V_s^2}{K};$$

$$\frac{\rho}{\rho_0} = e^{-\beta y} \qquad (3\text{-}6)$$

where

$$V_s = \sqrt{gr_0},$$

$$K = \frac{W}{C_L A},$$

C_L is the lift coefficient,

$$\frac{L}{D} = \frac{C_L}{C_D}, \text{ and}$$

$$0 \leq \Psi \leq \Phi.$$

The initial velocity required for a given range is shown plotted for values of L/D in Figure 3-2, based on the relation

$$\left(\frac{V_i}{V_s}\right)^2 = 1 - \exp\left[\frac{-2\Phi}{L/D}\right] \qquad (3\text{-}7)$$

The desirability of having large L/D is clearly indicated. For low values of L/D, longer range is achieved with a *nonlifting* vehicle for a given V_i.
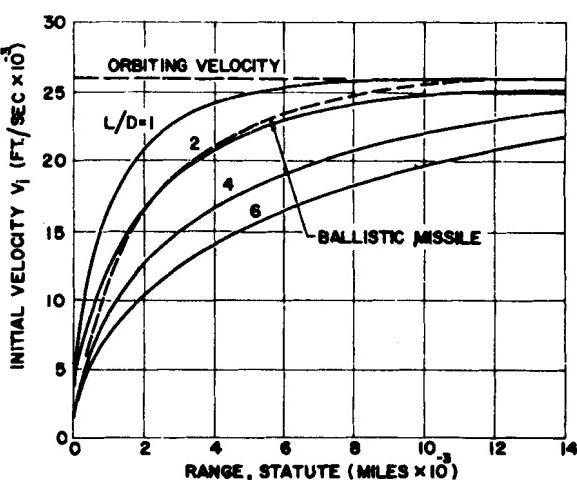
Figure 3-2. Initial Velocity of Glide Vehicles Required to Achieve a Given Range, Showing the Effect of the Lift-to-Drag Ratio

By maximizing the quantity $\sqrt{\rho}V^3$ it can be shown that the maximum stagnation point heating rate occurs at the point of the trajectory where the velocity $V = \sqrt{\frac{2}{3}} V_i = 21{,}000$ ft/sec provided that the initial velocity $V_i \geq 21{,}000$ ft/sec. Likewise, a peak value of the average surface heating which is proportional to ρV^3, occurs when $V = V_i / \sqrt{3} = 15{,}000$ ft/sec, provided that $V_i \geq 15{,}000$ ft/sec. Otherwise the peak heating occurs at the start of glide when $V = V_i$. For values of the lift parameter $K > 100$ lb/ft^2, peak heating occurs below an altitude of 220,000 ft. Rarefied gas phenomena will have a negligible or at most a minor influence on the heating of glide vehicles in the regime of peak heating.

REFERENCES

1. K. R. Eukenhus, *The Flight Environment of Long-Range Ballistic Missiles and Glide Vehicles*, U. S. Naval Ordnance Laboratory, NAVORD Report 6745, 1959.

2. A. J. Eggers, H. A. Allen and S. E. Niece, *A Comparative Analysis of the Performance of Long-Range Hypervelocity Vehicles*, National Advisory Committee for Aeronautics Technical Note 4046, 1957.

3. H. A. Allen and A. J. Eggers, *A Study of the Motion and Aerodynamic Heating of Missiles Entering the Earth's Atmosphere at High Supersonic Speeds*, National Advisory Committee for Aeronautics Technical Note 4047, 1957.

CHAPTER 4

PHYSICAL AND THERMODYNAMIC PROPERTIES OF AIR

4-1 EQUILIBRIUM THERMODYNAMIC AND TRANSPORT PROPERTIES

In Chapter 2 the properties of air are given from the standpoint of their variation with altitude. In this chapter the equilibrium thermodynamic and transport properties of air are presented in more general terms for use in flow calculations (See References 25, 28–38 in Chapter 1). It is recalled that the thermodynamic properties such as enthalpy, specific heat and composition, etc., are characteristics of the medium which are not dependent upon flow or time. On the other hand, the transport properties such as viscosity, thermal conductivity and diffusion coefficients are each essentially proportionality factors between gradients of quantities such as velocity, temperature and component concentrations and their respective fluxes such as shear stress, heat flux and component-diffusion flux.

The thermodynamic properties of equilibrium air presented here in tabular and graphical form, Tables 4-1 through 4-4 and Figures 4-1 through 4-10, (from Reference 31 in Chapter 1) may also be represented in the form of Mollier diagrams. Such Mollier diagram are available elsewhere (References 25, 28, 29 in Chapter 1).

TABLE 4-1. TRANSPORT PROPERTIES OF AIR FOR VARIOUS TEMPERATURES AND PRESSURES

(A) Coefficient of Viscosity

T, ° K	Ratio η/η_0 Pressure, atmospheres							Reference coefficient, η_0, in 10^{-6}	
	100	10	1.0	0.1	0.01	0.001	0.0001	$\dfrac{\text{lb sec}}{\text{ft}^2}$	$\dfrac{\text{gm}}{\text{cm sec}}$
500	1.000	1.000	1.000	1.000	1.000	1.000	1.000	0.558	287
1000	1.000	1.000	1.000	1.000	1.000	1.000	1.000	.868	416
1500	1.000	1.000	1.000	1.000	1.000	1.000	1.000	1.100	527
2000	1.000	1.000	1.000	1.000	1.000	1.000	1.000	1.293	619
2500	1.000	1.000	1.000	1.000	1.000	1.000	1.000	1.461	700
3000	1.000	1.000	1.000	1.000	1.000	1.000	1.000	1.612	772
3500	1.000	1.001	1.003	1.006	1.010	1.010	1.011	1.751	838
4000	1.003	1.008	1.016	1.020	1.022	1.024	1.032	1.879	899
4500	1.010	1.022	1.029	1.033	1.038	1.055	1.096	1.999	957
5000	1.022	1.036	1.043	1.051	1.074	1.128	1.181	2.11	1011
5500	1.036	1.052	1.060	1.086	1.146	1.209	1.227	2.22	1062
6000	1.050	1.067	1.090	1.148	1.228	1.257	1.256	2.32	1112
6500	1.072	1.090	1.139	1.229	1.276	1.286	1.271	2.42	1159
7000	1.089	1.124	1.208	1.294	1.317	1.303	1.264	2.52	1204
7500	1.112	1.175	1.283	1.332	1.337	1.307	1.210	2.61	1247
8000	1.143	1.238	1.342	1.371	1.347	1.280	1.072	2.69	1289
8500	1.185	1.307	1.386	1.386	1.343	1.207	.826	2.78	1330
9000	1.238	1.368	1.425	1.396	1.314	1.068	.517	2.86	1370
9500	1.298	1.418	1.438	1.393	1.251	.853	.261	2.94	1408
10000	1.361	1.468	1.445	1.375	1.143	.595	.118	3.02	1446
10500	1.418	1.496	1.448	1.335	.983	.361	.055	3.10	1482
11000	1.467	1.501	1.442	1.267	.782	.200	.029	3.17	1518
11500	1.509	1.511	1.424	1.168	.571	.108	.018	3.24	1552
12000	1.549	1.520	1.394	1.040	.387	.063	.012	3.31	1586
12500	1.577	1.516	1.342	.881	.249	.036	.009	3.38	1620
13000	1.581	1.508	1.274	.711	.158	.024	.008	3.45	1652
13500	1.594	1.492	1.187	.547	.100	.018	.007	3.52	1684
14000	1.599	1.468	1.082	.408	.067	.015	.007	3.58	1716
14500	1.601	1.415	.940	.288	.042	.013	.008	3.65	1747
15000	1.604	1.387	.828	.212	.016	.012	.008	3.71	1777

TABLE 4-1. TRANSPORT PROPERTIES OF AIR FOR VARIOUS TEMPERATURES AND PRESSURES (continued)

(B) Coefficient of Thermal Conductivity

T, °K	Ratio k/k_e — Pressure, atmospheres							Reference coefficient, k_e, in 10^{-6}	
	100	10	1.0	0.1	0.01	0.001	0.0001	$\dfrac{\text{Btu}}{\text{ft sec }°R}$	$\dfrac{\text{watt}}{\text{cm }°K}$
500	1.021	1.021	1.021	1.021	1.021	1.021	1.021	5.84	364
1000	1.100	1.100	1.100	1.100	1.100	1.100	1.100	9.10	567
1500	1.150	1.150	1.150	1.150	1.150	1.150	1.150	11.53	719
2000	1.177	1.177	1.177	1.251	1.460	2.09	3.99	13.55	844
2500	1.256	1.317	1.619	2.50	4.63	7.67	5.50	15.31	954
3000	1.421	1.928	3.20	5.48	5.02	2.19	1.465	16.90	1053
3500	1.941	3.15	4.72	3.96	1.719	2.11	3.71	18.35	1143
4000	2.69	3.94	2.99	1.600	2.91	6.04	15.03	19.09	1227
4500	3.22	3.06	1.714	3.32	7.34	17.65	30.5	21.0	1305
5000	3.07	1.997	3.29	7.18	16.63	25.8	11.84	22.1	1379
5500	2.46	2.91	5.99	13.71	22.2	11.40	3.54	23.3	1449
6000	1.930	4.53	10.19	18.74	13.09	3.96	6.14	24.3	1516
6500	3.35	6.98	14.50	15.39	5.49	5.92	12.99	25.4	1580
7000	4.69	9.97	15.69	8.32	3.28	10.95	26.9	26.4	1642
7500	6.31	12.48	12.24	5.92	8.62	19.97	51.9	27.3	1701
8000	8.21	13.19	7.80	3.42	13.99	34.7	84.8	28.2	1759
8500	9.86	11.55	5.10	9.72	22.1	56.3	107.6	29.1	1814
9000	10.90	8.79	3.26	14.03	34.1	78.8	93.8	30.0	1868
9500	10.88	6.38	6.66	20.3	49.1	92.6	54.9	30.8	1921
10000	9.87	4.07	10.95	28.2	64.8	84.8	25.6	31.6	1972
10500	8.33	6.50	14.40	37.6	76.6	59.9	11.45	32.4	2020
11000	6.84	8.47	19.17	48.3	78.6	35.2	5.81	33.2	2070
11500	5.59	10.48	24.5	58.2	68.6	19.04	3.40	34.0	2120
12000	4.79	12.96	30.9	65.4	51.6	10.75	2.29	34.7	2160
12500	3.34	15.55	37.0	67.3	34.8	6.09	1.807	35.5	2210
13000	5.78	18.77	43.3	63.4	22.5	4.08	1.622	36.2	2250
13500	9.95	22.3	48.7	54.5	14.28	3.18	1.461	36.9	2300
14000	11.44	25.9	52.3	43.5	9.58	2.76	1.586	37.6	2340
14500	13.73	31.4	54.2	30.4	6.25	2.43	1.670	38.2	2380
15000	14.95	33.8	52.4	24.3	3.04	2.33	1.754	38.9	2420

TABLE 4-1. TRANSPORT PROPERTIES OF AIR FOR VARIOUS TEMPERATURES AND PRESSURES (continued)

(C) Prandtl Number

T, °K	Pressure, atmospheres						
	100	10	1.0	0.1	0.01	0.001	0.0001
500	0.738	0.738	0.738	0.738	0.738	0.738	0.738
1000	.756	.756	.756	.756	.756	.756	.756
1500	.767	.767	.767	.767	.767	.767	.767
2000	.773	.773	.773	.766	.724	.668	.614
2500	.762	.751	.696	.645	.611	.654	.771
3000	.740	.680	.627	.636	.740	.745	.714
3500	.678	.631	.660	.744	.737	.658	.606
4000	.640	.662	.762	.759	.619	.580	.587
4500	.654	.743	.752	.610	.578	.611	.764
5000	.702	.767	.611	.581	.624	.799	.993
5500	.748	.620	.583	.617	.785	.989	.871
6000	.763	.592	.602	.736	.969	.891	.455
6500	.610	.592	.673	.906	.955	.464	.392
7000	.593	.620	.796	.986	.830	.404	.361
7500	.595	.688	.927	.969	.424	.371	.342
8000	.620	.788	.983	.648	.387	.351	.322
8500	.666	.891	.943	.411	.363	.335	.279
9000	.730	.961	.807	.382	.348	.316	.200
9500	.806	.966	.497	.364	.336	.279	.114
10000	.886	.872	.429	.348	.319	.216	.0576
10500	.937	.532	.404	.339	.295	.145	.0314
11000	.955	.463	.382	.327	.254	.0677	.0213
11500	.947	.434	.369	.312	.201	.0524	.0167
12000	.908	.412	.355	.292	.146	.0346	.0143
12500	.728	.396	.343	.263	.101	.0238	.0129
13000	.525	.383	.333	.227	.0688	.0190	.0121
13500	.436	.369	.319	.185	.0470	.0162	.0110
14000	.421	.360	.302	.144	.0345	.0149	.0108
14500	.401	.349	.277	.0986	.0245	.0130	.0109
15000	.394	.341	.253	.0819	.0129	.0120	.0110

TABLE 4-2. THERMAL PROPERTIES OF AIR FOR VARIOUS TEMPERATURES AND PRESSURES

(A) Specific Heat $\quad\dfrac{ZC_p'}{R} = z\sum\left(\dfrac{C_i}{R}+1\right)$ (B) Thermal Conductivity Ratio, k_n/k_o

T_k °K	\(A\) Pressure, atmospheres 100	10	1.0	0.1	0.01	0.001	0.0001	\(B\) Pressure, atmospheres 100	10	1.0	0.1	0.01	0.001	0.0001
500	3.59	3.59	3.59	3.59	3.59	3.59	3.59	1.021	1.021	1.021	1.021	1.021	1.021	1.021
1000	3.96	3.96	3.96	3.96	3.96	3.96	3.96	1.100	1.100	1.100	1.100	1.100	1.100	1.100
1500	4.20	4.20	4.20	4.20	4.20	4.20	4.20	1.150	1.150	1.150	1.150	1.150	1.150	1.150
2000	4.33	4.33	4.33	4.33	4.33	4.33	4.34	1.177	1.177	1.177	1.177	1.177	1.178	1.181
2500	4.41	4.41	4.41	4.41	4.42	4.45	4.47	1.195	1.195	1.196	1.198	1.206	1.225	1.252
3000	4.46	4.47	4.47	4.48	4.51	4.52	4.53	1.205	1.208	1.215	1.235	1.268	1.285	1.289
3500	4.50	4.52	4.52	4.54	4.56	4.55	4.56	1.218	1.230	1.259	1.289	1.310	1.314	1.320
4000	4.53	4.55	4.57	4.58	4.58	4.60	4.65	1.238	1.270	1.312	1.329	1.340	1.356	1.406
4500	4.57	4.59	4.60	4.61	4.64	4.74	4.97	1.269	1.319	1.346	1.366	1.396	1.482	1.674
5000	4.60	4.61	4.64	4.68	4.81	5.12	5.46	1.311	1.357	1.389	1.428	1.541	1.777	1.983
5500	4.62	4.66	4.71	4.85	5.20	5.62	5.76	1.351	1.406	1.448	1.569	1.829	2.08	2.14
6000	4.64	4.71	4.85	5.20	5.73	5.94	6.00	1.383	1.457	1.566	1.824	2.14	2.25	2.50
6500	4.72	4.82	5.12	5.71	6.11	6.21	6.25	1.459	1.543	1.767	2.14	2.33	2.69	2.67
7000	4.78	5.00	5.53	6.16	6.35	6.44	6.56	1.519	1.685	2.05	2.38	2.47	2.86	2.79
7500	4.89	5.28	6.02	6.40	6.58	6.68	6.97	1.606	1.889	2.33	2.52	3.14	3.04	2.90
8000	5.04	5.68	6.42	6.66	6.78	6.97	7.57	1.733	2.14	2.55	2.66	3.33	3.11	2.75
8500	5.27	6.06	6.66	6.91	6.97	7.34	8.41	1.898	2.40	2.70	3.64	3.47	3.29	2.29
9000	5.55	6.42	6.87	6.98	7.20	7.85	9.35	2.10	2.61	2.83	3.85	3.56	2.95	1.771
9500	5.85	6.66	6.98	7.11	7.49	8.54	10.11	2.32	2.78	2.96	4.03	3.62	2.66	1.307
10000	6.15	6.99	7.07	7.26	7.86	9.29	10.52	2.53	2.93	3.03	4.21	3.54	2.23	1.105
10500	6.41	7.02	7.12	7.45	8.34	9.95	10.73	2.71	3.15	3.04	4.34	3.38	1.883	1.061
11000	6.59	7.05	7.20	7.67	8.91	10.41	10.84	2.86	3.18	3.06	4.41	3.10	1.643	1.092
11500	6.71	7.06	7.33	7.97	9.49	10.67	10.91	2.97	3.24	3.02	4.45	2.84	1.582	1.152
12000	6.76	7.07	7.39	8.33	9.99	10.82	10.94	3.06	3.29	2.99	4.39	2.59	1.573	1.223
12500	6.88	7.10	7.54	8.75	10.37	10.90	10.98	3.17	3.26	2.88	4.28	2.44	1.643	1.301
13000	6.86	7.11	7.71	9.20	10.62	10.96	10.99	3.37	3.27	2.76	4.13	2.42	1.702	1.381
13500	6.91	7.17	7.95	9.63	10.77	10.99	11.01	3.51	3.27	2.58	3.97	2.43	1.814	1.461
14000	6.90	7.23	8.24	10.01	10.87	11.00	11.02	3.55	3.20	2.41	3.90	2.49	1.893	1.586
14500	6.90	7.37	8.66	10.37	10.94	11.01	11.02	3.56	3.12	2.11	3.79	2.56	2.01	1.670
15000	6.88	7.44	8.88	10.52	11.02	11.02	11.03	3.59	3.09	1.930	3.84	2.64	2.13	1.754

TABLE 4-3. THERMODYNAMIC PROPERTIES OF AIR FOR VARIOUS TEMPERATURES AND PRESSURES

(A) Compressibility, Z

T, °K	Pressure, atmospheres						
	100	10	1.0	0.1	0.01	0.001	0.0001
500	1.000	1.000	1.000	1.000	1.000	1.000	1.000
1000	1.000	1.000	1.000	1.000	1.000	1.000	1.000
1500	1.000	1.000	1.000	1.000	1.000	1.000	1.000
2000	1.000	1.000	1.000	1.001	1.002	1.005	1.016
2500	1.000	1.001	1.004	1.011	1.033	1.088	1.163
3000	1.003	1.009	1.026	1.072	1.149	1.192	1.200
3500	1.012	1.035	1.092	1.167	1.197	1.203	1.211
4000	1.033	1.089	1.165	1.198	1.208	1.228	1.287
4500	1.071	1.149	1.196	1.213	1.245	1.337	1.577
5000	1.118	1.186	1.214	1.252	1.359	1.622	1.910
5500	1.159	1.208	1.248	1.348	1.599	1.898	1.990
6000	1.189	1.235	1.316	1.529	1.849	1.983	2.008
6500	1.214	1.279	1.437	1.752	1.961	2.006	2.032
7000	1.243	1.351	1.607	1.904	1.997	2.027	2.088
7500	1.284	1.457	1.778	1.971	2.017	2.067	2.210
8000	1.341	1.590	1.896	2.001	2.044	2.144	2.446
8500	1.418	1.727	1.959	2.023	2.090	2.284	2.826
9000	1.512	1.838	1.993	2.050	2.166	2.510	3.282
9500	1.616	1.914	2.018	2.090	2.286	2.832	3.645
10000	1.718	1.962	2.042	2.149	2.462	3.202	3.843
10500	1.807	1.993	2.071	2.234	2.700	3.526	3.932
11000	1.876	2.018	2.111	2.351	2.983	3.745	3.969
11500	1.927	2.042	2.163	2.505	3.272	3.867	3.985
12000	1.965	2.067	2.232	2.694	3.520	3.931	3.993
12500	1.993	2.098	2.318	2.910	3.700	3.963	3.996
13000	2.017	2.135	2.426	3.135	3.818	3.979	3.998
13500	2.039	2.180	2.553	3.347	3.889	3.988	3.999
14000	2.062	2.233	2.700	3.527	3.932	3.993	3.999
14500	2.086	2.297	2.861	3.667	3.957	3.996	4.000
15000	2.113	2.372	3.028	3.769	3.973	3.997	4.000

(B) Dimensionless Enthalpy, ZH/RT

T, °K	Pressure, atmospheres						
	100	10	1.0	0.1	0.01	0.001	0.0001
500	3.52	3.52	3.52	3.52	3.52	3.52	3.52
1000	3.65	3.65	3.65	3.65	3.65	3.65	3.65
1500	3.80	3.80	3.80	3.80	3.80	3.80	3.80
2000	3.92	3.92	3.92	3.93	3.97	4.07	4.41
2500	4.01	4.03	4.09	4.27	4.81	6.16	8.02
3000	4.13	4.25	4.61	5.55	7.13	8.02	8.19
3500	4.34	4.75	5.75	7.08	7.62	7.77	8.03
4000	4.70	5.56	6.74	7.28	7.53	8.09	9.82
4500	5.20	6.29	6.98	7.33	8.14	10.55	16.80
5000	5.73	6.62	7.10	7.96	10.48	16.68	23.46
5500	6.13	6.80	7.58	9.73	15.14	21.58	23.58
6000	6.38	7.11	8.70	12.93	19.30	21.97	22.54
6500	6.62	7.72	10.64	16.46	20.35	21.24	21.93
7000	6.95	8.76	13.20	18.34	20.01	20.69	22.29
7500	7.44	10.24	15.48	18.66	19.54	20.72	24.26
8000	8.16	11.99	16.73	18.43	19.34	21.65	28.65
8500	9.10	13.63	17.09	18.17	19.60	23.85	35.75
9000	10.20	14.79	17.04	18.09	20.49	27.66	43.74
9500	11.36	15.40	16.91	18.29	22.17	33.00	49.15
10000	12.42	15.61	16.84	18.85	24.78	38.79	50.96
10500	13.23	15.64	16.90	19.84	28.28	43.28	50.64
11000	13.77	15.60	17.13	21.31	32.31	45.57	49.48
11500	14.08	15.58	17.57	23.28	36.13	46.09	48.07
12000	14.22	15.62	18.24	25.69	39.01	45.64	46.64
12500	14.28	15.74	19.16	28.36	40.66	44.74	45.26
13000	14.30	15.96	20.32	30.99	41.26	43.69	.43.97
13500	14.31	16.28	21.72	33.27	41.17	42.61	42.76
14000	14.34	16.71	23.29	34.97	40.69	41.55	41.64
14500	14.40	17.26	24.98	36.02	40.01	40.53	40.58
15000	14.49	17.92	26.66	36.53	39.24	39.57	39.60

(C) Dimensionless Entropy, ZS/R

T, °K	100	10	1.0	0.1	0.01	0.001	0.0001
500	21.1	23.4	25.7	28.0	30.3	32.6	34.9
1000	23.7	26.0	28.3	30.6	32.9	35.2	37.5
1500	25.3	27.6	29.9	32.2	34.5	36.8	39.2
2000	26.6	28.9	31.2	33.5	35.8	38.2	40.9
2500	27.5	29.9	32.2	34.7	37.6	41.4	45.9
3000	28.4	30.8	33.5	36.9	41.0	44.6	47.5
3500	29.3	32.0	35.5	39.4	42.7	45.6	48.6
4000	30.2	33.5	37.3	40.6	43.6	46.9	51.6
4500	31.3	34.9	38.3	41.5	45.1	50.5	60.0
5000	32.4	36.0	39.2	42.9	48.4	58.0	68.9
5500	33.4	36.8	40.4	45.5	54.3	64.8	71.3
6000	34.2	37.7	42.2	49.7	59.9	67.1	72.2
6500	34.9	38.9	44.9	54.4	62.6	68.1	73.4
7000	35.8	40.5	48.3	57.6	63.8	69.1	75.4
7500	36.8	42.7	51.6	59.2	64.6	70.5	79.0
8000	38.0	45.1	53.9	60.1	65.7	72.8	85.0
8500	39.4	47.6	55.3	61.0	67.1	76.4	94.1
9000	41.1	49.5	56.2	61.9	69.2	81.6	104.3
9500	42.8	51.0	57.0	63.1	72.0	88.6	112.2
10000	44.5	52.0	57.8	64.6	75.8	96.2	116.6
10500	45.9	52.8	58.7	66.6	80.6	102.7	118.8
11000	47.1	53.4	59.7	69.0	86.0	107.1	119.9
11500	48.0	54.1	60.9	71.9	91.4	109.6	120.7
12000	48.8	54.8	62.4	75.4	95.8	111.1	121.3
12500	49.4	55.6	64.0	79.1	99.1	112.1	121.8
13000	50.0	56.4	66.0	82.9	101.3	112.8	122.3
13500	50.5	57.3	68.2	86.4	102.8	113.3	122.7
14000	51.1	58.4	70.5	89.4	103.8	113.8	123.1
14500	51.7	59.5	73.1	91.7	104.5	114.2	123.5
15000	52.2	60.8	75.6	93.4	105.1	114.6	123.9

(D) Dimensionless Specific Heat at Constant Pressure, ZC_p/R

T, °K	100	10	1.0	0.1	0.01	0.001	0.0001
500	3.59	3.59	3.59	3.59	3.59	3.59	3.59
1000	3.96	3.96	3.96	3.96	3.96	3.96	3.96
1500	4.20	4.20	4.20	4.20	4.21	4.23	4.29
2000	4.34	4.35	4.41	4.57	5.10	6.73	11.57
2500	4.51	4.74	5.46	7.63	13.58	24.00	20.03
3000	5.03	6.23	9.62	16.64	17.66	7.88	5.41
3500	6.27	9.50	14.90	12.31	6.51	6.64	10.69
4000	8.24	12.47	11.05	6.91	8.49	16.46	40.78
4500	10.12	11.06	7.63	9.61	19.68	49.06	101.49
5000	10.53	8.57	9.58	18.98	46.22	87.18	47.49
5500	9.56	9.06	15.85	37.24	72.70	44.58	12.82
6000	9.05	12.38	26.95	57.60	49.37	15.16	11.43
6500	10.05	18.31	41.13	54.37	20.60	11.76	19.13
7000	12.59	26.50	49.61	31.18	12.89	16.38	36.82
7500	16.48	35.19	42.69	17.32	13.99	27.02	70.02
8000	21.42	40.33	28.27	13.68	19.40	45.62	121.60
8500	26.70	38.14	18.58	14.91	28.85	74.32	173.36
9000	31.05	30.38	14.83	18.90	43.11	111.46	173.32
9500	32.90	22.50	14.65	25.26	62.69	143.94	114.86
10000	31.43	17.46	16.53	34.11	86.43	147.10	60.29
10500	27.46	15.19	19.86	45.53	109.34	114.76	31.99
11000	22.82	14.83	24.46	59.25	121.78	73.50	19.92
11500	18.96	15.71	30.27	74.10	115.48	44.18	14.93
12000	16.39	17.45	37.23	87.57	93.38	27.91	12.82
12500	15.01	19.88	45.17	96.01	67.36	19.67	11.89
13000	14.57	22.89	53.70	96.15	46.35	15.56	11.47
13500	14.80	26.42	62.12	87.59	32.30	13.49	11.26
14000	15.52	30.41	69.41	73.42	23.72	12.41	11.16
14500	16.62	34.77	74.36	58.06	18.66	11.83	11.10
15000	18.02	39.37	75.95	44.65	15.70	11.51	11.06

TABLE 4-3. THERMODYNAMIC PROPERTIES OF AIR FOR VARIOUS TEMPERATURES AND PRESSURES (continued)

(E) Ratio of Specific Heats, γ (F) Dimensionless Speed of Sound Parameter, $a^2 \rho / p$

$T,$ °K	\multicolumn{7}{c}{Pressure, atmospheres}	\multicolumn{7}{c}{Pressure, atmospheres}
	100	10	1.0	0.1	0.01	0.001	0.0001	100	10	1.0	0.1	0.01	0.001	0.0001
500	1.387	1.387	1.387	1.387	1.387	1.387	1.387	1.387	1.387	1.387	1.387	1.387	1.387	1.387
1000	1.337	1.337	1.337	1.337	1.337	1.337	1.337	1.337	1.337	1.337	1.337	1.337	1.337	1.337
1500	1.312	1.312	1.312	1.312	1.312	1.310	1.306	1.312	1.312	1.312	1.312	1.312	1.310	1.306
2000	1.300	1.299	1.296	1.286	1.260	1.209	1.153	1.300	1.299	1.296	1.285	1.259	1.206	1.144
2500	1.288	1.277	1.249	1.202	1.161	1.152	1.157	1.288	1.276	1.247	1.196	1.144	1.119	1.132
3000	1.266	1.235	1.195	1.178	1.181	1.239	1.304	1.265	1.229	1.181	1.147	1.150	1.232	1.302
3500	1.241	1.211	1.202	1.212	1.270	1.252	1.176	1.234	1.192	1.166	1.187	1.265	1.250	1.171
4000	1.230	1.223	1.230	1.260	1.213	1.150	1.133	1.212	1.187	1.204	1.254	1.208	1.137	1.097
4500	1.240	1.243	1.251	1.204	1.154	1.155	1.190	1.208	1.210	1.241	1.196	1.133	1.101	1.092
5000	1.256	1.252	1.212	1.166	1.172	1.203	1.168	1.217	1.233	1.202	1.143	1.111	1.103	1.124
5500	1.262	1.231	1.183	1.182	1.214	1.183	1.257	1.229	1.217	1.161	1.124	1.113	1.133	1.249
6000	1.253	1.206	1.190	1.221	1.202	1.237	1.266	1.230	1.186	1.141	1.124	1.135	1.225	1.263
6500	1.235	1.201	1.220	1.228	1.217	1.265	1.188	1.214	1.165	1.137	1.136	1.193	1.260	1.183
7000	1.223	1.217	1.246	1.216	1.258	1.210	1.155	1.195	1.155	1.142	1.167	1.249	1.205	1.140
7500	1.223	1.243	1.244	1.237	1.237	1.173	1.164	1.182	1.154	1.156	1.216	1.231	1.162	1.128
8000	1.235	1.264	1.235	1.252	1.201	1.168	1.201	1.175	1.159	1.181	1.242	1.193	1.143	1.130
8500	1.255	1.267	1.243	1.235	1.183	1.188	1.242	1.174	1.169	1.214	1.228	1.168	1.140	1.136
9000	1.275	1.260	1.252	1.213	1.185	1.224	1.244	1.176	1.185	1.237	1.203	1.157	1.144	1.145
9500	1.288	1.265	1.248	1.201	1.203	1.256	1.216	1.181	1.206	1.237	1.185	1.155	1.151	1.157
10000	1.291	1.259	1.236	1.201	1.232	1.263	1.211	1.190	1.228	1.225	1.176	1.159	1.159	1.185
10500	1.287	1.262	1.226	1.213	1.263	1.244	1.256	1.201	1.242	1.212	1.173	1.165	1.169	1.244
11000	1.282	1.261	1.222	1.233	1.281	1.230	1.339	1.216	1.246	1.202	1.175	1.173	1.187	1.334
11500	1.280	1.256	1.226	1.258	1.280	1.243	1.427	1.232	1.242	1.198	1.180	1.181	1.221	1.424
12000	1.282	1.252	1.236	1.283	1.267	1.288	1.491	1.247	1.236	1.197	1.187	1.192	1.276	1.489
12500	1.284	1.250	1.251	1.301	1.257	1.352	1.528	1.257	1.231	1.198	1.194	1.207	1.346	1.528
13000	1.285	1.251	1.271	1.307	1.263	1.419	1.548	1.263	1.227	1.202	1.202	1.232	1.415	1.548
13500	1.284	1.257	1.291	1.303	1.288	1.472	1.558	1.265	1.226	1.208	1.210	1.269	1.470	1.558
14000	1.284	1.266	1.311	1.295	1.329	1.509	1.563	1.265	1.226	1.214	1.221	1.317	1.508	1.563
14500	1.284	1.278	1.326	1.290	1.377	1.532	1.565	1.264	1.228	1.221	1.235	1.370	1.532	1.565
15000	1.286	1.293	1.336	1.253	1.425	1.547	1.567	1.263	1.232	1.228	1.254	1.420	1.546	1.567

TABLE 4-4. CONVERSION TABLE FOR OBTAINING THERMODYNAMIC PROPERTIES FROM THE DIMENSIONLESS QUANTITIES

Multiply	By	To get	In
$\dfrac{ZE}{RT}$ or $\dfrac{ZH}{RT}$	0.0686 T (°K) 0.287 T (°K) 0.0686 T (°R) 1716 T (°R)	Energy or enthalpy	cal/gm Joule/gm Btu/lb mass ft-lb/slug
$\dfrac{ZS}{R}$, $\dfrac{ZC_v}{R}$, $\dfrac{ZC_p}{R}$, or $\dfrac{ZC_v'}{R}$	0.0686 0.287 0.0686 1716	Entropy or specific heat	cal/gm °K Joule/gm °K Btu/lb mass °R ft-lb/slug °R
μ/μ_0	$1.462 \times 10^{-6} \, T^{1/2} \left(1 + \dfrac{112}{T}\right)^{-1}$ (T in °K) $2.28 \times 10^{-6} \, T^{1/2} \left(1 + \dfrac{202}{T}\right)^{-1}$ (T in °R)	Coefficient of viscosity	gm/cm-sec lb sec/ft²
$\dfrac{k}{k_0}$ or $\dfrac{k_a}{k_0}$	$4.76 \times 10^{-6} \, T^{1/2} \left(1 + \dfrac{112}{T}\right)^{-1}$ (T in °K) $1.994 \times 10^{-5} \, T^{1/2} \left(1 + \dfrac{112}{T}\right)^{-1}$ (T in °K) $2.39 \times 10^{-7} \, T^{1/2} \left(1 + \dfrac{202}{T}\right)^{-1}$ (T in °R) $1.866 \times 10^{-5} \, T^{1/2} \left(1 + \dfrac{202}{T}\right)^{-1}$ (T in °R)	Coefficient of thermal conductivity	$\dfrac{cal}{cm\text{-sec }°K}$ $\dfrac{watt}{cm \, °K}$ $\dfrac{Btu}{ft\text{-sec }°R}$ $\dfrac{ft\text{-}lb}{ft\text{-sec }°R}$
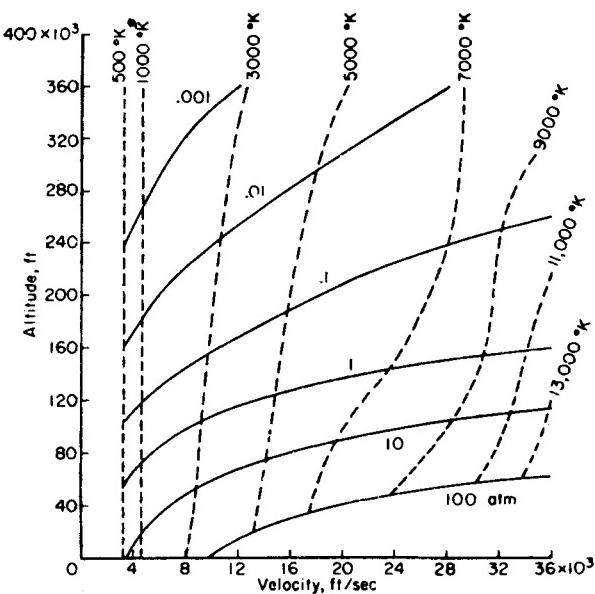
Figure 4-1. Stagnation Temperature and Pressure in Air as a Function of Altitude and Velocity
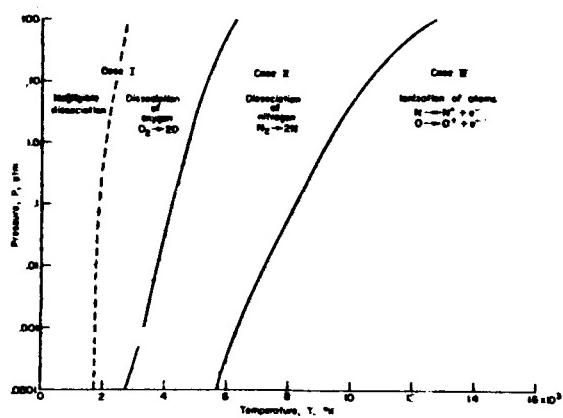
Figure 4-2. Domains of Pressure and Temperature for the Major Chemical Reactions in Air
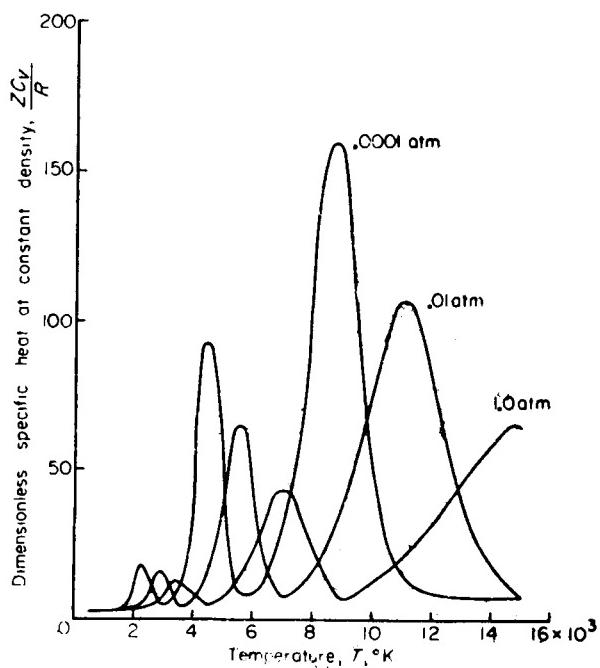
Figure 4-3 Specific Heat of Air at Constant Density as a Function of Temperature

4-7
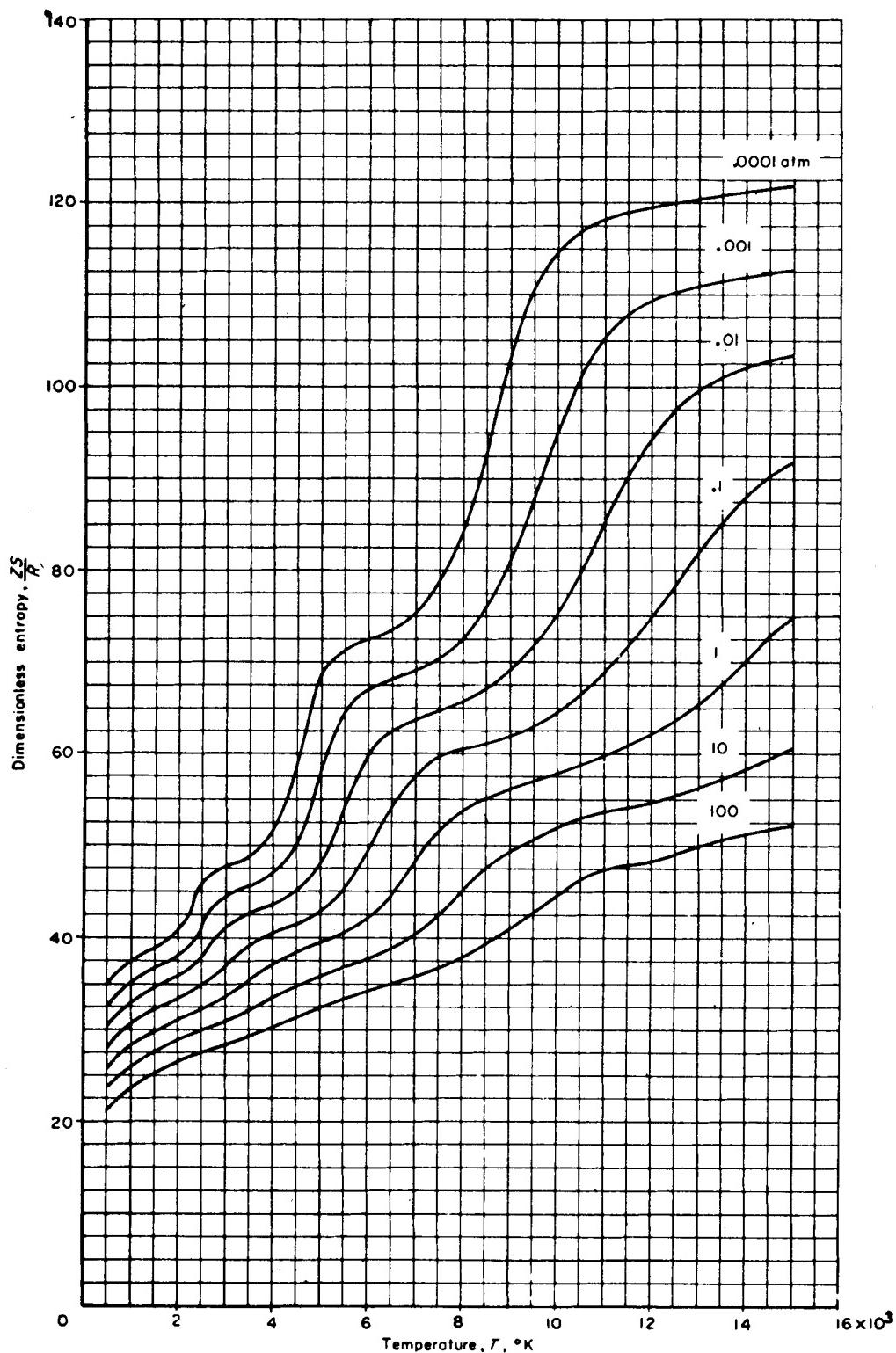
Figure 4-4. Entropy of Air as a Function of Temperature
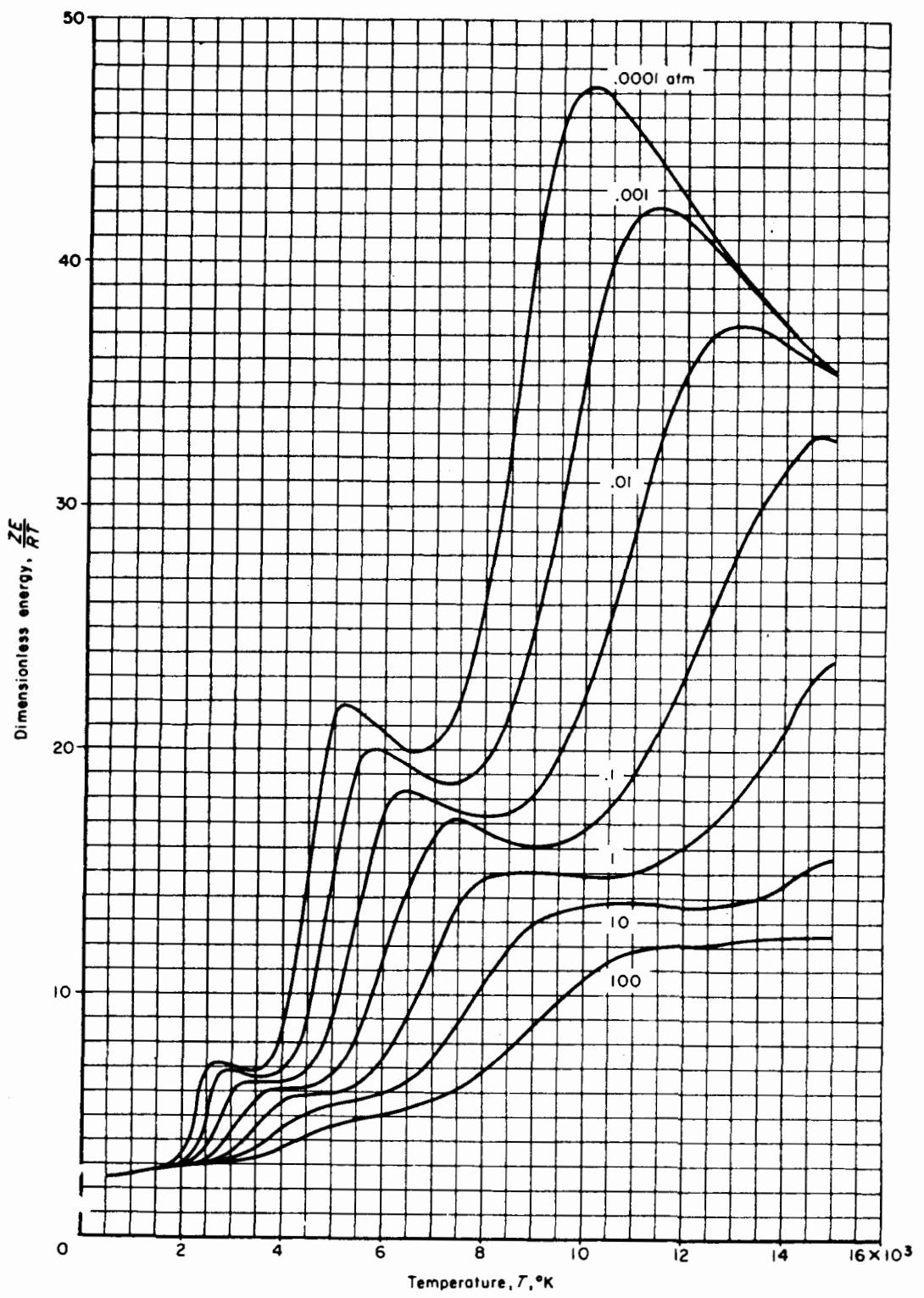
Figure 4-5. Energy of Air as a Function of Temperature
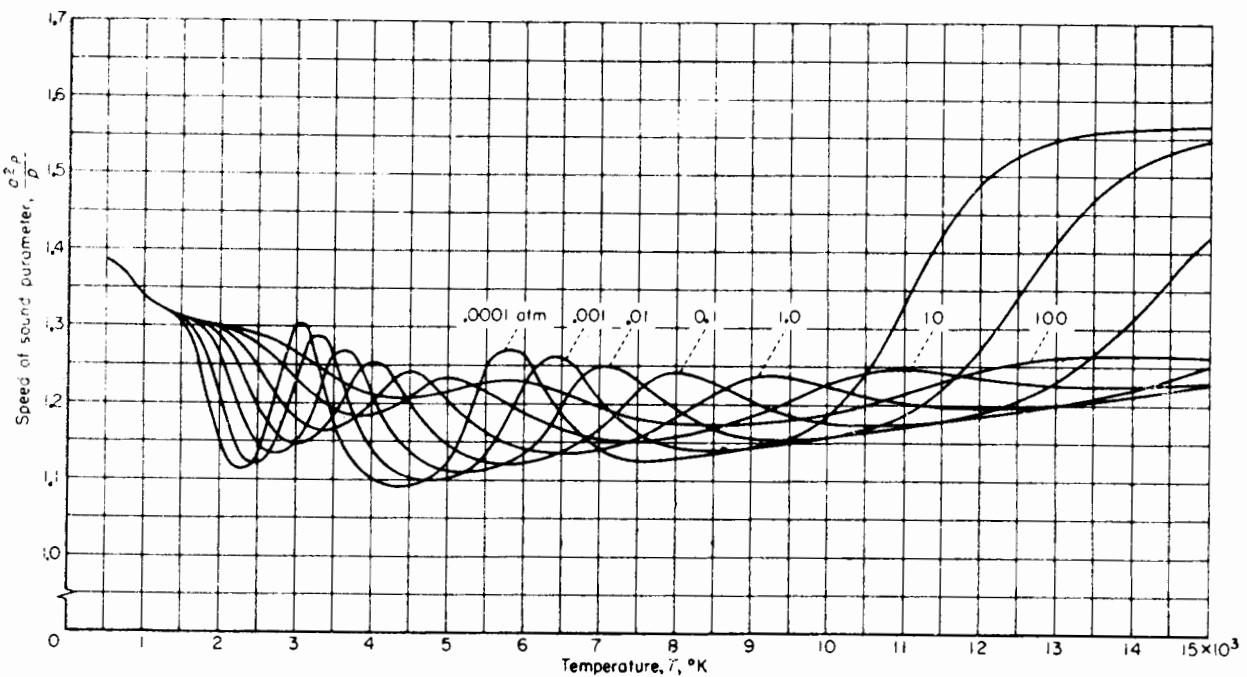
Figure 4-6. Zero Frequency Speed of Sound Parameter for Air as a Function of Temperature
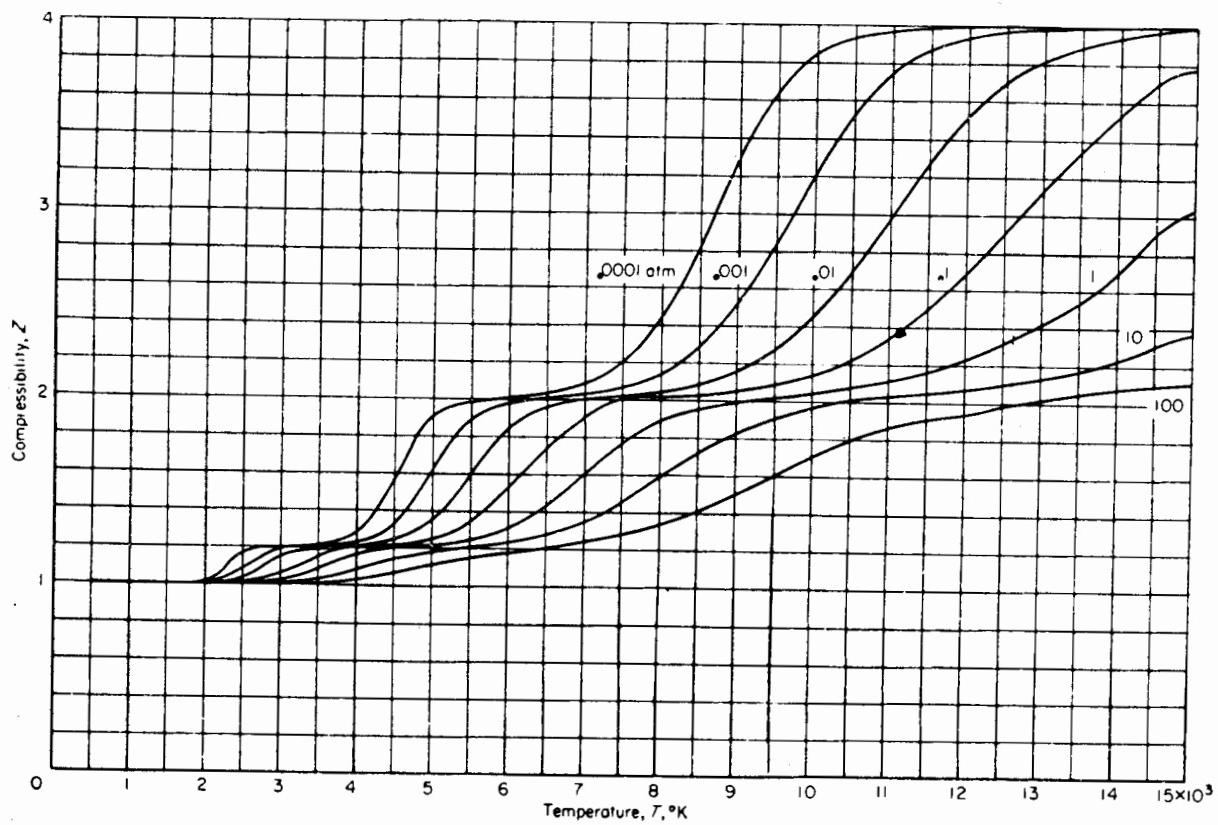
Figure 4-7. Compressibility of Air as a Function of Temperature
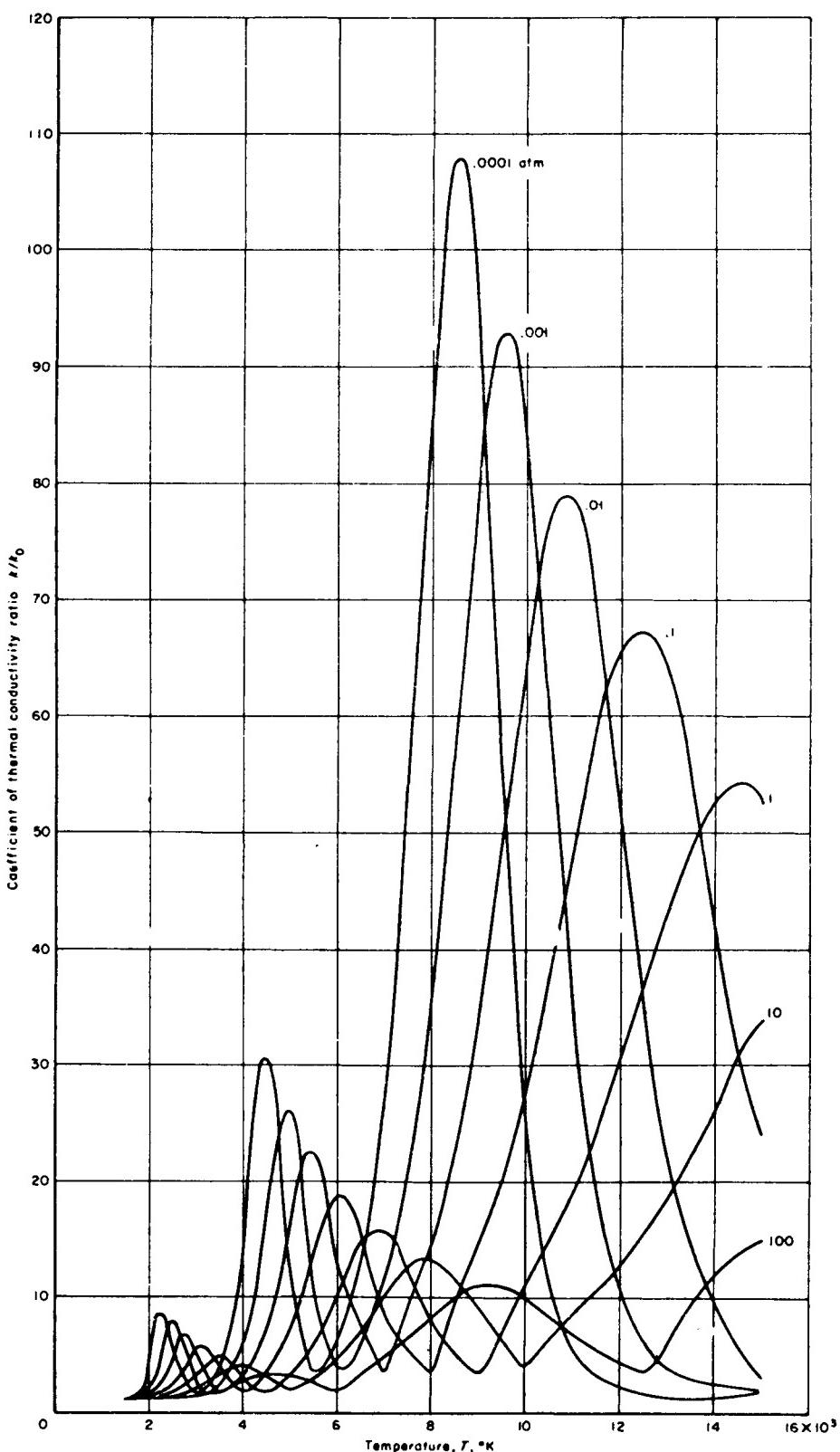
Figure 4-8. Ratio of the Coefficient of Thermal Conductivity of Air to the
Reference Coefficient, k_0, as a Function of Temperature
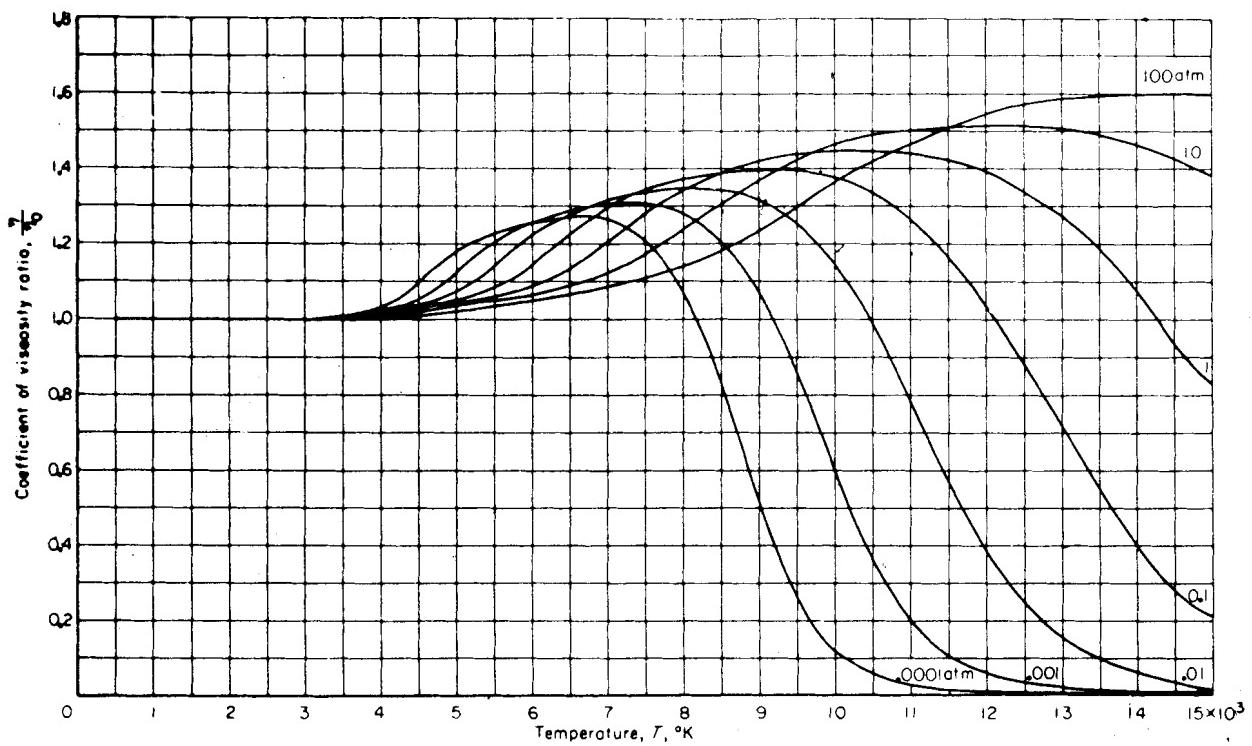
Figure 4-9. *Ratio of the Coefficient of Viscosity for Air to the Reference Coefficient, η_0, as a Function of Temperature*
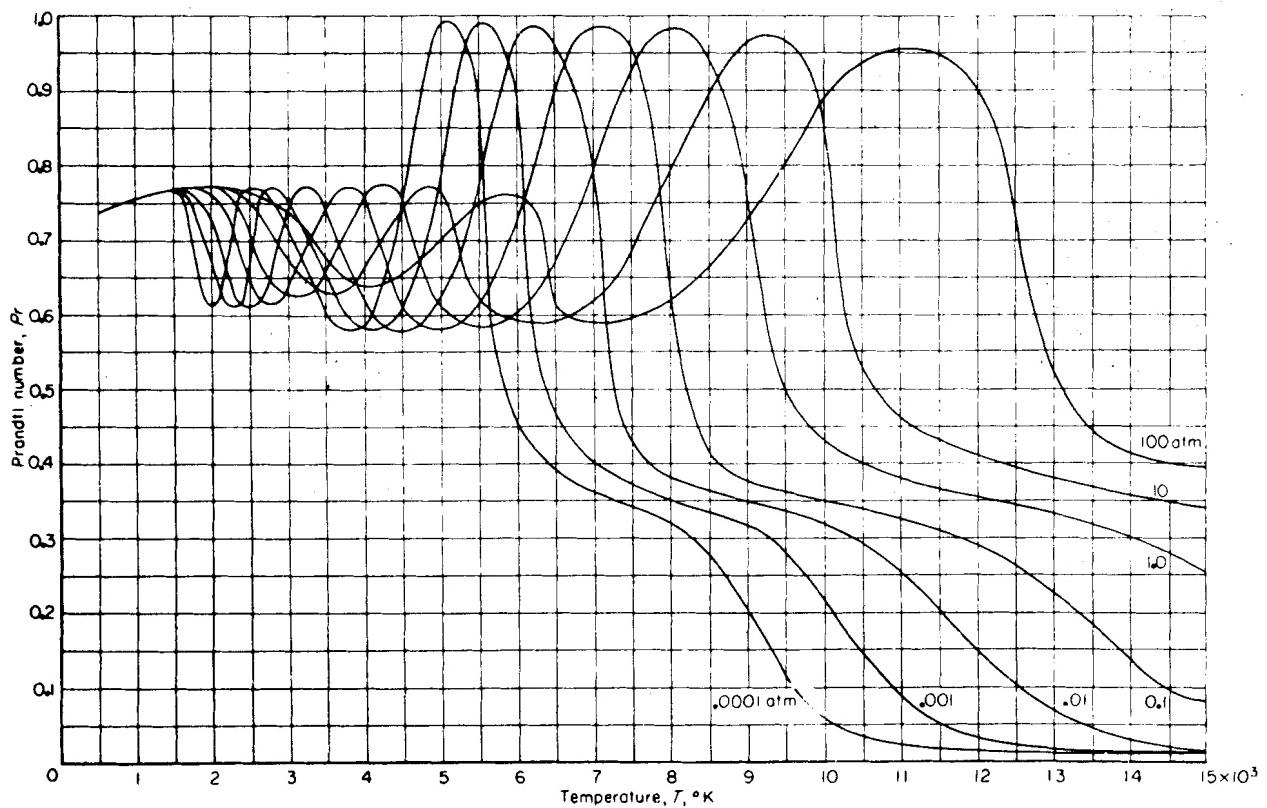
Figure 4-10. *Prandtl Number for Air as a Function of Temperature*

CHAPTER 5

PRESSURE DISTRIBUTIONS

5-1 INTRODUCTION

The pressure distribution over the surface of a vehicle must be known to permit an evaluation of the skin friction, heat transfer, and other diffusive phenomena which occur in the boundary layer over the vehicle, and to permit an evaluation of the forces other than those due to skin friction. A detailed determination of the pressure distribution requires complex calculations of the flow field about the body. Methods by which such complete analyses may be carried out are the subject of numerous standard works on aerodynamics and are outside the scope of this work. However, approximate methods have been developed which give estimates with accuracy sufficient for present purposes and indeed for preliminary design. The main part of this chapter will be devoted to these approximate procedures to provide a "feel" for the possible values which may be encountered.

5-2 "NEWTONIAN" PRESSURE DISTRIBUTION

Primary interest for ballistic missile applications centers on the hypersonic speed range, which, for present purposes can be defined as being in excess of 5000 ft/sec. In this regime surfaces which make significant contributions to the forces acting on the body are usually inclined at angles δ with the flight velocity vector $\vec{V}$ which are not "very small". This is particularly true of blunt noses which are roughly spherical in shape, of conical surfaces whose angles are not small, and of the surfaces of inclined bodies. Moreover, on bodies of the type usually employed, surfaces which are "shaded" from the oncoming velocity vector (i.e., those whose surface-normals make oblique angles with $\vec{V}$) usually make minor contributions to the forces and heat inputs to the body.

As a result, the following empirical estimate can be applied as a first approximation to surfaces which are "seen" by the vector $\vec{V}$:

$$\frac{p - p_f}{p_* - p_f} = \sin^2 \delta \qquad (5-1)$$

Here p_f denotes the undisturbed pressure at a given flight altitude and p_* is the maximum pressure to be found on the body surface and is usually equal to the stagnation pressure on the body (i.e., the pressure at a point where the velocity is zero on a body of revolution). A reasonable estimate for p_* at hypersonic speeds is given as follows:

$$p_* \simeq \rho V^2 \gg p_f \qquad (5-2)$$

where ρ is the density at the flight altitude and V is the flight velocity.

The pressure relation cited above is termed the "Newtonian" distribution because of associated reasoning of Newton who deduced a form of this kind by assuming that the component of momentum normal to the surface in a molecular gas is completely lost on impact. Many theoretical discussions of the rigorous range and conditions of validity of this relation can be found in the literature, e.g., Ref. 7 of Chapter 1. However, it is presented here in an empirical sense without further justification.

It is seen that when $\delta \to 0$ the Newtonian relation predicts that $p \to p_f$, a result which is not quite correct because of the presence of a shock wave around the body. As a result, another method is often used to continue the estimate of pressures into regions of small surface inclination. This method of estimation employs the "Prandtl-Meyer Expansion" relation which is discussed in Paragraph 5-3.

The pressure alone is not sufficient to permit the calculation of the velocity and other properties at the body surface which are required for estimating the heat transfer and other boundary layer characteristics. This procedure requires a knowledge of the equations of motion governing isentropic flow and may be found in most textbooks of aerodynamics. An indication of the general nature of the procedure can be given for the highly simplified conditions wherein there are no chemical reactions occurring in the gas, and when the body is blunted so that a stagnation point exists. In this case

$$\frac{p}{p_*} = f(\gamma, M_L^2) \qquad (5-3)$$

where

M_L is the local Mach number V_L/a_L,

V_L is the local velocity on the surface,

$a_L \simeq 50\, T_L$ is the local sound speed in ft/sec,

T_L is the local temperature in °R, and

γ is the ratio of specific heats for the air mixture (1.4 at low temperatures).

Thus a knowledge of p/p_s and γ determines M_L^2. Next, energy conservation considerations give a relation

$$\frac{T_L}{T_s} = g(\gamma M_L^2) \qquad (5\text{-}4)$$

where

T_s is termed the stagnation temperature and has the approximate value $V^2/2C_p$,

C_p is the specific heat at constant pressure, and

V is the flight velocity.

In this manner, the local properties of the flow at the surface of the body can be determined. For flows with chemical reactions the estimation of local properties may be carried out with the use of a Mollier chart when the flow is in chemical equilibrium. Otherwise, the equations governing chemical rate processes must be coupled with the flow equations to permit the remaining properties to be evaluated. Pertinent tabulations of flow properties have been cited in Chapter 1 as References 22–25.

A final word of caution is in order concerning the value of p_s which is required in conjunction with p to give local flow properties. For a blunt body in which the viscous boundary layer is thin, the foregoing procedure can be applied with good accuracy. However, on a sharp-nosed body, where the stagnation point is enveloped within the boundary layer near the sharp apex, the value of p_s may be somewhat higher than ρV^2. Indeed it rigorously would be the "stagnation" pressure behind the inclined bow shock along a streamline which pierces the boundary layer at the local point of interest on the body. For example, on a sharp cone, the value of p_s to be used in Equation 5-3 is that corresponding to the oblique shock about the body.

5-3 "PRANDTL-MEYER" EXPANSION AND FLOW FIELDS OF CONES

Exact solutions of the equations of motion can be carried out for special types of flow. These solutions are useful in estimating pressures over bodies. One of these, the Prandtl-Meyer expansion, provides a relation between the local surface inclination δ and the local Mach number M_L for a given initial
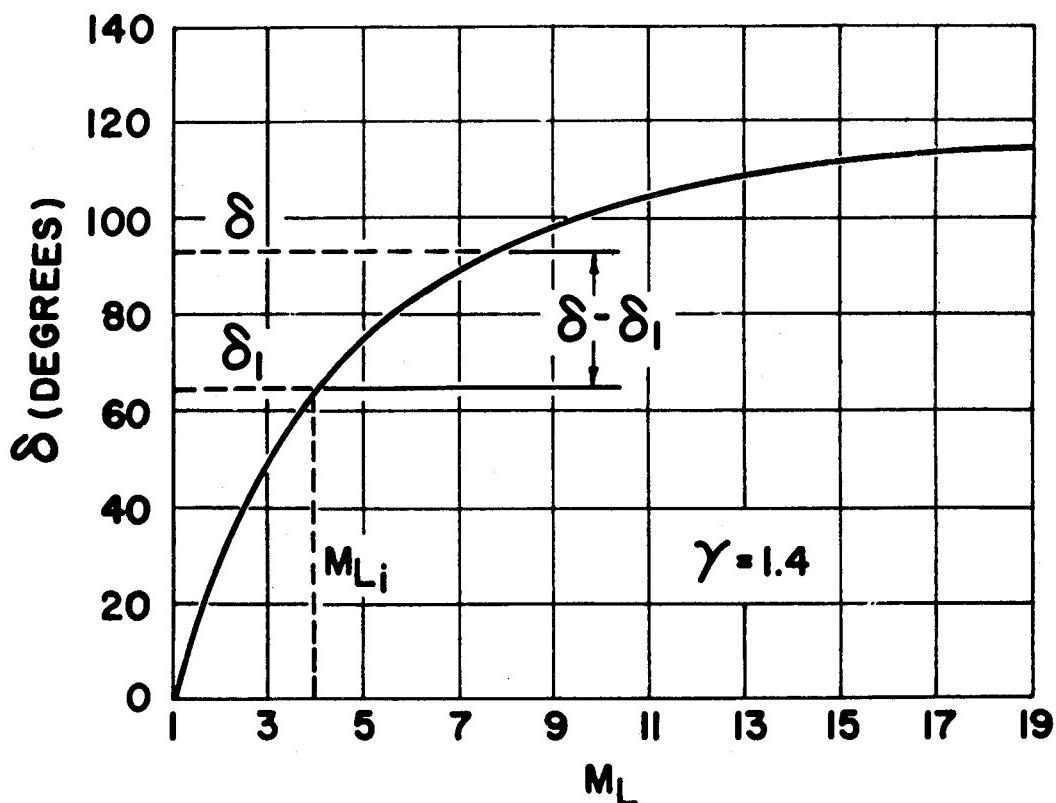
Figure 5-1. Prandtl-Meyer Expansion Relation

set of values δ_i and M_{L_i} and for a given γ. There-fore, if one ends an estimate of p at a given point on the surface where δ and M_L are known, one can continue the estimate for usual values of δ by means of the Prandtl-Meyer relation.

A plot of this relation for $\gamma = 1.4$ is given in Figure 5-1. Tabulations for other values of γ are available in the literature. Some calculations are also available which take into account equilibrium high temperature air chemistry.

Tabulations of the properties of flows about sharp cones which represent another useful set of exact aerodynamic calculations can be found in NACA TR 1135 (Reference 4) and are described in standard texts of supersonic aerodynamics. The pressures on cones are sometimes used empirically to give the pressure on a body of revolution whose inclination γ is assumed to be part of a fictitious cone of half angle δ.

An example of how some of these methods are
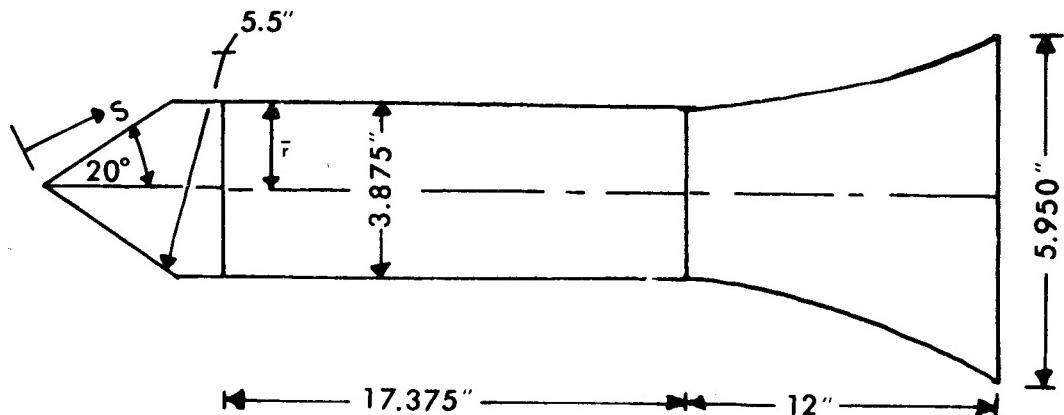
Figure 5-2. *The Cone-Cylinder-Flare Configuration, Overall Model*[3]
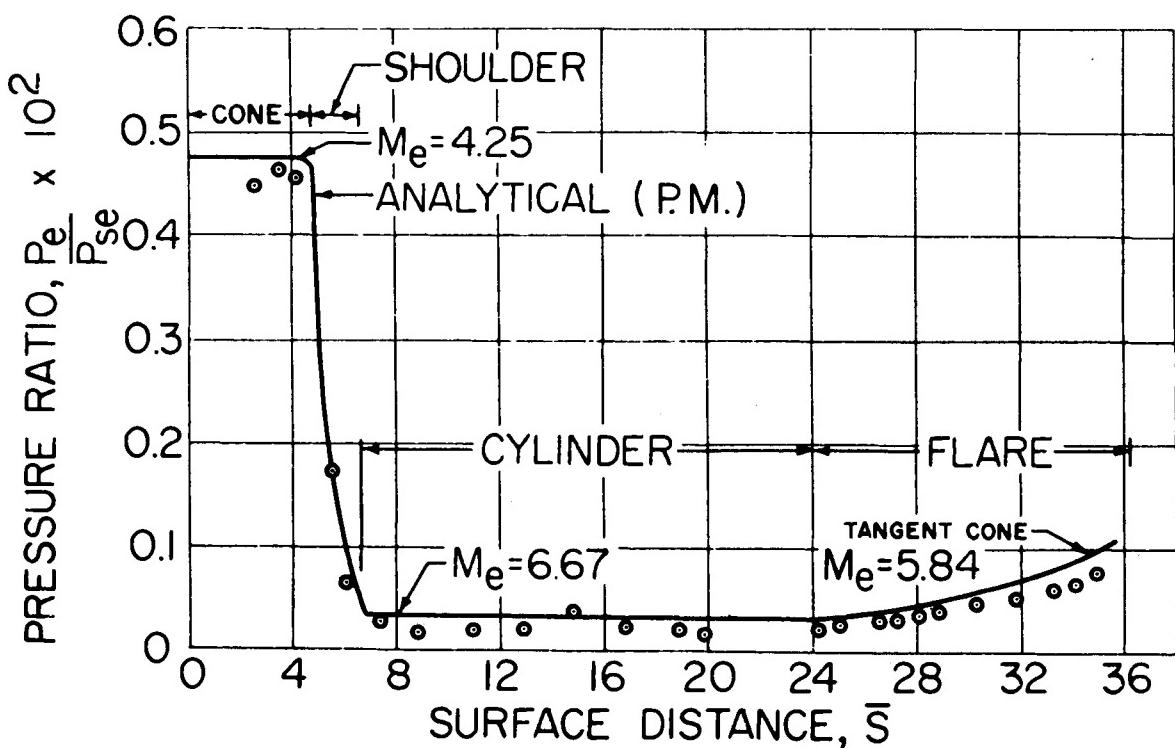
Figure 5-3. *Analytical and Experimental Pressure Distributions*[3]

applied to a typical missile shape to permit a determination of theoretical heat rates is given in Reference 3. For the cone-cylinder-flare configuration shown in Figure 5-2, pressures were measured at $M_f = 8$. The experimentally determined pressures are shown in Figure 5-3 together with approximate theoretical estimate. Methods used are indicated on the figures.

REFERENCES

1. S. Feldman, *Hypersonic Gas Dynamic Charts for Equilibrium Air*, AVCO Research Laboratory, Everett, Mass., 1957.

2. M. H. Bloom and M. H. Steiger, "Inviscid Flow with Nonequilibrium Molecular Dissociation for Pressure Distributions Encountered in Hypersonic Flight, J. Aeronaut. Sci. **27**, 821–835 (1960).

3. V. Zakkay and C. J. Callahan, *Laminar, Transitional and Turbulent Heat Transfer to a Cone-Cylinder-Flare Body at Mach 8*, Polytechnic Institute of Brooklyn Aerospace Laboratory, Air Force Office of Scientific Research Report 2359, 1962.

4. Ames Research Staff, *Equations, Tables and Charts for Compressible Flow*, National Advisory Committee for Aeronautics Technical Report 1135, 1953.

CHAPTER 6

THERMAL EFFECTS

6-1 INTRODUCTION

In high speed flight, high temperatures are generated around a missile and consequently within its structural components. Conditions on the exposed surface of the missile form the connecting link between the air flow and the interior thermal state of the structure. Therefore, interfacial conditions such as surface temperature or rate of heat flow through the surface must be expressed in terms of the surface contour and flight parameters (e.g., flight velocity, etc.). On the other hand, the surface conditions must be related to properties within the structure so that the internal temperature distribution can be established. The joining of these two classes of information through their common boundary condition provides the relation between the flight situation and the thermal characteristics of the structure.

The first step in estimating structural effects, such as thermal stresses, consists of determining the internal temperature level or *temperature distribution*. Theoretically, this problem is governed by the classical heat conduction equation which expresses the energy balance within the material. The following parameters influence the temperature distribution: (i) structural geometry; (ii) material properties, i.e., both termal conductivity $k(T)$ and thermal diffusivity $\alpha(T) = k/wc$ (where w is the specific weight and c the specific heat) in time-dependent cases, and only $k(T)$ in steady-state cases; (iii) rate of energy transfer through the boundaries or energy generated within the material; or alternatively, the surface temperature, which implies the heat transfer necessary to maintain this temperature.

Using the known temperature distribution or temperature level in the structure, one can examine excessive temperatures or other destructive conditions, probable cooling requirements, possibility of surface melting or ablation (mass loss) which may be useful for cooling, as well as evaluating thermal stresses and required thermal materials. Changes in body-geometry or flight-programs may be employed to alleviate or circumvent an unfavorable situation.

6-2 CONDITIONS FOR APPLICATION OF STEADY FLOW ANALYSIS

It is worthwhile to recall here that flow and transfer processes are usually viewed from a *coordinate system fixed to the body*. In this frame of reference a body moving through stationary air is aerodynamically equivalent to the same body held fixed with respect to the ground and subjected to an airstream; the ground-reference approximates an inertial coordinate system. The airstream is initially uniform, undisturbed, parallel to the flight velocity vector, and equal in velocity to the flight velocity. The state parameters of this relative flow, that is, its pressure, temperature and density, are equal to those of the stationary air at a given altitude. In this coordinate system the flow may be regarded as *steady* or at least *quasi-steady* for all but the most refined heat transfer purposes. By quasi-steady we mean that time-dependent flows may be treated as a continuous series of instantaneously steady states, and that explicit time-derivatives of the flow field are negligible, with respect to spatial derivatives.

Some effects of unsteadiness, such as those due to the acceleration of a missile, can be taken into account by considering the consequent inertia forces to act as additional body forces, augmenting the body forces such as those of gravity. Only recently have studies of time-dependent boundary layer and heat transfer phenomena received appreciable attention. For example, special types of oscillating flows have been studied[1-4] and have indicated effects of unsteadiness on shear and heat transfer which are important only in a secondary way. More general treatments of the effects of time-dependent flight on boundary layer phenomena including heat transfer have recently appeared[5-7] and will be discussed further in a later chapter.

A useful approximate criterion for judging when the direct effects of unsteadiness may be neglected in boundary layers is that the following inequality be satisfied:

$$\frac{x^n}{u_e^{n+1}} \frac{d^n u_e}{dt^n} \ll 1, \qquad n = 1, 2, \cdots \qquad (6-1)$$

where u_e is a characteristic velocity, (e.g., the velocity external to the boundary layer at the station x), x a streamwise distance and t denotes time. These conditions are usually satisfied in current missile applications. For example, for a body 100 ft long, traveling at 1000 ft/sec with an acceleration of 30 g

$$\frac{x}{u_e^2}\frac{du_e}{dt} = \frac{1}{10} \ll 1, \quad \text{for} \quad n = 1 \qquad (6\text{-}2)$$

Shock-tube experimentation has indicated that flows over forebodies become established in the order of tens of microseconds in high-speed flow. Wakes in the base region take somewhat longer to become steady, perhaps on the order of milliseconds. These times are negligible from the flight standpoint.

It is well to note here that thermodynamic relations and other physical laws, such as the equation of state of a gas and the law of heat conduction, which strictly apply only to gases macroscopically "at rest," are usually applied without alteration to gases in motion. This procedure yields excellent results in practice.

6-3 PROCESSES OF ENERGY TRANSFER NEAR A MISSILE

A high speed missile imparts energy to a limited mass of air in the vicinity of the vehicle. Here "air" is used to denote the ambient atmosphere regardless of its actual composition). Primarily this energy transfer takes place by compression of the displaced air and by heat-dissipation due to the shear stresses in the boundary layer. Part of the compression-energy is lost to the surrounding atmosphere through the dissipative action of shock waves which extend outward from the body. These shock losses increase as the bluffness or pressure drag of the body increases, and as the shock wave compression becomes correspondingly stronger. In ballistic flight this increase in drag leads to additional deceleration.

A further loss of energy to the surroundings takes place as the energized boundary layer is shed rearward, while a much smaller amount is lost by radiation from the hot gas surrounding the body. Energy also may be gained or lost by the missile surface by radiation which is not directly concerned with the surrounding air, for instance, by radiation to the surface directly from the sun or earth, and by radiation from the surface itself to the local surroundings. This radiation transfer is influenced by the atomic-scale characteristics of the air surrounding the missile, among other things, and will be discussed in a later section.

The portion of the energy transmitted by the missile to its surroundings and not permanently lost to the atmosphere is returned to the missile surface by several possible heat transfer mechanisms described below.

6-3.1. Conduction and Convection[6-22]

Conduction is a primary energy transfer process characterized by the proportionality between the heat flux q and the temperature gradient at a point. Within the boundary layer the governing relation is

$$q\left[\frac{\text{Btu}}{\text{ft}^2\,\text{sec}}\right] = -k\left[\frac{\text{Btu}}{\text{ft}^2\,\text{sec}\cdot\dfrac{^\circ\text{F}}{\text{ft}}}\right]\frac{\partial T}{\partial y}\left[\frac{^\circ\text{F}}{\text{ft}}\right] \qquad (6\text{-}3)$$

where q is transmitted along y, i.e., the outward normal to the surface. The thermal conductivity k is a property of this mode of energy transport on a molecular scale. With this sign convention, negative q indicates the heat transfered *to* the body *from* the gas.

Forced convection denotes mechanically-enforced (e.g., by pressure gradients) fluid motion which brings fluid masses into contact permitting conduction to take place more readily. Free convection denotes fluid motion induced by body forces such as gravity; it has a negligible direct effect on heat transfer to missiles although body forces may influence the transition from laminar to turbulent flow and thereby stimulate increased heat transfer rates. A special class of body forces resulting from the presence of electromagnetic fields may influence the motion of conducting fluids such as ionized air, or air artificially "seeded" with materials which enhance its conductivity. As a result, the convection properties of the fluid may be altered; these latter effects fall into the category of "magneto-hydrodynamics".

In *turbulent flow* random motion exists on a macroscopic scale as distinguished from the molecular activity which leads to the basic conductive transport previously described. Here turbulent eddying motion results in violent and initimate mixing of small discrete fluid segments of different momenta and temperature and consequently cause a significant increase in both the heat transport and the effective (turbulent) shear stress. By analogy with *laminar flow*, i.e., flows devoid of random eddies, attempts are made to relate the turbulent heat flux to the local gradient of the mean temperature by an empirical proportionality factor. This factor is often termed the *turbulent eddy conductivity* $[k_T]$. Unlike its laminar counterpart k, the turbulent factor k_T is not simply a physical property of the fluid, but

is quite sensitive to the nature of the turbulent flow. For example, the value of k_T may be quite different in a boundary layer near a surface than in a free jet. The analogous turbulent shear parameter, the *turbulent eddy viscosity* [ϵ_T], is sometimes considered to be dependent on the local derivatives of the mean velocity profile such that the turbulent shear is considered to be proportional to the *square* of the mean-velocity derivative rather than to the first power of this derivative, as in laminar flow.

6-3.2. Mass Diffusion[28-33]

In some cases the air flowing over the surface may not be of a homogeneous nature. This occurs when air is dissociated into a mixture of atoms and molecules at high temperature, or when foreign coolants or material ablated from the solid surface mix into the airstream. In nonhomogeneous mixtures currents are set up which tend to promote homogeneity. The phenomena associated with this mixing process are known as "diffusion" processes. In addition to the diffusion of the various components through each other (i.e., "mass diffusion") certain secondary processes occur. These are known as "temperature diffusion" and "pressure diffusion." They are observed experimentally in nonhomogeneous mixtures which are at rest on the average; when the different species diffuse through each other; and when the molecular motion sets up temperature and pressure differences[33]. For example, the mean diffusion velocity of species 1 in a binary (two component) mixture can be expressed as follows:

$$\vec{V}_1 = -D_{12}\Bigg[\text{grad}\,(ln\,C_1) + \frac{W_2 - W_1}{W} C_2\,\text{grad}\,(ln\,P)$$
$$+ \frac{W_1 W_2}{W^2} C_1^{-1}\left(\frac{D_T}{D_{12}}\right) \text{grad}\,(ln\,T)\Bigg] \qquad (6\text{-}4)$$

where W_i is the molecular weight of species i,

$$W = \left[\sum_i C_i/W_i \right]^{-1},$$

and

$$C_i = \cdot\,'\rho$$

An identical relation is obtained for $\vec{V}_2$ if C_1 and C_2 are interchanged. The diffusion coefficient D_{12} is virtually independent of concentration. Thermal diffusion (characterized by thermal diffusion coefficient D_T) tends to concentrate lighter and smaller spec: .n the warmer region. The thermal term is usually less than 10% of the leading term, while the pressure term is negligible (on the order of the inverse of the momentum-thickness Reynolds number) compared to the concentration

gradient term.[23] Thus only the concentration gradient term remains for present application, and the mass transport is usually expressed as follows for species 1:

$$\rho C_1 \vec{V}_1 = -\rho D_{12}\,\text{grad}\,(C_1) \qquad (6\text{-}5)$$

This relation is known as Fick's law.

This transport influences the gas composition as well as the flow properties at a point, and thereby affects transport properties such as thermal conductivity and viscosity coefficient.

It is noted that a "diffusion process" can be defined as any process in which the net transport of a substance is directly proportional to the gradient of a given property. The proportionality constant is the "diffusion coefficient." The term "mutual diffusion" describes the intermixing of 2 different gases, while "self diffusion" describes the intermixing of 2 types (e.g., isotopes) of the same gas.

The energy absorption and release by gas components which dissociate and recombine, or which react chemically with other components, are linked with the diffusion process. For instance, absorbed energy may be released near a surface due to the diffusion of the reacting component across the boundary layer.

In most technical applications it will suffice to consider only the diffusion in binary (2-component) mixtures. For example, dissociated air can be considered for some purposes to behave as a mixture of 2 species: molecules and atoms. The differences in the atomic weights of oxygen (atomic weight 16) and nitrogen (atomic weight 14) in these cases can be neglected within a good approximation. In this connection it will be seen that binary diffusion can be accounted for in a rather simple way when the "Lewis number" ($Le \equiv \rho D_{12} C_p/k$) which characterizes the effectiveness of diffusion, as compared to conduction, in the energy transfer is equal to unity.

We note here that the shear stresses set up by the intermingling of species in a mixture are negligible with respect to the usual viscous stresses under the high Reynolds number conditions of practical flight. For a more advanced treatment of chemical effects in flow systems see References 32 and 33.

6-3.3. Heat Transport in a Binary Mixture

Consider dissociated air as a binary mixture of atoms and molecules (species 1 and 2, respectively). The enthalpy of each species is then

$$h_i = \int_0^T C_{p_i}\,dT + h_i^0 \qquad i = 1, 2 \qquad (6\text{-}6)$$

where h_i^0 is the heat of formation of the ith species. We may take

for atoms $h_1^0 \cong 5\text{–}10$ ev
for molecules $h_2^0 = 0$

Thus we may write the heat flux q in a direction n as follows (in practice n will be the outward normal to the body surface):

$$q = -k\frac{\partial T}{\partial n} + \sum_{1,2} \rho C_i V_i h_i \qquad (6\text{-}7)$$

where V_i is given by Equation 6-5 neglecting pressure and temperature diffusion, and body force differences on the species. Thus we obtain

$$q = -\frac{k}{\overline{C}_p}\left[\left(\frac{\partial h}{\partial n} - \sum_{1,2} h_i \frac{\partial C_i}{\partial n}\right) + Le \sum_{1,2} h_i \frac{\partial C_i}{\partial n}\right] \quad (6\text{-}8)$$

where

the static enthalpy $h = \sum_{1,2} C_i h_i$,

the mass averaged specific heat $\overline{C}_p = \sum_{1,2} C_i C_{p_i}$; and

the Lewis–Semenov number or Lewis number $Le = \rho D_{1,2}\overline{C}_p/k$.

For $Le = 1$, a reasonable approximation for gas mixtures in which the molecular weights of the components differ by a factor of only 2 or 3 as encountered in most missile problems, Equation 6-8 becomes simply

$$q = -\frac{k}{\overline{C}_p}\frac{\partial h}{\partial n} \qquad (6\text{-}9)$$

This relation is identical to the expression for the heat flux in the simple case where no dissociation or other chemical reactions occur, and where the gas is homogeneous. It represents a *major simplification* in the analytic treatment of flows with chemical reactions since for this case the heat transfer rate is independent of the *mechanism* of heat transfer and explicitly *independent of chemical reaction* rates to an excellent approximation. Of course, the fluid properties k and $\overline{C}_p$ are dependent on the state and concentration of species at a point. However, Equation 6-9 reduces the role of the temperature (explicitly) in influencing the *heat flux* in flows with chemical reactions of which dissociation is a special case. It is emphasized that ionization (freeing of electrons) has not been considered as yet.

6-3.4. Radiation[34-37]

Radiation heat transfer rates are usually proportional to T^4. However, at very high gas temperatures the gas emissivity becomes sharply tempera-ture-dependent, being proportional, e.g., to T^8. Thus the radiation flux from the gas can well vary like T^{12} and become appreciable. Conditions of this kind may be encountered during satellite and interplanetary re-entry.[34-36]

Although the detailed mechanism of radiation energy transfer is quite complex, its engineering treatment may be somewhat simplified. Radiation energy is transferred by electromagnetic waves or the equivalent quanta. Most monatomic and diatomic gases such as helium, hydrogen, oxygen and nitrogen are transparent to (i.e., emit but do not appreciably absorb) thermal radiation, except at very high temperatures; while polyatomic gases such as water vapor and carbon dioxide may absorb or emit in certain wave lengths. A cogent introduction to the role of radiative effects in aerodynamics may be found in Ref. 37.

6-4 PARAMETERS FOR CALCULATION OF CONVECTIVE HEAT RATES

Heat flux to a surface can be viewed as occurring under the driving force of a temperature or enthalpy difference termed the "potential." The proportionality factor between the flux and potential is termed the heat transfer coefficient. This concept of the heat flux is borne out by theoretical analysis and experiments which are based on the Prandtl boundary layer concept, and show that the following more definite quantities are of prime importance in determining the heat rates.

6-4.1. Stagnation Enthalpy (h_s)

This is the value of enthalpy which would be acquired by a moving air mass if an adiabatic deceleration to zero velocity were to occur. It is derived from the conservation of energy principle which states that under adiabatic conditions the sum of the local enthalpy and kinetic energy per unit mass remains constant, i.e.,

$$h + \frac{u^2}{2gJ} = h_s \qquad (6\text{-}10)$$

where J is the mechanical equivalent of heat (778 ft-lb/Btu) and g is the gravitational acceleration.

For constant values of specific heat, Equation 6-10 becomes

$$\frac{T_s}{T} = 1 + (\gamma - 1)M^2/2 \qquad (6\text{-}11)$$

For conditions in the atmosphere where $T \leq 500°R$ and $h \leq 125$ Btu/lb, the dominant

factor in determining h_c at speeds above say 6000 ft/sec is the right side of Equation 6-10; that is, the effect of altitude variations on stagnation enthalpy is negligible. This is not the case at lower velocities.

6-4.2. Adiabatic Surface Enthalpy (h_{aw})

This is the value which hypothetically would occur at a totally insulated (zero net heat transfer) surface in the absence of any heating or cooling devices or substances except those naturally in the air. It is the value which that portion of the boundary layer fluid in immediate contact with the surface would acquire in the absence of heat sources and sinks. It differs from h_s because of viscous, conductive and heat storage effects in the fluid, and, in cases of low-density or rarefied gas flow, because the fluid may not adhere perfectly to the surface. It is given with excellent accuracy by

$$\frac{h_{aw} - h_s}{h_s - h_s} = \begin{cases} (Pr)^{1/2} \text{ for laminar flow} \\ (Pr)^{1/3} \text{ for turbulent flow} \end{cases} \quad (6\text{-}12)$$

where Pr is the Prandtl number. The form of Equation 6-12 for constant C_p, in terms of T, is obvious. The quantity h_s denotes the local enthalpy directly outside the boundary layer.

6-4.3. Equilibrium Surface Enthalpy (h_{eq})

The actual temperature of a point on the surface of a body (and its corresponding enthalpy in the fluid directly adjacent to the surface) is established by the heat between the heat input to the surface by all possible means, the heat re-emitted, e.g., by radiation, and the heat transferred to the interior of the body. Under steady state conditions the final surface temperature is termed the "equilibrium temperature" T_{eq} having a corresponding enthalpy h_{eq}.

For example, if a coolant is injected into the flow at one point on an otherwise insulated body, the surface acquires a temperature level and variation different from h_{aw}. The same is true for a completely insulated surface which loses heat by radiation.

6-5 CONVECTIVE HEAT RATES FOR CONSTANT PRESSURE AND TEMPERATURE

6-5.1. Two–Dimensional Laminar Flow

The convective heat rates for two–dimensional laminar flow at a station s along a surface having constant pressure and temperature are described by

the following equation:

$$\frac{Nu}{(R_N)^{1/2}(Pr)^{1/3}} = 0.32$$

where

$$Nu = \frac{qs}{\frac{k_e}{C_{pe}}(h_w - h_{aw})} \text{ is the Nusselt number,}$$

$$R_N = \frac{\rho_e u_e s}{\mu_e} \text{ is the Reynolds number based on } S, \text{ and}$$

$$\quad (6\text{-}13)$$

$$Pr = \frac{\mu_e C_{pe}}{k_e} \text{ is the Prandtl number.}$$

It is often specified[8] that, for good agreement with experiments, the "subscript-e" quantities in Equation 6-13 should be evaluated at a "reference enthalpy" given by

$$h^* = h_{se} + 0.5(h_w - h_{se}) + 0.22(h_{aw} - h_{se}) \quad (6\text{-}14)$$

However, in Reference 9, Gold shows that, for temperatures below the dissociation level, Equation 6-13 is virtually independent of the evaluation temperature and may be expressed in a simplified form as follows:

$$\frac{q}{T_w - T_{aw}} = 2.06 \times 10^{-6} \left(\frac{u_e P_e}{S}\right)^{1/2} \quad (6\text{-}15)$$

where all quantities are in British Units. A nomograph for Equation 6-16 is given in Figure 6-1.

Furthermore, shock-tube experiments under conditions of dissociated inviscid flow (Reference 31) have shown that Equation 6-13 represents the data within the same order of accuracy as the "reference enthalpy" method. Equation 6-13 applies when the outer flow is not dissociated although the flow within the boundary layer may be dissociated.

For laminar flow over cones the constants in Equations 6-13 and 6-15 are multiplied by $\sqrt{3}$ to give:[8]

$$\frac{Nu}{(R_N)^{1/2}(Pr)^{1/3}} = 0.55 \quad (6.16)$$

$$\frac{q}{T_w - T_{aw}} = 3.56 \times 10^{-6} \left(\frac{u_e P_e}{S}\right)^{1/2} \quad (6\text{-}17)$$

Figure 6-1 also shows a nomograph for Equation 6-17.[10]

6-5.2. Two–Dimensional Turbulent Flow

For this type of flow the equation for convective heat transfer is

$$\frac{Nu}{(R_N)^{4/5}(Pr)^{1/3}} = 0.0296 \quad (6\text{-}18)$$

NOTE: $(h_L)_{CONE} = \sqrt{3} \ (h_L)_{FLAT \ PLATE}$
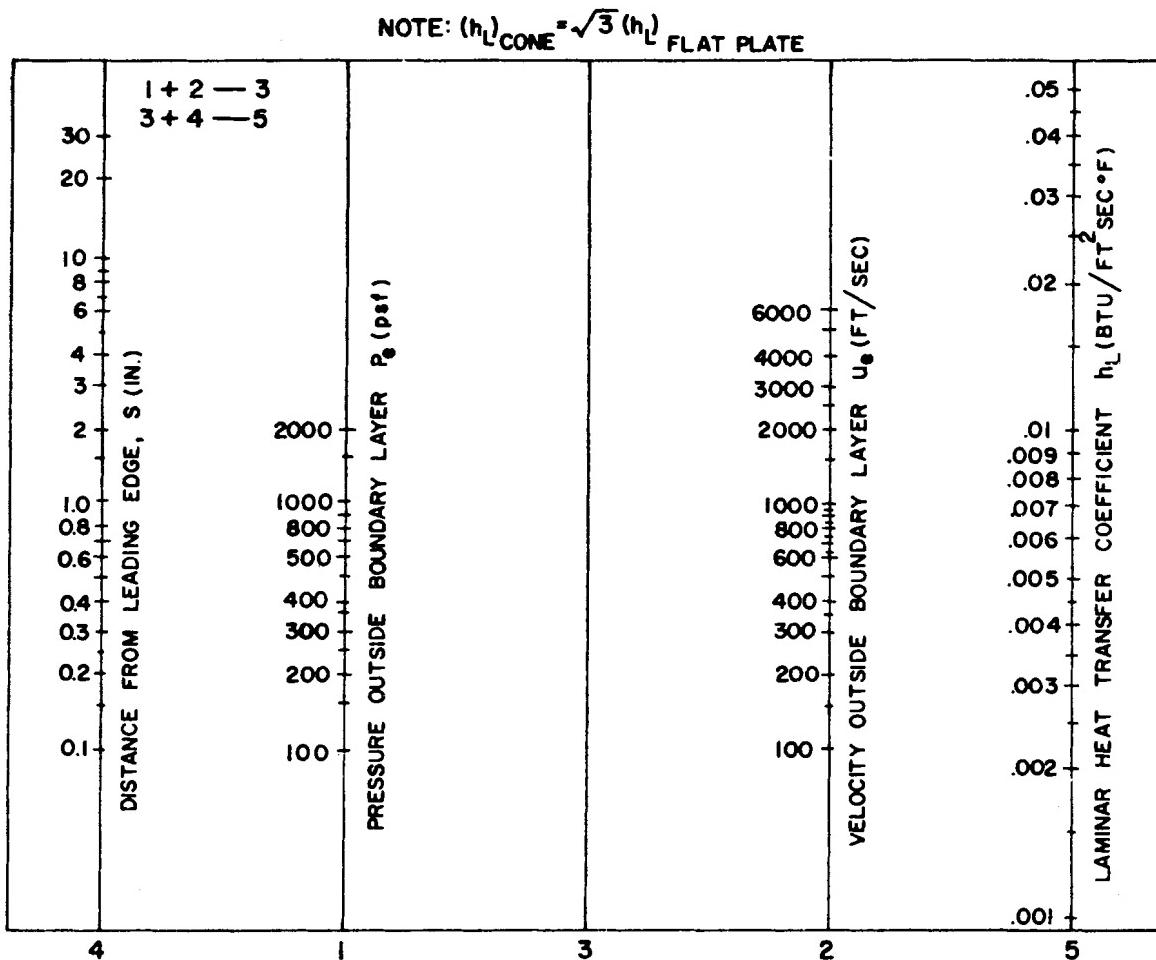
Figure 6-1. Flat Plate Heat Transfer Coefficient (h_L), Laminar Boundary Layer[10]

In this expression the "reference enthalpy" evaluation should be used for best accuracy. A simplified form has been derived[9] for Equation 6-18, but it is not independent of temperature. The simplified form is

$$\frac{q}{T_w - T'_{aw}} = 10.25 \times 10^{-6} \frac{(u_s Pr)^{4/5}}{.2(T^*)^{3/5}} \qquad (6\text{-}19)$$

where T^* is the temperature obtained by replacing the h values by T in Equation 6-14. A nomograph for Equation 6-19 is shown in Figure 6-2.[10]

For a cone in turbulent flow, the right sides of Equations 6-18 and 6-19 must be multiplied by 1.15.[11]

It has also been shown[12] that Equation 6-19 can be applied locally as a good approximation in turbulent flow over blunt bodies in hypersonic flow, a case of utmost importance in missile design. Evaluations of this formula for a range of local

surface pressures, altitudes, and Mach number are given in Figure 6-3. These charts take into account the effects of dissociation equilibrium.

The charts are expressed in terms of the local value of the ratio P/P_s, where P is the local surface pressure and P_s is the local surface stagnation pressure.

A critical point of heating on a spherical nose of radius R_n over which the flow has turned turbulent occurs in the neighborhood of the sonic point, generally found at an angular position of about 40° from the stagnation point (i.e., at about 0.7 R_n in arc length along the body from the stagnation point). At this point the following rough estimate may be deduced from the "local flat plate" formula for hypersonic conditions.

$$\frac{qR_n^{0.2}}{1 - \dfrac{h_w}{h_{ss}}} \cong A \rho_f^{0.8} u_f^3 \qquad (6\text{-}19a)$$

6-6

where

$A = 9.6$ when R_n is in ft,
ρ_f in slugs/ft³,
u_f in kilo-ft/sec and
q is in Btu/ft²-sec.

In most hypersonic cases $h_w/h_{ae} \ll 1$.

6-6 CONVECTIVE HEAT RATE AT THE STAGNATION POINT OF A BLUNT BODY

In practice, the stagnation-point laminar heat rates are among the most important parameters for design. Since the growth of the boundary layer is initiated in the stagnation region, the flow will always be laminar in this area, at least for a short distance from the stagnation point or line.

The stagnation region is an area of maximum heat flux when the flow over the body is completely laminar. If, however, the boundary layer becomes turbulent at a downstream position the heat flux in some downstream area, e.g., near a sonic point, may be larger than at the stagnation point. This peak turbulent flux may be on the order of twice the stagnation point laminar value. Nevertheless, the calculation of the heat flux to a blunt body always starts with the laminar stagnation point computation. This is so for two-dimensional (wing-like) bodies; axially-symmetric bodies (bodies of revolution at zero angle of attack); bodies with almost spherical noses even when at an angle of attack (provided the stagnation point remains on the sphere); and nonaxially symmetric bodies (such as those with ellipsoid-like noses). In nonaxially symmetric cases the heat rate is not single-valued at the stagnation point, but takes on different values along each of the streamlines emerging from the stagnation point.
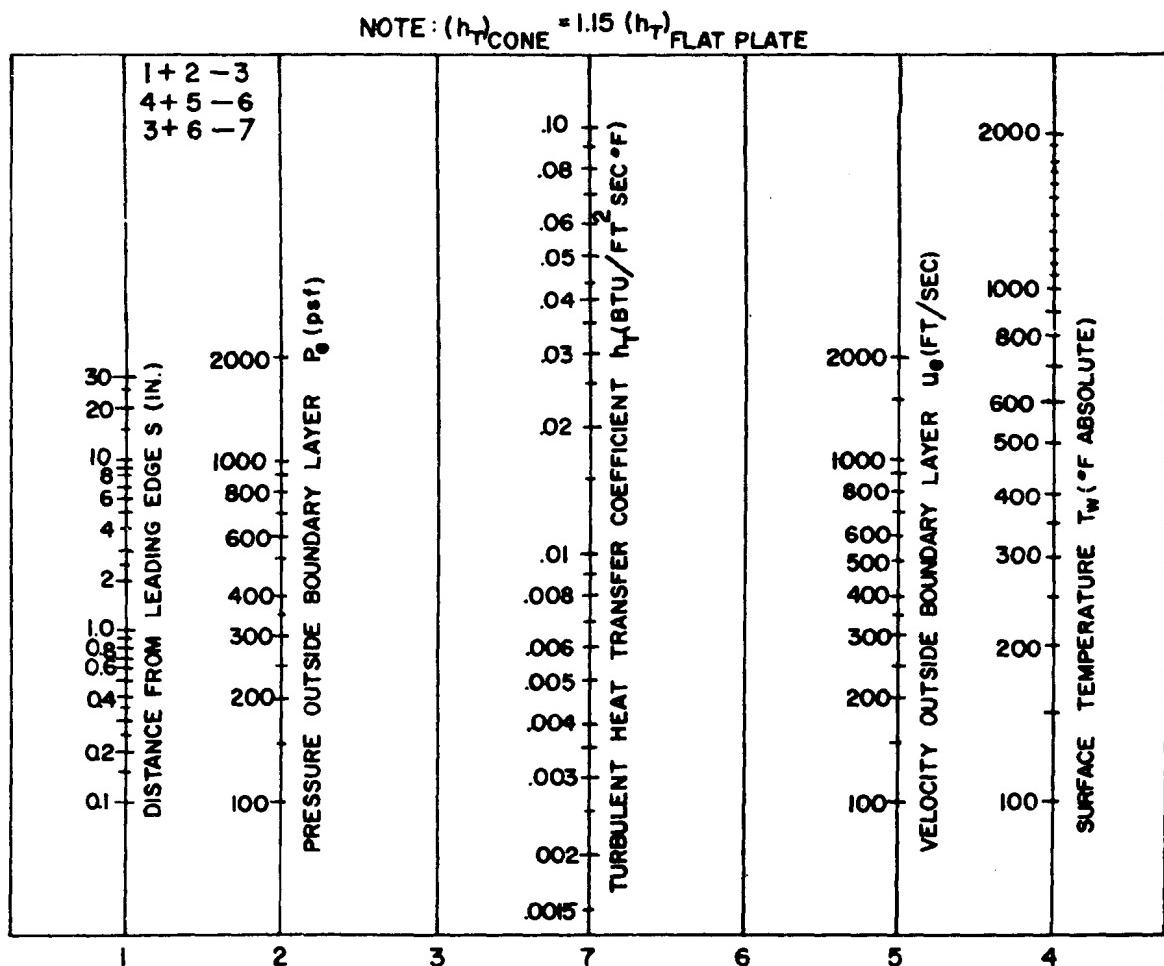
Figure 6-2. Flat Plate Heat Transfer Coefficient (h_T), Turbulent Boundary Layer[10]
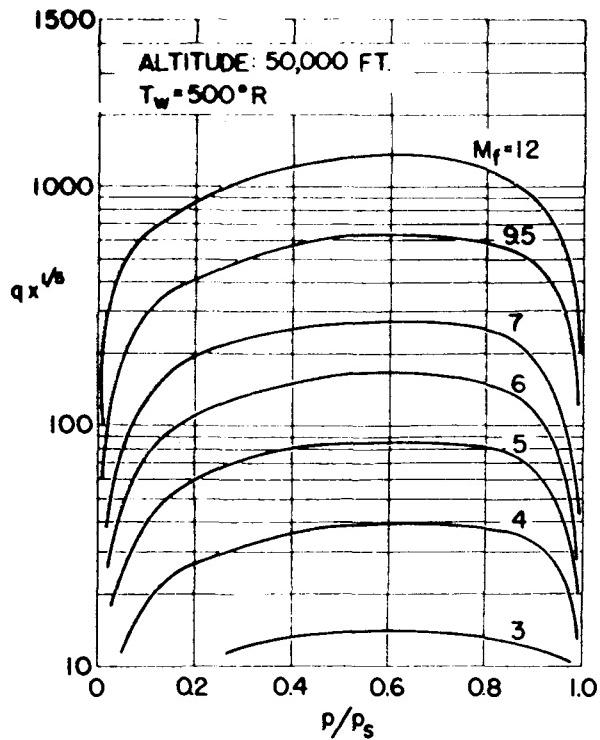
(A) Altitude: 50,000 ft $T_w = 500°R$
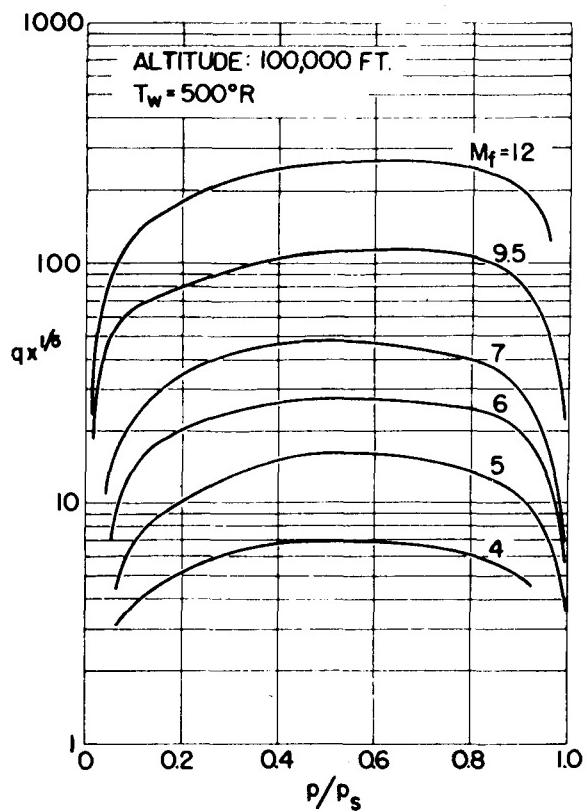
(B) Altitude: 100,000 ft $T_w = 500°R$
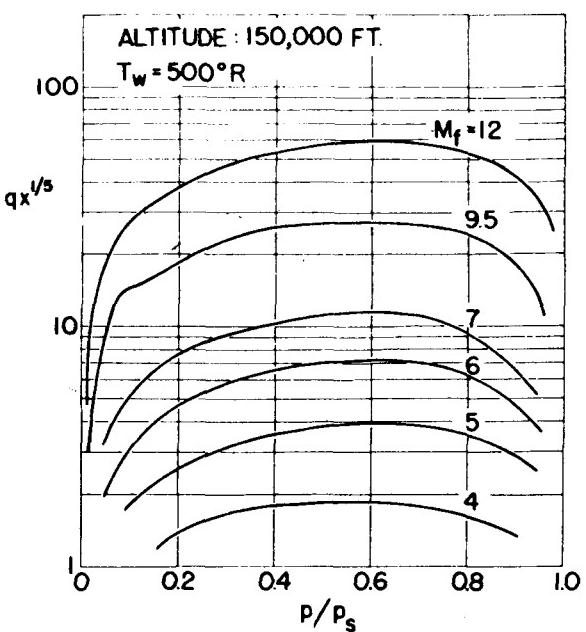
(C) Altitude: 150,000 ft $T_w = 500°R$
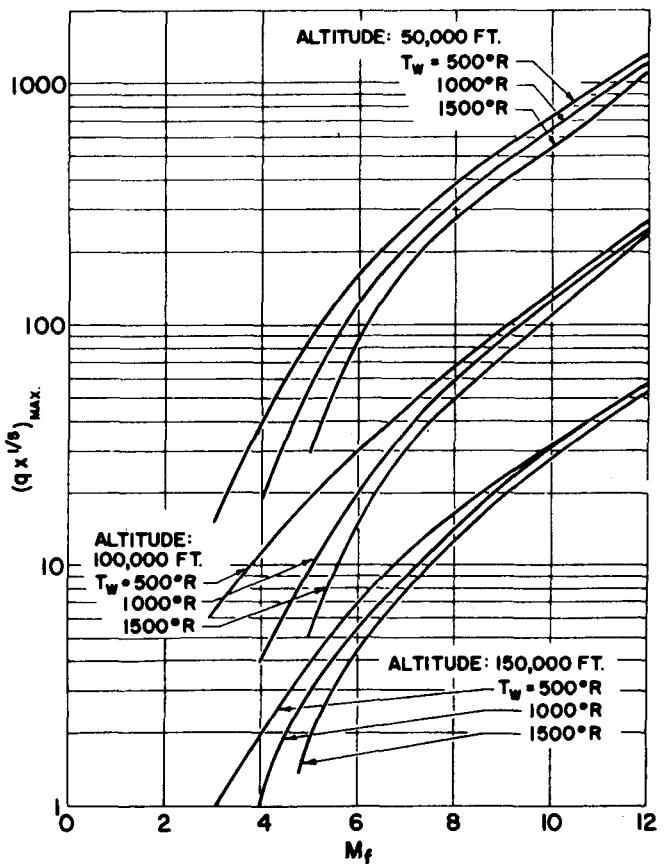
(D) Maximum Heating Rates as a Function of Flight Mach Number for Various Altitudes and Wall Temperatures

Figure 6-3. Turbulent Heat Transfer Rates as a Function of Static-to-Stagnation-Pressure Ratio

The stagnation region heat rates depend strongly on the magnitude of the velocity gradient (du_e/ds) along streamlines emerging from the stagnation point. In fact, they are directly proportional to $(du_e/ds)^{1/2}$. Thus for nonaxially symmetric bodies the heat rates will change along the various streamlines as du_e/ds changes.

A very accurate relation for the laminar stagnation point heat rate had been obtained theoretically[23,31] and verified experimentally. This relation takes into account the "real gas" effects of molecular dissociation in the two limiting cases of "very fast" and "very slow" rates of dissociation and brackets the values for intermediate reaction rates. It is given by

$$\frac{q_e}{(h_{ee} - h_w)} = 0.54(2)^{n/2}(\overline{P})^{-0.6}\left(\frac{\rho_w\mu_w}{\rho_e\mu_e}\right)^{0.1}(\rho_e\mu_e)^{1/2}$$

$$\times \left[1 + (Le^m - 1)\frac{h_D}{h_{ee}}\right]\left(\frac{du_e}{ds}\right)^{1/2} \quad (6\text{-}20)$$

where $h_D = \sum_i C_i(-h_i)$ is the chemical formation enthalpy produced by dissociation of molecules and

$$n \begin{cases} = 0 \text{ for two-dimensional flow} \\ = 1 \text{ for axially-symmetric flow.} \end{cases}$$

Here the constant $m = 0.52$ for very rapid dissociation (i.e., for the case of chemical equilibrium) and $m = 0.63$ for very slow dissociation (i.e., for the case of constant or "frozen" chemical composition) with a catalytic surface. According to the modified Newtonian outer flow approximation, the velocity gradient in the stagnation region is

$$\frac{du_e}{ds} = R_n^{-1}\left[\frac{2(p_e - p_f)}{\rho_e}\right]^{1/2}$$

For values of $Le \simeq 1.4$, as is the case for dissociated air, the term in square brackets in Equation 6-20 takes on a maximum value of about 1.2. Thus, Equation 6-20, which was derived in a very complex fashion, agrees quite closely with the earlier results of more approximate calculations.

A simplified engineering form for Equation 6-20 would be[31]

$$\frac{q_e R_n^{1/2}}{\left(1 - \frac{h_w}{h_{ee}}\right)} = 2^{n/2}A\rho_f^{1/2}u_f^3 \quad (6\text{-}21)$$

For R_n in feet, the flight conditions ρ_f and u_f in slugs/ft³, and in kiloft/sec, respectively, and q_e in Btu/ft²-sec, the constant A is equal to 15.5.

The value of A is 4710 when R_n is in cm, ρ_f in gm/cm³, u_f in km/sec, and q_e in watts/cm². Lees

also suggests that this value of A may probably apply to the atmosphere of Venus and Mars as well as the Earth.

As previously mentioned, Equations 6-20 and 6-21 also apply for the stagnation point or line of bodies having nearly spherical or nearly-cylindrical noses at angles of attack provided the stagnation region remains on the nose, i.e., for moderate angles of attack.

A nomograph giving the stagnation-point heat transfer rates for ballistic re-entry of a body with an approximately spherical nose is given in Fig. 6-4.[12]

More recently, Hoshizaki[31], presented a simple relation for determining the heat transfer rate at an axisymmetric stagnation point in the velocity range of 6 to 50 kilo-feet/sec. This expression includes the effect of variable Prandtl and Lewis number as well as ionization, for *equilibrium* chemistry, and has the following form

$$q_e \sqrt{R_n} = C_{air}\left[\frac{R_n}{u_f}\frac{du_e}{ds}\right]^{1/2}\rho_f^{1/2}\left(\frac{u_f}{10^4}\right)^{3.19}\left(1 - \frac{h_w}{h_e}\right)$$

where

$$C_{air} = 2.59 \times 10^4 \text{ Btu-ft}^{1/2}/\text{lb}^{1/2}\text{-sec}^2$$

A comparison of experimental and theoretical results for stagnation point heat transfer at high velocities is given in Figure 6-5.

A nonspherical stagnation region with two planes of symmetry may be approximated using an ellipsoidal local body geometry. Thus, Equations 6-20 and 6-21 may be applied in this case with slight modifications.[13] For this approximation, the value of du_e/ds in Equation 6-20, or the corresponding value of R_n in the Newtonian approximation, must be interpreted as the velocity gradient and radius of curvature corresponding to the plane of the smaller principle radius of curvature, i.e., $(du_e/ds)_1$ and $R_{n,1}$, respectively. On the right side of Equation 6-20 the factor $(2)^{n/2}$ must be replaced by $(1 + B)^{1/2}$ where B is the ratio of the two perpendicular velocity gradients, i.e., $B = (du_e/ds)_2/(du_e/ds)_1$. Similarly in the Newtonian approximation [Equation 6-21] $B = R_{n,1}/R_{n,2}$. Note that for $R_{n,2} = R_{n,1}$, $B = 1$, thus giving the axially symmetric case; while for $R_{n,i} \to \infty$, $B \to 0$ giving the two-dimensional case.

6-7 LAMINAR HEAT TRANSFER ALONG A STREAMLINE OF A BLUNT BODY

With good approximation, particularly for high supersonic and hypersonic flow conditions over blunt bodies, we may consider the flow along an inviscid streamline emerging from the stagnation region as
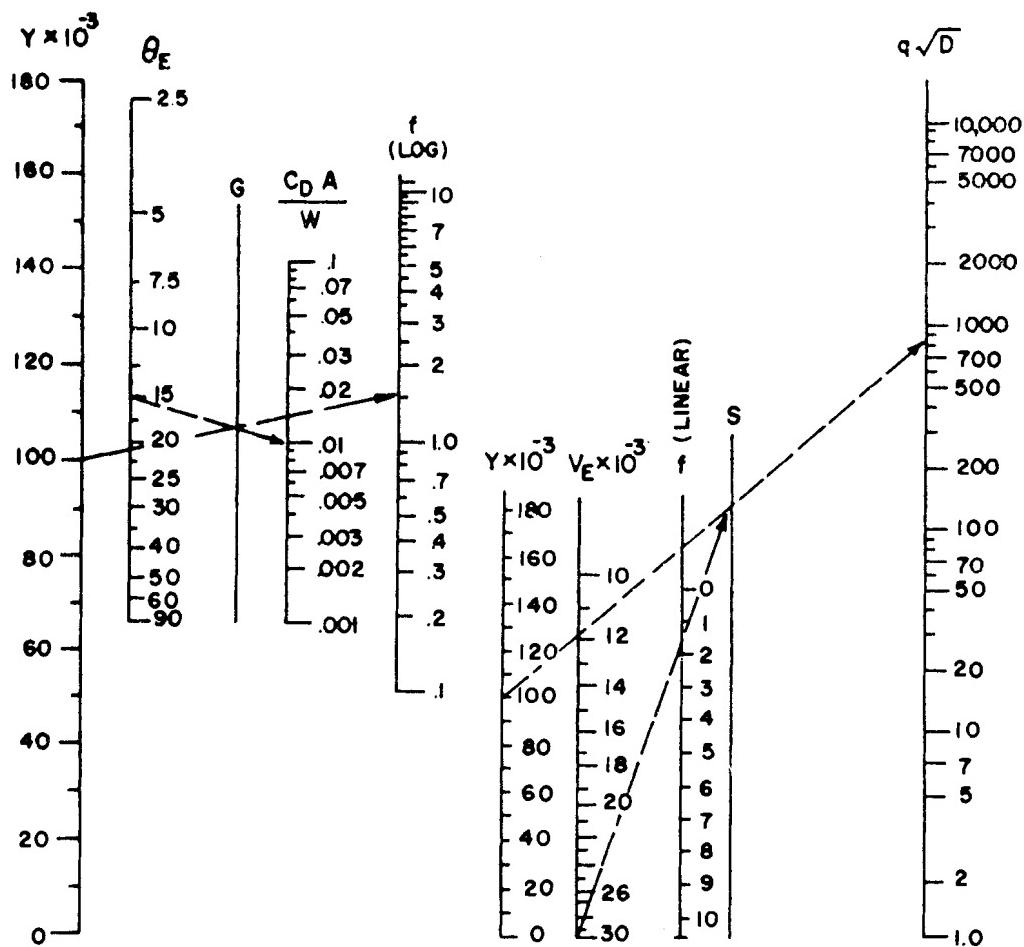
Figure 6-4. Nomograph of Stagnation Point Heat Transfer for Hypersonic Re-entry[12]

if that streamline were everywhere a local body of revolution. The pressure variation along this streamline must be known apriori, of course. Then the following ratio of local heat transfer to the stagnation point heat rate can be obtained.

$$\frac{q}{q_s} = \frac{1}{2^{\frac{(n+1)}{2}} \left(\frac{du_s}{ds}\right)_s^{1/2}} \frac{\left(\frac{\rho_s \mu_s}{\rho_s \mu_s}\right) u_s r_0^n}{\left[\int_0^s \left(\frac{\rho_s \mu_s}{\rho_s \mu_s}\right) u_s r_0^{2n} \cdot ds\right]^{1/2}} \quad (6\text{-}22)$$

where

r_0 = radius of cross section of bodies of revolution and

n = 1 for bodies which are like bodies of revolution.

Equation 6-22 was derived by Lees[14] strictly for the case of axially symmetric or two-dimensional flow assuming "local similarity." However, it can

be shown to hold for the aforementioned cases within good engineering accuracy.[23,24]

6-8 MASS TRANSFER AND ABLATION COOLING

The "first generation" of ballistic missiles have generally employed "heat-sink" methods of maintaining sufficiently cool structural temperatures. That is, a mass of metal, otherwise structurally extraneous, was applied to the body usually in the form of a sheath. Theis material absorbed the heat generated during flight and thereby maintained tolerable surface temperatures. Copper was found to be a particularly desirable heat sink material because of its conductive and absorptive properties.

An upper limit to the utility of metallic heat sinks is given by their maximum absorptive capacity prior to melting or structural deterioration. For copper this absorptive capacity is on the order of 400 Btu/lb. For missile performance requiring total

heat inputs over the trajectory greater than several hundred Btu/lb other cooling methods than pure absorption must be utilized.

In the "second generation" missiles which require higher impact velocities than can be achieved with simple nondestructive heat-sink methods, materials have been utilized which melt or evaporate in a relatively orderly fashion. These materials, primarily plastic in nature (e.g., bonded resins such as Fiberglas, or materials like Teflon) have been used as coatings or external caps on the nose cone. Their latent heat of melting, vaporization or sublimation augment their effective heat absorptive capacity, increasing it to the order of several thousand Btu/lb. These materials are expendable and their removal due to thermal effects during flight is termed "ablation."

Of course, ablating materials must have not only desirable absorptive capabilities but also must have desirable structural properties to resist surface shear by the air and other aerodynamic loads.

An additional desirable characteristic of ablation cooling is derived from the fact that the material which is sublimed or evaporated from the surface acts as a gaseous coolant blocking the usual entry of heat to the surface, such as if a cooling fluid were being blown out of the surface itself. Also accompanying this process may be chemical reactions between the gaseous ablated material and the high temperature air around the body. It has been found that these chemical reactions may actually be beneficial for the cooling process.

Naturally, these complicated processes are somewhat difficult to treat analytically. However, some progress has been made toward an understanding and simplified theoretical treatment of boundary layer flows subjected to mass addition and chemical reaction. (References 22, 23, 24)

Both theory and experiments indicate that Teflon placed in the stagnation region of a spherical nose in hypersonic flow has an effective absorptivity or "effective heat of ablation" which varies linearly from about 3,000 Btu/lb when the flight velocity is 15,000 ft/sec to about 5,000 Btu/lb at a velocity of 20,000 ft/sec. This dependence upon velocity and position of the material on the body reflects the
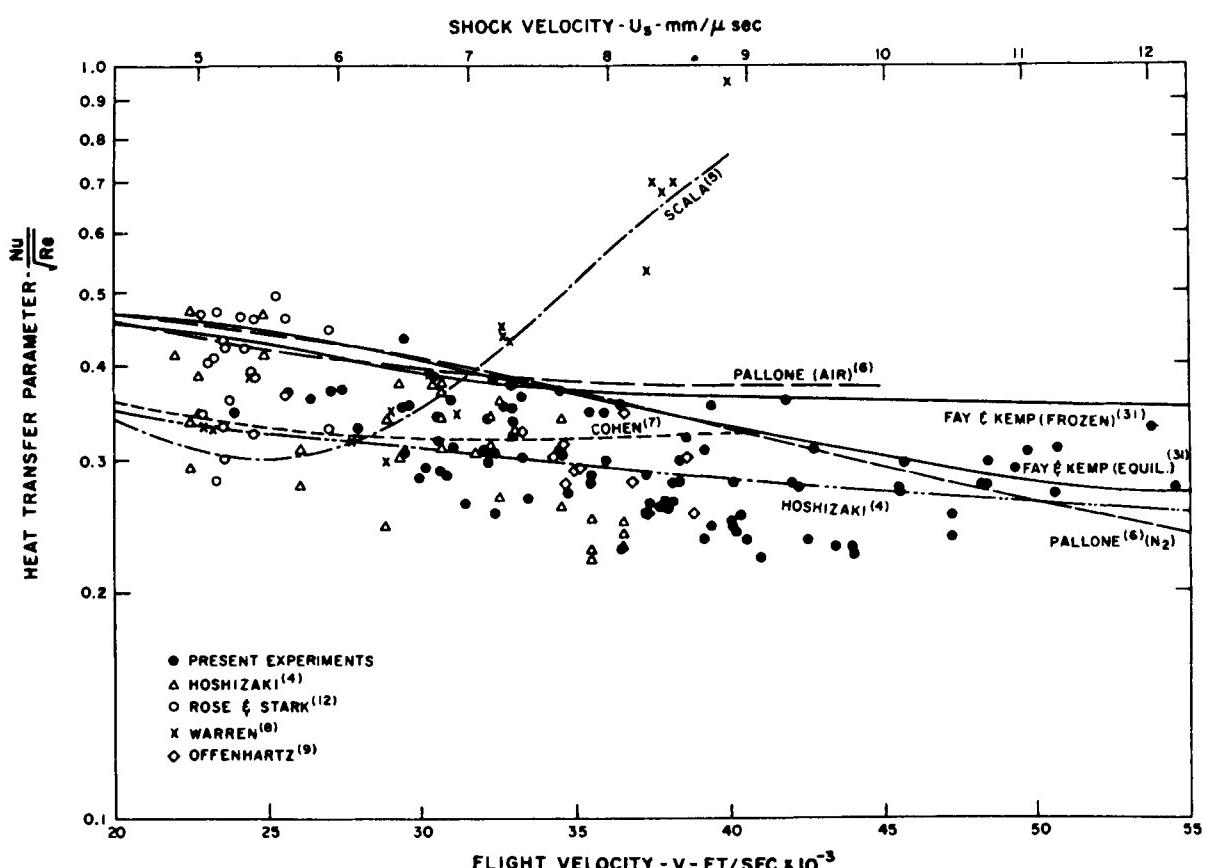

Figure 6-5. Heat Transfer Parameter $Nu/\sqrt{Re}$ for High Speed

complex fluid-mechanical and physico-chemical processes which continue to give the engineering quantity termed the "effective heat of ablation" denoted by H_{eff}.

For engineering purposes one estimates the mass lost from an ablating material by computing the theoretical heat input to the body as if there were no mass addition due to material loss (i.e., the value q as previously discussed in this chapter). Then the quantity q/H_{eff} yields the lb of material lost per ft^2 of exposed surface per second during the course of exposure.

For these purposes it is of interest to note that the order of magnitude of the average heat input to the entire surface of a spherical nose is characterized by the stagnation point heating value when the flow is laminar and by the sonic point value when the flow is turbulent. Integration of the heat transfer rate over a hemispheric surface at a given instant of time shows a mean heat rate equal to about $\frac{1}{2}$ the peak heat rate. On pointed or slender bodies with large amounts of lateral surface, the flat-plate or cone heat rate levels are more characteristic of the overall heat inputs to the body than are the local peak values which occur at the tip and which may require special local cooling methods for the preservation thereof.

An idea of the theoretical methods by which the actual heat transfer to an ablating material may be studied in detail, and whereby the effective heat of ablation may be estimated, is given in the paragraphs which follow.

A simplified expression for oxygen-and-nitrogen-limited chemical reactions with a pure ablating surface material E is treated in detail by Lees[24,25]. Here the salient points of interest are outlined. If q_s is the net rate of convective heat transfer to the solid interior available for heating fresh surface material, where subscript s denotes solid and g denotes gas, then for reactions occurring between atomic and molecular oxygen and nitrogen and a surface material E (here an *element*) there results the expression

$$q_s = \left[k\frac{\partial T}{\partial n} + \rho D_{12} \sum_i h_i \frac{\partial C_i}{\partial n} \right] - (\rho v)_w h_w(g) + (\rho v)_w h_{E,w}(s). \tag{6-23}$$

For $\rho D_{12}\bar{C}_p/k = 1$ this yields

$$q_s \doteq \rho_e u_e C_H(\Delta h - B'L_E) \tag{6-24}$$

where C_H is the Stanton number,

$$\Delta h = \sum_i C_{i,e}(h_{i,e} - h_{i,w})$$

$$+ \frac{u_e^2}{2} + \sum_{i \ne E} h_{i,w}[C_{i,e} - (B'+1)C_{i,w}]$$

$$+ [B' - (B'+1)C_{E,w}]h_{E,w}(g) \tag{6-25}$$

$$B' = \frac{(\rho v)_w}{\rho_e u_e C_H} \tag{6-26}$$

and L_E is the latent heat of sublimation per gram of E. For oxygen-nitrogen-limited reactions, wherein the mass fractions of individual chemical *elements* $\tilde{C}$ are introduced rather than each species C_i, this expression may be simplified to

$$q_s = \rho_e u_e C_H\{h_{e,e} - \sum_J \tilde{C}_{J,e} h_{J,w}$$

$$+ \sum_J \tilde{C}_{J,e} \Delta Q_{E,J} - B'L_E\} \tag{6-27}$$

where ΔQ denotes the heat released in a chemical reaction per unit mass, and

$$\tilde{C}_J = W_J \sum_k \frac{\mu_{J,k} C_k}{W_k}$$

where $\mu_{J,k}$ is the number of atoms (or molecules) of the element J in the species k:

For the complete combustion of carbon by oxygen and nitrogen the added chemical enthalpy potential is about 24,000 Btu/lb, about twice the potential without combustion. However, this is relieved by the heat absorption due to sublimation, about 28,500 Btu/lb, about ten times that of unburnt carbon. Thus the net effect is not catastrophic but may be somewhat beneficial in reducing heat inputs.

The "heat blockage" or reduction in C_H brought about by the mass transfer can be regarded as an increase in effective heat sink capacity, i.e.,

$$\frac{L_{eff}}{L_E + L_T} = \frac{C_{H,0}}{C_H}$$

where $C_{H,0}$ is the Stanton number for zero mass transfer. The ratio $C_{H,0}/C_H$ depends only on

$$B' = \frac{\Delta h_{eff}}{L_E + L_T}$$

as given by Fig. 6-6. Here L_T is the thermal capacity of the solid material from some interior temperature T_i up to the surface temperature T_w, i.e.,

$$L_T = \frac{q_s - q_R}{(\rho v)_W}$$

where q_R is the net radiative heat transfer away
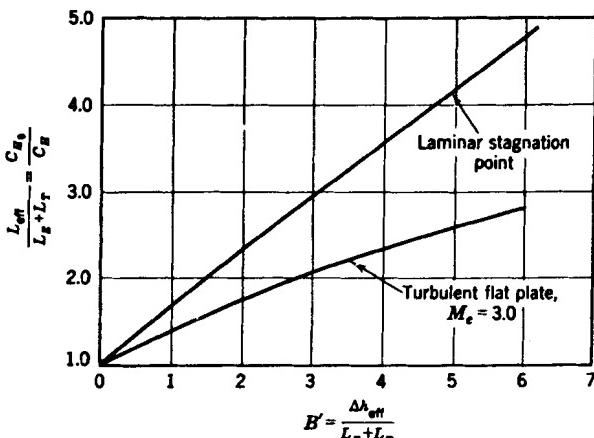
Figure 6-6. Effective Heat-Sink Capacity with Mass Addition[15]

from the wall. Furthermore, the term Δh_{eff} is an "effective" enthalpy potential defined by

$$\Delta h_{eff} = \Delta h - \frac{q_R}{\rho_e u_e C_H}$$

6-9 RADIATION HEAT TRANSFER

The emissivity ϵ for air considered as an optically thin layer ($\epsilon < 1$) has been tabulated in Ref. 39 and approximately correlated in Ref. 24

as follows:

$$\frac{\epsilon}{L} \simeq 0.75 \left(\frac{\rho_{ss}}{\rho_{sea\ level}}\right)^{1.3} \left(\frac{T_{ss}}{8000}\right)^{8.6}$$

where L is a characteristic length of the body (in cm) and T_{ss} is the stagnation temperature external to the boundary layer (in °K). If chemical equilibrium is assumed, one estimates, for the flight regimes of interest:

$$\frac{\rho_{ss}}{\rho_f} \simeq 17, \qquad T_{ss} \simeq 0.32 u_f$$

where u_f is the flight velocity (in ft/sec).

With an approximate shock layer geometry and data for equilibrium states from Ref. 39, estimates of the heat flux to the stagnation region of a blunt body have been made in Ref. 35. The graphical representation of such estimates is presented in Fig. 6-7. These results may be correlated adequately by the expression developed in Ref. 40. In this case, i.e., $\epsilon < 1$, the heat flux due to radiation is given by

$$q_R \simeq 100 R_n \left(\frac{\rho_f}{\rho_{sea\ level}}\right)^{1.60} \left(\frac{u_f}{10^4}\right)^{8.5}$$

where

q_R is the radiative heat flux (in Btu/ft^2 − sec),
R_n is the nose radius (in ft) and
ρ_f is the density at flight altitude.
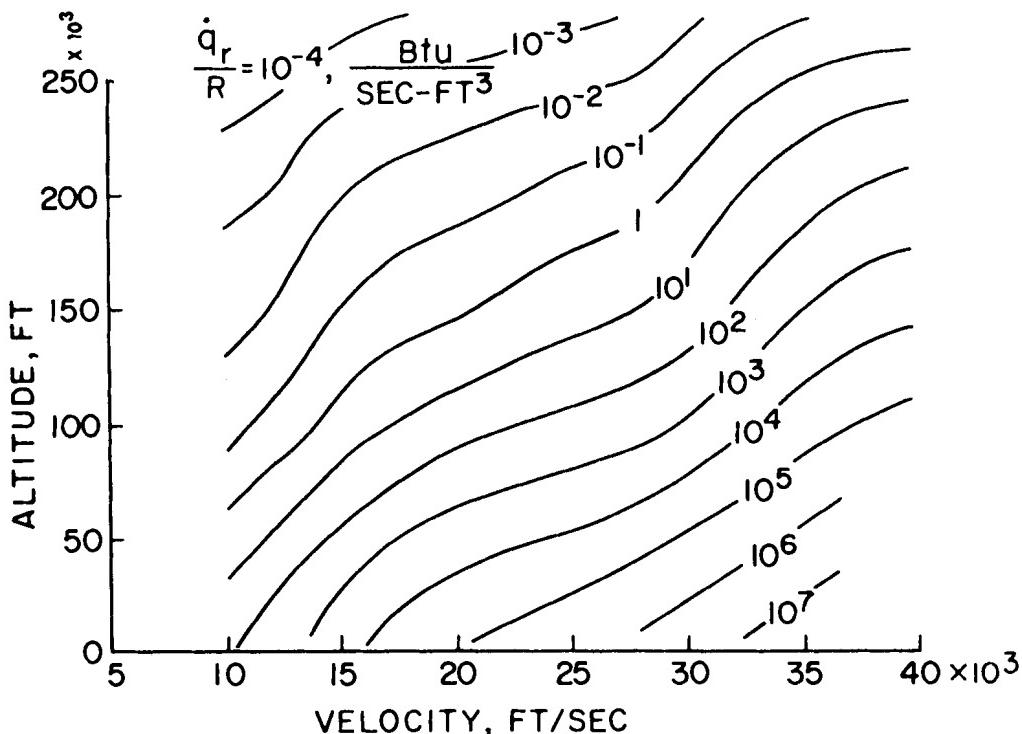
Figure 6-7. Radiative Heating as a Function of a Flight Altitude and Velocity[35]

However, if the air is not in chemical equilibrium in the shock layer, the local temperatures may be much higher than those obtained assuming chemical equilibrium. As an approximation, a first estimate of the radiant heat flux can be made if the non-equilibrium temperature is known, by evaluating the expression for ϵ/L given above at the non-equilibrium state and using the relation $q_R \simeq \epsilon \sigma T^4$, where σ is the Stefan-Boltzmann constant.

Additional work relative to radiative heat transfer effects is given in References 29, 36 and 37.

6-10 CONCLUDING REMARKS

There are numerous special problems concerning the heat transfer to missiles which have not been treated explicitly in this Chapter.[41] For example, the augmented heat rates which may be engendered by protuberances from a surface have been considered in Reference 42, and the heat transfer and pressures over the blunt base of a body has been studied in Reference 43. The reader should consult the references for the solution of other heat transfer problems.

REFERENCES

1. F. K. Moore, *Unsteady Laminar Boundary Layer Flow*, National Advisory Committee for Aeronautics Technical Note 2471, 1951.

2. F. K. Moore and S. Ostrach, *Average Properties of Compressible Laminar Boundary Layer on Flat Plate with Unsteady Flight Velocity*, National Advisory Committee for Aeronautics Technical Note 3886, 1956.

3. M. J. Lighthill, "The Response of Laminar Skin Friction and Heat Transfer to Fluctuations in the Stream Velocity," Proc. Roy. Soc. (London) **224**, 1–23 (1954).

4. N. Rott, "Unsteady Viscous Flow in the Vicinity of a Stagnation Point," Quart. Appl. Math. **13**, 444 (1956).

5. H. Schuli, "Calculation of Unsteady Boundary Layers in Two-Dimensional Laminar Flow," Zeitschrift fur Flugwissenschaften **1**, 122–131 (1953).

6. K. T. Yang, *Unsteady Laminar Boundary Layers in an Incompressible Stagnation Flow*, ASME Paper 58-A-3. Presented at ASME Annual Meeting, December 1958.

7. K. T. Yang, *Unsteady Laminar Boundary Layers Over an Arbitrary Cylinder with Heat Transfer in an Incompressible Flow*, ASME Paper 58-A-49. Presented at ASME Annual Meeting, December 1958.

8. E. R. G. Eckert, "Engineering Relations for Friction and Heat Transfer to Surfaces in High Velocity Flow," J. Aeronaut. Sci. **22**, 585 (1955).

9. R. R. Gold, "A Note on the Expressions for the Local Heat Transfer Coefficient," J. Aeronaut. Sci. **25**, 208 (1958).

10. R. R. Gold, *Thermal Environment of Radomes in High Speed Flight*, Hughes Aircraft Co. Presented at Wright Air Development Center 05V Radome Symposium held at Ohio State University, 1958.

11. M. H. Bloom, *Thermal Conditions Associated with Aircraft in Flight*, Wright Air Development Center Technical Report 55-169, 1956.

12. R. J. Cresci, D. A. MacKenzie and P. A. Libby, "An Investigation of Laminar, Transitional and Turbulent Heat Transfer on Blunt-Nosed Bodies in Hypersonic Flow," J. Aeronaut. Sci. **27**, 401 (1960).

13. E. Reshotko, "Heat Transfer to a General Three-Dimensional Stagnation Point," Jet Propulsion **28**, 58 (1958).

14. L. Lees, "Laminar Heat Transfer Over Blunt-Nosed Bodies at Hypersonic Flight Speeds," Jet Propulsion **26**, 259 (1956).

15. R. Vaglio-Laurin, "Laminar Heat Transfer on Three-Dimensional Blunt-Nosed Bodies in Hypersonic Flow," ARS Journ. **29**, 123 (1959).

16. V. Zakkay, *Pressure and Laminar Heat Transfer Results in Three-Dimensional Hypersonic Flow*, Wright Air Development Center Technical Note 58-182, 1958, AD 155679. (Also J. Aeronaut. Sci. **25**, 794 (1958).)

17. R. J. Wisniewski, *Methods of Predicting Laminar Heat Rates On Hypersonic Vehicles*, National Aeronautics and Space Administration Technical Note D-201, 1959.

18. R. Vaglio-Laurin, *Turbulent Heat Transfer on Blunt-Nosed Bodies in Two-Dimensional and General Three-Dimensional Hypersonic Flow*, Wright Air Development Center Technical Note 58-301, 1958, AD 206050.

19. V. Zakkay and C. J. Callahan, *Laminar, Transitional and Turbulent Heat Transfer to a Cone-Cylinder-Flare Body at Mach 8.0*, Polytechnic Institute of Brooklyn Aerospace Laboratory PIBAL Report 737, Air Force Office of Scientific Research 2359, 1962.

20. W. L. Hankey, R. D. Neumann and E. H. Flinn, *Design Procedures for Computing Aerodynamic Heating at Hypersonic Speeds*, Wright Air Development Center Technical Report 59-610, 1960, AD 239943.

21. M. F. Romig, "Stagnation Point Heat Transfer for Hypersonic Re-entry," *Aviation Age R and D Handbook, 1958–1959*, p. C-10.

22. M. H. Bloom, "External Sources of Heat (In Aeronautics)", *AGARDograph 28*, Pergamon Press, London, 1958.

23. J. A. Fay and F. R. Riddell, "Theory of Stagnation Point Heat Transfer in Dissociated Air," J. Aeronaut. Sci. **25**, 73 (1958).

24. L. Lees, "Recovery Dynamics—Heat Transfer at Hypersonic Speeds in a Planetary Atmosphere," *Space Technology*, John Wiley & Sons, N.Y., 1959.

25. L. Lees, "Ablation in Hypersonic Flows," *Proceedings of Seventh Anglo-American Aeronautical Conference, October 1959*, published by Institute of Aerospace Sciences, N. Y.

26. L. Steg, "Materials for Re-entry Heat Protection of Satellites," ARS Journ. **30**, 815 (1960).

27. L. Roberts, *An Analysis of Ablation—Shield Requirements for Unmanned Re-entry Vehicles*, National Aeronautics and Space Administration Technical Report R-62, 1960.

28. R. Vaglio-Laurin and M. H. Bloom, "Chemical Effects in Hypersonic Flows," *Hypersonic Flow Research*, Academic Press, N. Y., 1962.

29. P. R. Rose and D. Teare, *On Chemical Effects and Radiation in Hypersonic Aerodynamics*, AVCO Research Laboratory, Everett, Mass., AGARD Fluid Mechanics Panel, Brussels, 1962.

30. P. H. Rose and J. O. Stankevics, *Stagnation Point Heat Transfer Measurements in Partially Ionized Air*, AVCO Research Laboratory, Everett, Mass., Research Report 143, 1963.

31. N. H. Kemp, P. H. Rose and R. W. Detra, "Laminar Heat Transfer Around Blunt Bodies in Dissociated Air," J. Aerospace Sci. **26**, 421 (1959).

32. S. S. Penner, *Chemistry Problems in Jet Propulsion*, Pergamon Press, London, 1957.

33. J. O. Hirschfelder, C. F. Curtiss and R. B. Bird, *Molecular Theory of Gases and Liquids*, John Wiley & Sons, N. Y., 1954.

34. C. E. Treanor, *Radiation at Hypersonic Speeds*, ARS Reprint 1938–61, 1961.

35. K. K. Yoshikawa and B. H. Wick, *Radiative Heat Transfer During Atmosphere Entry at Parebolic Velocity*, National Aeronautics and Space Administration Technical Note D-1074, 1961.

36. R. A. Allen, P. H. Rose and J. C. Camm, *Non-Equilibrium and Equilibrium Radiation at Super Satellite Re-Entry Velocities*, AVCO Research Laboratory, Everett, Mass., Technical Note 324, 1962.

37. R. Goulard, *Similarity Parameters in Radiation Gas Dynamics*, Purdue University, A&ES Report No. 62-8, 1962.

38. H. Hoshizaki, *Convective Heat Transfer Measurements at Super-Orbital Speeds*, Fluid Mechanics Research Note #2, Lockheed Missiles and Space Co., LMSC-6-90-62-50, 1962.

39. B. Kivel and K. Baily, *Tables of Radiation from High Temperature Air*, AVCO Research Laboratory, Everett, Mass., Research Report 121, 1957.

40. M. H. Bloom and A. Miele, "Aerodynamics Heating of Hypervelocity Vehicles," *Flight Mechanics*, Addison-Wesley Publishing Co., Cambridge, Mass., 1962.

41. H. J. Allen, "Hypersonic Aerodynamic Problems of the Future," "High Temperature Aspects of Hypersonic Flow," *AGARDograph 68*, N 62-10713, Pergamon Press, London, 1964.

42. M. H. Bloom and A. Pallone, "Heat Transfer to Surfaces in the Neighborhood of Protuberances in Hypersonic Flow," *Heat Transfer and Fluid Mechanics Institute*, Stanford University Press, 1957.

43. M. H. Bloom and A. Pallone, "Shroud Tests of Pressure and Heat Transfer Over Short Afterbodies with Separated Wakes," J. Aeronaut. Sci. **26**, 643 (1959).

44. R. W. Detra and H. Hidalgo, *Generalized Heat Transfer Formulae and Graphs*, AVCO Research Laboratory, Everett, Mass., Research Report 72, 1960.

CHAPTER 7

HYPERSONIC AERODYNAMIC FORCES

7-1 INTRODUCTION

Considerable information has been compiled concerning forces and moments on bodies in subsonic and supersonic flight. Much of this information concerns wings, wing-like shapes, and sharp-nosed slender bodies in the low or moderate supersonic range, e.g., below Mach 4. For the purpose of this discussion, the speed range below roughly Mach 4 will be termed "low-speed" and the range above Mach 4 will be referred to as "hypersonic."

The utility of low speed aerodynamic properties in connection with the consideration of modern ballistic missiles is somewhat limited inasmuch as low speed flight regimes are confined to the boost phase and the final 50,000 ft (roughly) of re-entry. In the boost phase the vehicle weight and engine thrust far exceed the aerodynamic forces; hence the aerodynamic forces are of secondary importance for preliminary analyses. This is not to say that they do not have an important role in the final phase of design, especially in connection with stability and control. However, the considerations involved are of a relatively detailed nature, and may be thought of as lying within the scope of more "conventional" aerodynamics.

In the final phase of re-entry which may involve low speeds if the re-entry vehicle is sufficiently light, the details of forces do not have a great influence on preliminary design since their dispersive effects cannot be great and since critical regions of peak heating and deceleration occur well above the low speed part of the trajectory.

Low-speed problems therefore will not be considered explicitly in this chapter. Properties of this regime are developed in sufficient detail in standard texts and in applied design works such as References 1 and 2. This chapter will emphasize instead the hypersonic flight conditions unique to ballistic missile design and performance. Similarly, we shall not emphasize the aspect of forces relating to lift (the force component normal to the flight velocity vector) since lift is employed primarily in satellite or manned re-entry to minimize heating and/or deceleration and to facilitate terminal guidance. Furthermore, wing-like surfaces which are usually used solely to provide lift or control, assume less importance in hypersonic flight, since their contribution to lift is dominated by that of the body itself. Thus the body shapes which will be of principle interest will be spheres, cones, sphere-cones and sphere-cone-cylinder-flare combinations.

An additional simplification arises from the fact that for many configurations the portion of the drag (force component parallel to the flight velocity vector) which stems from viscous skin friction is comparatively small and may be neglected or roughly estimated. This is not the case for very slender bodies, such as cones with included angles on the order of 10° or less, for which skin friction drag becomes important.

The protion of the drag not contributed by skin friction is termed *pressure drag*. This drag is determined by integrating the pressures over the surface and taking the component of the resultant parallel to the flight velocity vector. The body pressures, aside from those over the base, which have a minor effect on hypersonic forces are established essentially by the flow external to the boundary layer. In this external region viscosity may be neglected. Subclasses of pressure drag, termed wave drag and base drag, need not be distinguished here.

When the ratio of pressure drag to friction is large, the body is termed bluff; the opposite type of body is termed *streamlined*. Viscous and pressure force components normal to the flight velocity vector comprise the *lift*. This characteristic is dominated by the pressure forces.

Within the current state of the art it is quite possible to make detailed theoretical calculations of the hypersonic flow fields around missile configurations, even including the effects of flow chemistry. However the procedures required are highly complex and involve numerical integrations on large digital computers.

In fact, such calculation programs are considered to be "numerical experiments" and are used in touchstone cases to check approximate theories, or in the final stages of design. Examples of such calculations are given in References 3-6. These deal with bodies

at zero angle of attack, i.e., axially-symmetric flow. The cases of non-axial symmetry which arise due to angle of attack are much more difficult to obtain, and at present are at the limit of available techniques. Fortunately, however, the simpler problem of estimating surface forces in hypersonic flight does not require the aforementioned detail since it is amenable to approximation. Appropriate engineering approximations for the resultant forces and moments form the main subject of the subsequent paragraphs of this chapter.

7-2 STEADY FRAME OF REFERENCE

Aerodynamic effects, such as forces acting on a body in flight, are considered in terms of an equivalent system consisting of a fixed body subjected to an initially undisturbed stream moving relative to the body. This is the situation actually produced in wind tunnel testing. The initial flow is taken to have a velocity vector $\bar{u}_f^{\bullet}$ equal in magnitude and direction, but opposite in sense to the vehicle's flight velocity vector. The static pressure p_f, density ρ_f and temperature T_f of the initial stream are those of the undisturbed atmosphere at the flight altitude. In this frame of reference the flow relative to the

_____
• Here subscript f denotes freestream flight conditions.

body is steady; i.e., at each point there are no time-wise variations. Hence the determination of flow effects, such as forces, is simplified. The usual variations of flight conditions along a trajectory are taken into account by a "quasi-steady" approximation which considers a succession of instantaneously achieved steady-states along the flight path. Special conditions, involving extreme curvatures of trajectory, extreme time-variations in flight conditions, or vibrating surfaces, for which the quasi-steady approach may not be valid are too limited for consideration here.

7-3 QUALITATIVE STRUCTURE OF THE HYPERSONIC FLOW FIELD

Use of the approximate methods of force estimation to be given here does not require a detailed knowledge of hypersonic flow fields, whose complex structure can be observed from the typical schematic diagram shown in Figure 7-1 (from Ref. 6). However, several salient features are cited to serve as an introductory background.

Shock waves are formed in supersonic flows, wherein local velocities exceed local sound speeds, due to the coalescence of disturbances which cannot propagate away from the body more rapidly than
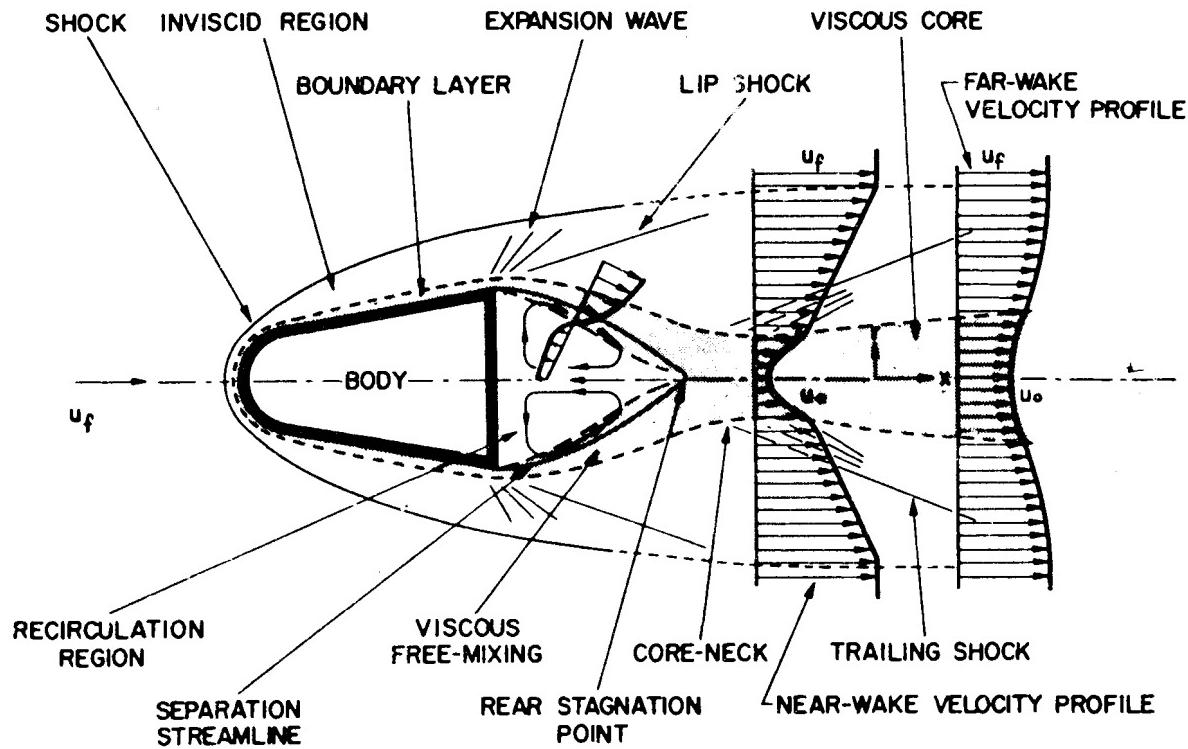

Figure 7-1. Schematic Diagram of Complete Flow Field Around a Blunt-Nosed Body[6]

the oncoming flow sweeps them back. As the flow traverses the shock its velocity decreases, whereas the static pressure, density and temperature increase. In hypersonic flow the bow shock lies very close to the body and is roughly parabolic in shape downstream of the nose. The region between the shock and the body is termed the *shock layer*. Its thickness in the nose region of a blunt body in hypersonic flow is on the order of $\frac{1}{5}$ of the nose radius.

The *boundary layer* is a region adjacent to the body wherein significant shear stresses are created by the adhesion of the fluid to the surface (no-slip condition). The surface shear stress has the rough magnitude $\tau_w \simeq \mu_w(2u_e/\delta)$, where

μ_w is the absolute viscosity evaluated at the surface temperature,

u_e is the local velocity outside the boundary layer

and

δ is the local thickness of the boundary layer.

The ratio $2u_e/\delta$ signifies the order of magnitude of the velocity gradient or rate of strain within the layer.

The thickness δ has the following order of magnitude at a distance x away from the initial point if the flow remains laminar:

$$\frac{\delta}{x} \simeq A\left(\frac{\rho_e u_e x}{\mu_e}\right)^{-1/2}$$

$$A \simeq 6 + \left(\frac{\gamma - 1}{2}\right)M_e^2$$

where

γ is the ratio of specific heats with typical values between 1.2 and 1.4 in air,

M is the Mach number and subscript e denotes values outside the boundary layer at the station x.

The term in parentheses is a dimensionless group called the *Reynolds number* (R_N), or in this instance the "local" Reynolds number because its parameters are evaluated at the local conditions indicated.

The local density ρ_e varies in rough proportion to the ambient density ρ_f, decreasing from about 10 ρ_f to 2ρ_f around a typical blunt body. The local velocity u_e increases from zero at the nose of the blunt body to about 0.5 u_f at the end. The temperatures which determine μ_e are more difficult to evaluate generally because of their sensitivity to chemical composition; however, they may decrease from levels around 20 to 100 T_f in the nose region

of a blunt body to 10 T at the rear. Thus $\rho_e u_e/\mu_e \simeq (\frac{1}{3})\rho_f u_f/\mu_f$ and $\delta/x \simeq 15(\rho_f u_f x/\mu_f)^{-1/2}$. At an altitude of 150,000 ft, flight Reynolds numbers per foot $(\rho_f u_f/\mu_f)$ are on the order of 10^5. Therefore for $x = 10$ ft a typical thickness $\delta \simeq 0.15$ ft is estimated. At 200,000 ft δ increases to about 0.5 ft, and at 100,000 ft it decreases to 0.05 ft.

The foregoing rough estimates indicate that at low altitudes (e.g., below 150,000 ft) the boundary layer thickness is relatively small compared to characteristic body dimensions and to the shock layer thickness, whereas at higher altitudes the boundary layer may become sufficiently thick to occupy a major part of the shock layer.

From the standpoint of forces, a key feature of the boundary layer is the fact that it is virtually parallel to the surface, and thus transmits the pressure at its outer edge essentially undistorted to the surface along a surface-normal. As a result, the effect of the boundary layer thickening on forces is twofold: First, the shear stress is decreased so that at high altitudes its contribution is smaller than at low altitudes. Secondly, its displacement effect causes an effective thickening of the body with respect to the flow outside the boundary layer. It has been shown both theoretically and experimentally[8] that this interaction has only a modest effect on pressures over bodies of revolution. For example on 10° half angle cones, pressures about 20% higher than those obtained with thin boundary layer are found. Although the effect is much more pronounced on two-dimensional wing-like surfaces, the effect of viscous-inviscid interactions on larger angle cones and on blunt bodies of revolution is diminished still further. Therefore, we are justified in neglecting this low Reynolds number phenomenon for present purposes. Indeed at the high altitudes where the interaction would be observed, the overall aerodynamic forces are small, and have only a minor influence on ballistic missile behavior.

A word may be said about the *separated flow* or *base region* of the body surface; denoted as the recirculation region in Figure 7-1. When the flow outside the boundary layer creates regions of increasing pressure over the boundary layer (and body surface), the boundary layer is usually forced to separate from the body and thus creates an eddying wake region. On wings, this condition is known as *stall* and leads to increased drag and decreased lift. On blunt-based bodies of revolution, the cause of separation is somewhat more complex, being related to the ultimate redeflection of the flow beyond the body. Estimates of the mean pressure in the re-

circulation region, i.e., the *base pressure*, are usually made by semi-empirical methods. In low-speed flow the contribution of the base force to the overall forces on the body is significant and requires accurate evaluation. However, in hypersonic flight the base force usually is negligible and therefore will not be considered here.

Finally, it may be remarked that the boundary layer flow may be laminar or turbulent. Usually turbulent boundary layers will not be found at the higher altitudes (above 150,000 ft). However, at low altitudes they are almost certain to arise. Estimates of where the transition from laminar to turbulent flow will occur are extremely difficult to make. For this purpose one usually relies on experiments or prior experience in similar cases and, when in doubt, makes alternative estimates based on both laminar and turbulent possibilities. The main effect of turbulence on the force is to increase the surface shear and thus the skin friction drag contribution. It also leads to boundary layers which are thicker than laminar ones.

Textbooks dealing in detail with the subject matter of the chapter are listed as Refs. 7, 10 and 11.

7-4 FORCE ESTIMATES BY THE NEWTONIAN IMPACT CONCEPT

The Newtonian impact concept, previously cited in Chapter 5 in connection with surface pressures, provides a very useful tool for making initial estimates of forces in hypersonic flow. In this approximation, the approaching stream is assumed to lose completely its momentum component normal to the surface, whereas the tangential momentum is unchanged. Thus the pressure is increased on a segment of the surface that can be "seen" by the oncoming stream, i.e., a segment whose surface-normal makes an oblique angle with the oncoming stream. The surface segments "shaded" from the oncoming stream are assumed to make a negligible contribution to the force impressed on the body, whereas those perpendicular to the stream are subject only to ambient stagnation pressure P_f. In principle the pressures over shaded or slightly inclined surfaces are not accurately represented by these assumptions, however, the errors involved have only a secondary effect on the overall forces which depend on the integrated pressures.

The impact theory, which arose from physical reasoning, has been studied on a rational analytic basis in limiting hypersonic cases for which the conditions $M_f \rightarrow \infty$ and $\gamma \rightarrow 1$ are considered (M_f is

the flight Mach number and γ the ratio of specific heats).

The aforementioned reasoning results in the local relation:

$$C_p \equiv \frac{(p - p_f)}{\left(\frac{\rho_f u_f^2}{2}\right)} = 2 \sin^2 \beta \qquad (7\text{-}1)$$

where C_p is termed a pressure coefficient (dimensionless) and β is the angle of inclination of the surface with respect to the direction of u_f. Use of this relation reduces all force determinations to geometric operations. Its nonlinear dependence on the deflection-measure β is characteristic of pressure and force relations in the hypersonic regime.

A correction to Eq. 7-1, which takes into account a decrease in the value of the absolute pressure p predicted by Eq. 7-1 as a result of centrifugal forces which accompany body curvature, will not be considered here for several reasons. First, the pressures over spheres and cylinders have been found to be in good agreement with experiment if Eq. 7-1 is modified for use in the following form:

$$\frac{C_p}{C_{p\,max}} = \sin^2 \beta \qquad (7\text{-}2)$$

where $C_{p\,max}$ is the value corresponding to the stagnation point on the body, and can be estimated quite accurately. Indeed for hypersonic flow over blunt bodies which produce strong bow shocks, an excellent approximation is

$$C_{p\,max} \simeq 2 \qquad (7\text{-}3)$$

Furthermore, when centrifugal forces are considered, it can be deduced that the value of p may decrease to zero at a point on the body where this value is not measured. Attempts have been made to explain this result by postulating the presence of regions of separated flow and by contending that the hypersonic theory which produces analytically the "Newtonian" pressure plus a centrifugal force correction is invalid near the zero-pressure point. Finally, on straight-sided surface, such as cones, the centrifugal force is zero. Thus force estimates in this section are based on either Eq. 7-1 or Eq. 7-2.

7-5 TYPICAL FORCE COEFFICIENTS

The pressure drag coefficient for a cone at zero angle of attack is

$$C_D \equiv \frac{DA}{\frac{\rho_f u_f^2}{2}} = 2 \sin^2 \beta_s \qquad (7\text{-}4)$$

where

D is the drag

A is the area of the base of the cone, and

β_c is the cone half-angle.

It is convenient to express the forces on bodies at angle of attack α in terms of force components F_N normal to the body axis x and F_c along the body axis. The corresponding force coefficients are, respectively,

$$C_c = \frac{F_c A}{\frac{\rho_f u_f^2}{2}} \quad \text{and} \quad C_N = \frac{F_N A}{\frac{\rho_f u_f^2}{2}},$$

where A is a reference area usually taken to be the maximum cross-sectional area of the body.

If M represents the moment of the forces on a body taken about an axis at the foremost point of the body, the moment coefficient may be defined as

$$C_M \equiv \frac{M A \lambda}{\frac{\rho_f u_f^2}{2}}$$

where λ is the body length. The center of pressure CP may be defined as

$$CP = \frac{M}{F_N} = \frac{\lambda C_M}{C_N} \tag{7-5}$$

The formulas which relate the lift and drag coefficients C_L and C_D to C_N and C_C are:

$$C_L = C_N \cos \alpha - C_c \sin \alpha$$
$$C_D = C_N \sin \alpha + C_c \cos \alpha \tag{7-6}$$

where α is the angle of attack.

For cones at angle of attack α there arise the following equations:

(i) $\alpha < \beta_c$:

$$C_N = \cos^2 \beta_c \sin 2\alpha$$

$$C_c = 2 \sin^2 \beta_c + \sin^2 \alpha (1 - 3 \sin^2 \beta_c); \tag{7-7a}$$

(ii) $\alpha > \beta_c$

$$C_N = (\cos^2 \beta_c \sin 2\alpha)\left(\frac{1}{3\pi}\right)[3(\psi + \pi/2)$$

$$+ \cos \psi (\cot \alpha \tan \beta_c + 2 \tan \alpha \cot \beta_c)]$$

$$C_c = \left(\psi + \frac{\pi}{2}\right)\left(\frac{1}{\pi}\right)[2 \sin^2 \beta_c + \sin^2 \alpha (1 - 3 \sin^2 \beta_c)]$$

$$+ \left(\frac{3}{4\pi}\right) \cos \psi \sin 2\alpha \sin 2\beta_c \tag{7-7b}$$

where $\psi = \arc \sin (\tan \beta_c / \tan \alpha)$ signifies the meridian angle at which the pressure has dropped to zero; the value $\psi = \pi/2$ represents the most leeward generator.

Relations 7-7 lead to the following expressions for the slope of the cone's lift curve and its center of pressure, respectively:

$$\left(\frac{dC_L}{d\alpha}\right)_{\alpha=0} = 2 \cos^2 \beta_c \tag{7-8}$$

$$CP = \frac{2\lambda}{3} \tag{7-9}$$

where λ is the cone length.

The coefficients for the *frustum of a cone* of minimum radius r_m and maximum radius r_B where the reference area $A = \pi r_B^2$ can be obtained from the cone values by simple subtraction of the force contributed by the initial section of a sharp cone of base radius r_B. The results may be expressed as follows:

$$(C_N)_{frustum} = (C_N)_{cone}\left(1 - \frac{r_m^2}{r_B^2}\right) \tag{7-10}$$

and similarly for C_c, i.e.,

$$(C_c)_{frustum} = (C_c)_{cone}(1 - r_m^2/r_B^2).$$

The center of pressure measured from the front of the frustum is given by:

$$CP = \frac{\lambda_f\left(2 + \frac{r_m}{r_B}\right)}{3\left(1 + \frac{r_m}{r_B}\right)} \tag{7-11}$$

where λ_f is the length of the frustum.

The force coefficients of a *circular cylinder* are obtained as special cases of the cone-frustum equations, equations in the $\alpha > \beta_c$ case, with the additional observations that

$$1 - \frac{r_m^2}{r_B^2} = \frac{(r_B + r_m)(r_B - r_m)}{r_B^2} = \frac{2\lambda}{r_B} \tan \beta_c$$

The above relations are substituted into Eq. 7-10 with the use of Eqs. 7-7b, and the limit $\beta_c \to 0$, imposed. The following result is obtained for the lateral surface of a circular cylinder:

$$C_N = \left(\frac{16}{3\pi}\right)\left(\frac{\lambda}{2r_B}\right) \sin^2 \alpha$$

$$C_c = 0 \tag{7-12}$$

It is of interest to note that an analysis taking into account pressure relief due to centrifugal effects, which are neglected completely in this chapter, leads

to a reduction of about 10 percent in the value of C_N given in Eq. 7-12. (See Ref. 7, p. 85.)

For a *flat surface* normal to the flow,

$$C_D = 2 \qquad (7\text{-}13)$$

For a *sphere* or a hemisphere whose axis is parallel to u_f,

$$C_D = 1 \qquad (7\text{-}14)$$

For a cone-frustum at zero angle of attack including the drag of the front face, and using $A = \pi r_B^2$,

$$C_D = 2\left(\frac{r_n}{r_B}\right)^2 + 2\sin^2\beta_c\left(1 - \frac{r_n^2}{r_B^2}\right) \qquad (7\text{-}15)$$

where

$$1 - \frac{r_n^2}{r^2} = \frac{2\lambda_f}{r_B}\tan\beta_c$$

It is readily seen that for a fixed base r_B and body length λ_f, the frustum of *minimum drag* is not a sharp cone but a frustum for which

$$\tan 2\beta_c = \frac{2r_B}{\lambda_f} \qquad (7\text{-}16)$$

For example, for $r_B/\lambda_f = 1$, the minimum drag is obtained when $\beta_c = 31.7°$ as compared to $\beta_c = 45°$ for the sharp cone. For the optimum frustum in this case $C_D = 0.77$, whereas the sharp cone gives $C_D = 1$, as does the hemisphere for which $r_B/\lambda = 1$ also.

There are many ramifications and refinements connected with the optimization of body forces under a variety of constraints such as fixed volume, fixed surface, etc. They are not considered to be within the scope of this chapter.

Bodies of a variety of shapes may be treated approximately as composites of segments of cones, cone-frustums, cylinders, etc. However, in this process it is probably most convenient to sum actual forces and moments in order to avoid confusing the various reference areas A which are used to form the different force and moment coefficients.

For sharp-nosed slender bodies of revolution, whose shape can be expressed in terms of a *power-law*

$$\frac{r}{\lambda} = \left(\frac{x}{\lambda}\right)^n$$

the drag coefficient may be approximated by

$$C_D\left(\frac{r_B}{\lambda}\right)^{-2} = \begin{cases} 2n^3(2n-1)^{-1}, \text{ no centrifugal forces;} \\ n^2(3n-1)(2n-1)^{-1}, \text{ including cen-} \\ \qquad\qquad\text{trifugal forces} \qquad (7\text{-}17) \end{cases}$$

For the case of no centrifugal forces, $n = \frac{3}{4}$ gives minimum drag and $C_D/(r_B/\lambda)^2 = \frac{27}{16}$; whereas

including centrifugal forces the terms are $n = \frac{2}{3}$ and $C_D/(r_b/\lambda)^2 = \frac{4}{3}$.

When these power-law bodies are at small angles of attack, the coefficients are approximately

$$C_N = K\sin 2\alpha$$
$$C_c = K(0.05 + \sin^2\alpha)$$
$$K = 1 + \left(\frac{1}{4}\right)\left[\frac{(r-1)}{(r+1)} + \frac{1}{\left(\frac{M_f r_B}{\lambda}\right)^2}\right] \qquad (7\text{-}18)$$

In practical use, slender bodies usually will be blunted somewhat because of thermal factors. Therefore, it is of interest to return to reexamine Eq. 7-15, which gives the drag coefficient of a blunted cone, to estimate the ratio of the blunt-nose drag to that contributed by the conical afterbody for small cone semi-angle β_c. The result is:

$$\frac{D_{nose}}{D_{afterbody}} = \frac{1}{2}\left(\frac{r_1}{\lambda\beta_c^2}\right)^2 \qquad (7\text{-}19)$$

which indicates that the effect of the blunted nose is strongly dominant for small cone angles.

7-6 AERODYNAMIC CHARACTERISTICS OF A FAMILY OF SPHERICAL-NOSED BODIES WITH CONVERGING CONICAL AFTERBODIES

The aerodynamic characteristics of this family of bodies have been calculated using impact theory by Dickey.[12] The importance of this report and the brevity of its presentation prompted the inclusion of it in its entirety. Another NASA report, by Rainey,[13] has a set of working charts to assist in the calculation of forces and pressure coefficients on arbitrary bodies of revolution; these calculations also being based on impact theory.

Reproduced below, in its original form is the report *Forces and Moments on Sphere-Cone Bodies in Newtonian Flow.*[12]

SUMMARY

The static longitudinal aerodynamic characteristics of a family of sphere-cone combinations (fineness ratios from 1.0 to 6.0) were computed by means of Newtonian impact theory. The effects of angle of attack, fineness ratio, and center-of-gravity location are shown. The results indicate that, with the center of gravity at or near the center of volume, the sphere-cone combinations are statically stable at trim points that provide low to moderate lift-drag ratios. In general, the lift-drag ratio increased with increasing fineness ratio. As an example, with the center of gravity at the center of volume, the lift-drag ratio at trim was increased from approximately

0.05 to 0.56 by increasing the fineness ratio from 1.2 to 6.0.

INTRODUCTION

Consideration of the heating, deceleration, guidance, and stability problems encountered during high-speed entry into the earth's atmosphere indicates that it would be desirable for an entry vehicle to have a blunt forward face and to be statically stable at a trim point which would provide a moderate lift-drag ratio. It would also be desirable for the launch configuration to have axial symmetry. Preliminary analysis indicated that a simple body of revolution consisting of a sphere with a converging conical afterbody possesses these desirable characteristics and, consequently, that such shapes merit further investigation. An analytical study utilizing Newtonian impact theory was therefore undertaken to gain further knowledge of the static aerodynamic characteristics of sphere-cone combinations. The purpose of this report is to present the results of that study. The effects of angle of attack, fineness ratio, and center of gravity on the lift, drag, and pitching-moment characteristics of a family of sphere-cone combinations having fineness ratios from 1.0 to 6.0 are shown.

NOTATION

A Axial force

C_A Axial-force coefficient, $\dfrac{A}{qS}$

C_A' Local axial-force coefficient per unit length, $\dfrac{dC_A}{d(x/d)}$

C_D Drag-force coefficient, $C_A \cos \alpha + C_N \sin \alpha$

C_L Lift-force coefficient, $C_N \cos \alpha - C_A \sin \alpha$

C_m Pitching-moment coefficient, $\dfrac{m}{qSd}$

C_m' Local pitching-moment coefficient per unit length, $\dfrac{dC_m}{d(x/d)}$

C_N Normal-force coefficient, $\dfrac{N}{qS}$

C_N' Local normal-force coefficient per unit length, $\dfrac{dC_N}{d(x/d)}$

C_p Pressure coefficient

D Drag force

d Diameter of the sphere

e Distance of the center of gravity from the longitudinal axis

$F.\,R.$ Fineness ratio of the sphere-cone combination, $\dfrac{\ell}{d}$

L Lift force

$\dfrac{L}{D}$ Lift-drag ratio

ℓ Length of the sphere-cone combination

m Pitching moment about the center of gravity

N Normal force (force perpendicular to the

longitudinal axis measured in the α plane)

q Free-stream dynamic pressure

R Radius of the sphere

r Local cross-sectional radius of the sphere-cone combination

S Frontal area of the sphere, πR^2

x Distance along the longitudinal axis from the nose of the sphere-cone combination

x_0 Distance along the longitudinal axis from the nose to the center of gravity of the sphere-cone combination

α Angle of attack (angle between the longitudinal axis and the free-stream velocity vector)

β Radial angle measured in a plane normal to the longitudinal axis (See Fig. 7-1.)

β_u Radial angle denoting the upper limit of the body surface exposed to the air stream (See Fig. 7-1.)

δ Local body slope with respect to the longitudinal axis (See Fig. 7-1.)

η Angle between the free-stream velocity vector and the perpendicular to the local surface of the body

SPHERE-CONE COMBINATIONS

The geometry of the family of sphere-cone combinations considered in this report is shown in Figure 7-2. Each combination consisted of a sphere with a converging conical afterbody tangent to the sphere. The length of the conical afterbody relative to the diameter of the sphere was varied so that the resultant fineness ratios of the sphere-cone combinations ranged from 1.0 to 6.0.

METHOD

In order to obtain the total force and moment coefficients of a sphere-cone combination, it is convenient to determine first the local force coefficients acting on a transverse section. The general expressions for the local axial-force and normal-force coefficients per unit length of an arbitrary body of revolution are given in Reference 1 as

$$C_A' = \frac{4r}{\pi R} \tan \delta \int_{-\pi/2}^{\beta_u} C_p \, d\beta \qquad (1)$$

and

$$C_N' = -\frac{4r}{\pi R} \int_{-\pi/2}^{\beta_u} C_p \sin \beta \, d\beta \qquad (2)$$

The foregoing equations are for that portion of the body exposed to the air stream. In the analysis the portion of the body shielded from the air stream is assumed to have a pressure coefficient of zero and therefore not to contribute to the body forces.

The pressure coefficient, C_p, of a surface exposed to the air stream is given by Newtonian theory as

$$C_p = 2 \cos^2 \eta \qquad (3)$$

where, for an arbitrary body of revolution

$$\cos \eta = \cos \alpha \sin \delta - \sin \alpha \cos \delta \sin \beta \qquad (4)$$

Side view

Transverse section
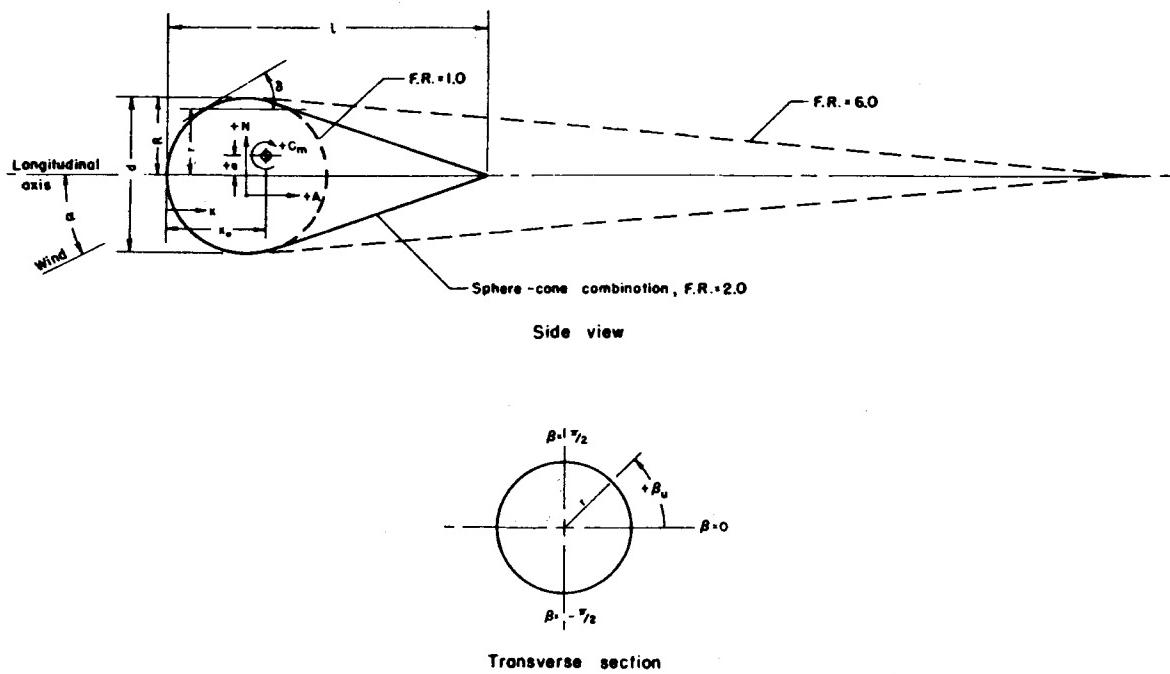
Figure 7-2. Geometry of Sphere-Cone Combinations

Substituting Equations 3 and 4 into Equations 1 and 2 and integrating yields

$$C_A' = \frac{4r}{\pi R} \tan \delta \left[\left(\beta_s + \frac{\pi}{2} \right) \right.$$

$$\cdot (2 \cos^2 \alpha \sin^2 \delta + \sin^2 \alpha \cos^2 \delta) + \cos \beta_u$$

$$\left. \cdot (\sin 2\alpha \sin 2\delta - \sin^2 \alpha \cos^2 \delta \sin \beta_u) \right] \qquad (5)$$

and

$$C_N' = \frac{4r}{\pi R} \left\{ \frac{1}{2} \left(\beta_u + \frac{\pi}{2} \right) \sin 2\alpha \sin 2\delta + \cos \beta_u \right.$$

$$\cdot \left[2 \cos^2 \alpha \sin^2 \delta - \frac{1}{2} \sin 2\alpha \sin 2\delta \sin \beta_u \right.$$

$$\left. \left. + \frac{2}{3} \sin^2 \alpha \cos^2 \delta (\sin^2 \beta_u + 2) \right] \right\} \qquad (6)$$

The local pitching-moment coefficient per unit length can be expressed in terms of the local geometric parameters and the local axial- and normal-force coefficients as

$$C_m' = \left(\frac{x_0}{d} - \frac{x}{d} \right) C_N' - \frac{r}{d} \tan \delta C_N' - \frac{e}{d} C_A' \qquad (7)$$

The total axial-force, normal-force, and pitching-moment coefficients presented in this report were obtained by graphically integrating the corresponding local force and moment coefficients per unit length (determined from Eqs. 5, 6 and 7 over the total length of the configuration as indicated below:

$$C_A = \int_0^{\ell/d} C_A' \, d(x/d) \qquad (8)$$

$$C_N = \int_0^{\ell/d} C_N' \, d(x/d) \qquad (9)$$

$$C_m = \int_0^{\ell/d} C_m' \, d(x/d) \qquad (10)$$

RESULTS

The static longitudinal aerodynamic characteristics of a family of sphere-cone combinations, with the center of gravity located at the center of volume, are presented in Figures 7-3 to 7-9. The results show that these blunt-faced bodies of revolution are statically stable at trim points that provide low to moderate lift-drag ratios. In general, for a given angle of attack, an increase in the fineness ratio results in an increase in the lift and drag coefficients and in the lift-drag ratio.

The trimmed ($C_m = 0$) aerodynamic characteristics of sphere-cone combinations, with center of gravity at the center of volume, are plotted as a function of the fineness ratio in Figure 7-10. The results show that increasing the fineness ratio from 1.2 to 6.0 decreased the trim angle from approximately 79° to 31° and increased the lift-drag ratio from approximately 0.05 to 0.56. It should be noted that because of the rotational symmetry of the sphere-cone combinations, the trim angles may be considered as angles in pitch or yaw or any vector combination thereof. In order to direct the lift force in the desired direction, some auxiliary method of
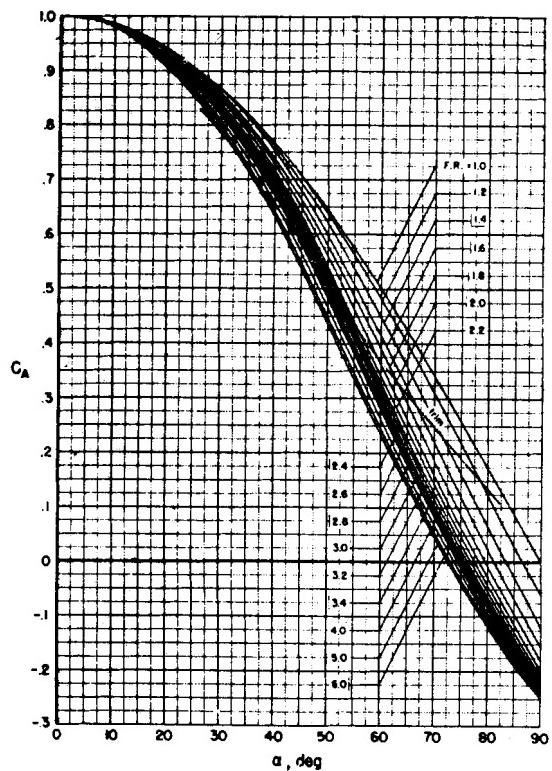
**Figure 7-3. Axial-Force Coefficients of Sphere-Cone Combinations**
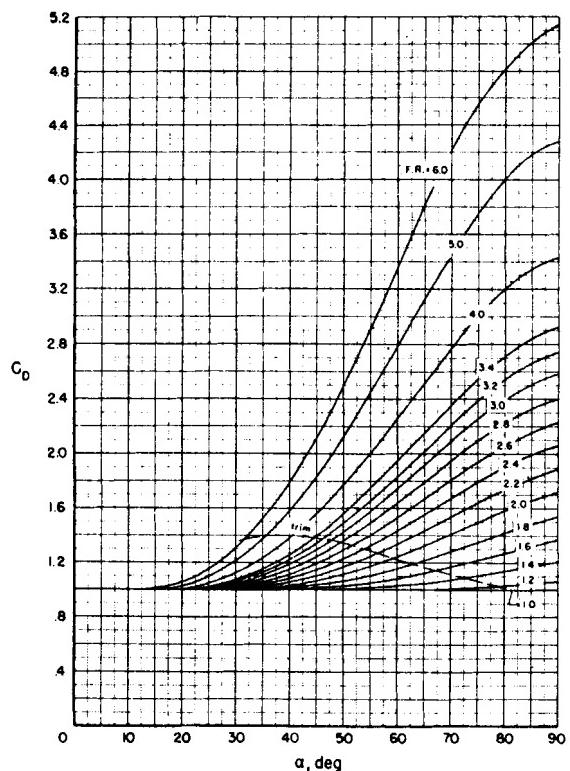
**Figure 7-4. Drag Coefficients of Sphere-Cone Combinations**
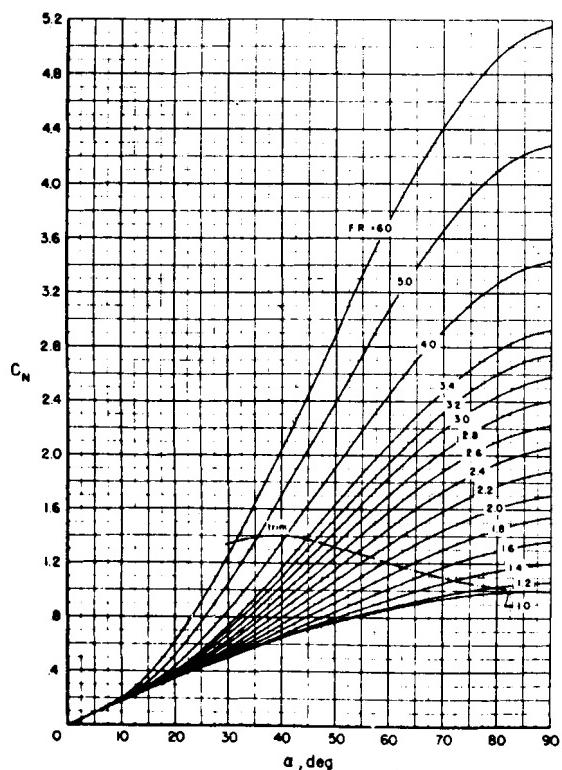
Figure 7-5. Normal-Force Coefficients of Sphere-Cone Combinations
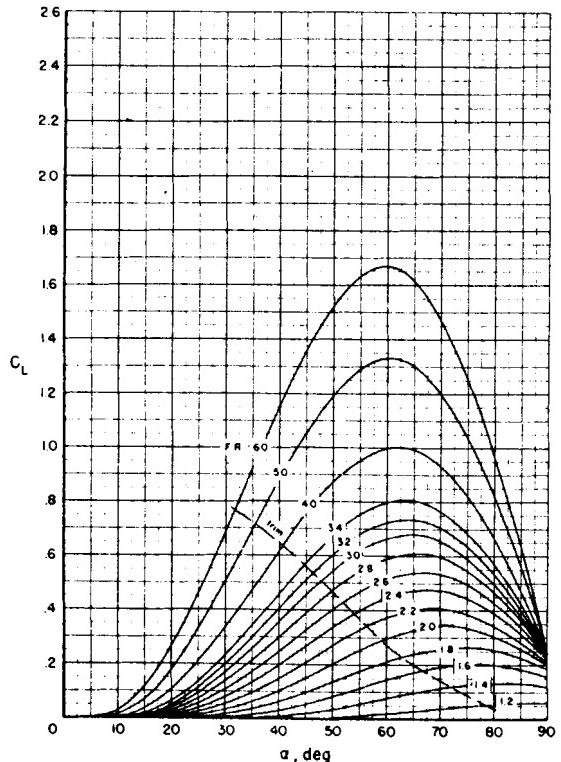

Figure 7-6. Lift Coefficients of Sphere-Cone Combinations

7-9

control (such as reaction jets) would be required for positioning and maintaining the configuration in the proper attitude of roll, pitch, and yaw. If, however, the rotational symmetry of the configuration is removed by locating the center of gravity off the longitudinal axis, the lift force could be placed in the desired direction by controlling only the roll attitude of the vehicle.

The effect of center-of-gravity location on the pitching-moment coefficients of a representative sphere-cone combination (fineness ratio = 2) is shown in Figure 7-11 for the complete 360° angle-of-attack range. The results shown in Figure 7-11(A) (effect of longitudinal shift of the center of gravity) indicate that the sphere-cone combination trims at a usable angle of attack only when the center of gravity is located very near the center of volume (i.e., closer than about 15 percent of the body length). For other center-of-gravity locations, the trim angle is either 0° or 180° and, as a result, no lift would be produced. With the center of gravity located on the longitudinal axis and near the center of volume, the configuration has two stable trim points, one at a positive angle of attach and one at a negative angle of attack. However, the results shown in Figure 7-11(B) (effect of transverse shift of the center of gravity) indicate that by locating the center of gravity off the longitudinal axis, the sphere-cone combination can be made to have only one stable trim point.


Figure 7-8. *Lift-Drag Ratios of Sphere-Cone Combinations*

Figure 7-7. *Pitching-Moment Coefficients of Sphere-Cone Combinations with Center of Gravity at the Center of Volume*
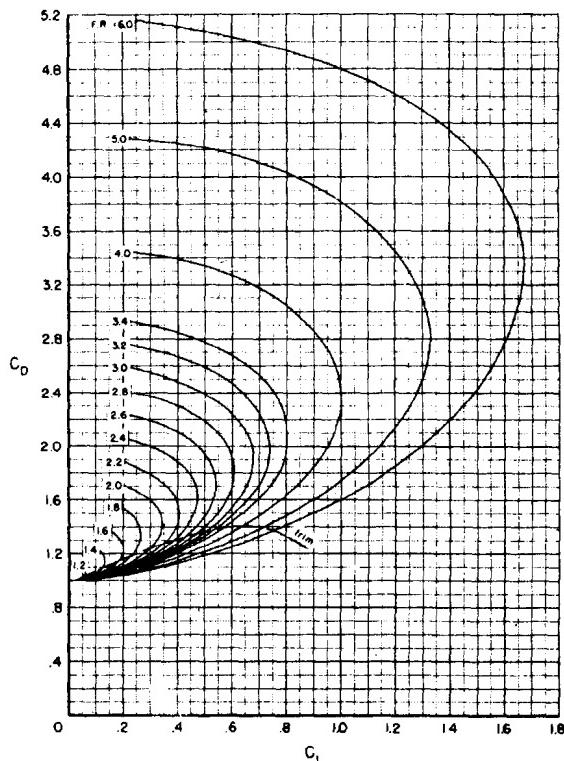

Figure 7-9. *Drag Polars of Sphere-Cone Combinations*
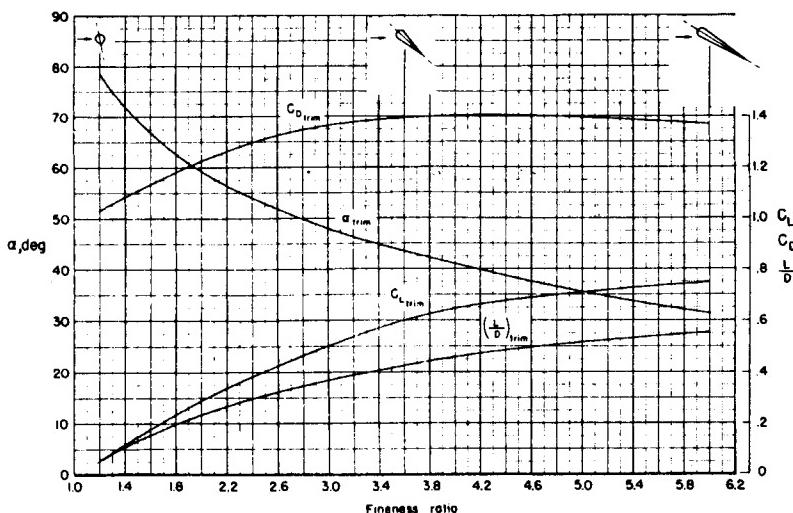
Figure 7-10. Aerodynamic Characteristics of Sphere-Cone Combinations at Trim with Center of Gravity at the Center of Volume
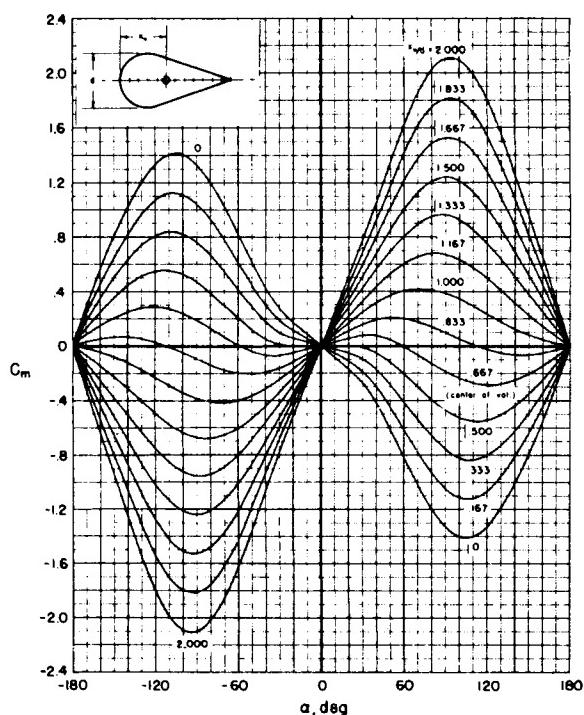
(A) Longitudinal Shift of Center of Gravity
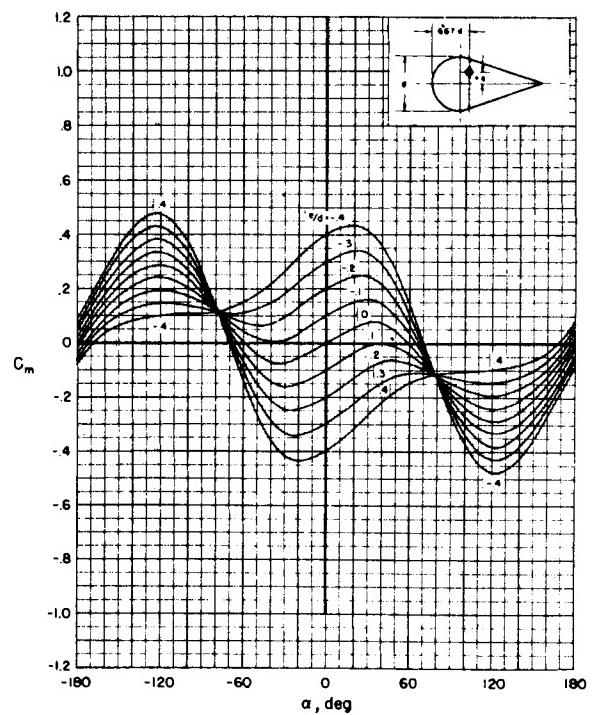
(B) Transverse Shift of Center of Gravity from the Center of Volume

Figure 7-11. Effect of Center-of-Gravity Location on the Pitching-Moment

7-11

REFERENCE

1. G. Grimminger, E. P. Williams and G. B. W. Young, "Lift on Inclined Bodies of Revolution in Hypersonic Flow", J. Aeronaut. Sci. **17**, 675–690 (1950).

7-7 FRICTIONAL EFFECTS

A fundamental idea in the understanding of fluid flow phenomena is the Prandtl boundary layer concept. According to this idea the behavior of air flowing over solid surfaces can usually be studied in two parts. One is a thin "boundary layer" region near the surface; thin in relation to distances measured along the surface. Within this region, shear forces caused by adhesion of the air to the surface, are stong, and the relative velocity drops off sharply to zero at the surface. The second part, outside the boundary layer, may be considered frictionless, its character being determined primarily by the disturbances caused by the surface contour.

The transmission of shear to adjacent layers within the boundary layer is termed a "transport process" and is attributable to the exchange of momentum between molecules of different velocities which intermix and collide. It is characterized by the "coefficient of absolute viscosity" μ. Other transport processes important in the boundary layer region are heat conduction and diffusion. Conduction involves an energy transport and exchange between intermixing molecules of different kinetic energies, i.e., temperatures. Diffusion involves a transport of mass, momentum and energy due to intermixing of various species of particles in a non-homogeneous mixture of different fluids. For example dissociated air may behave as a non-homogeneous mixture of molecules, atoms, ions and electrons. Likewise, injected or ablated coolants different from air form mixtures with the surrounding air.

The transport processes are important only in boundary layers, wakes and shock waves. Outside the boundary layer, their explicit effects are neglected. Under most practical circumstances the characteristic Reynolds number of the flow is not small, being on the order of 100,000 or more; while the Mach number is not extremely high. In these cases the deflection of the boundary layer streamlines does not alter appreciably the effective body shape, since the layer remains thin. Therefore, if the boundary layer does not separate from the surface, the outer flow values may be obtained by first disregarding the presence of the boundary layer, thereby considering the outer flow to slide without friction over the boundary layer. The pressure and velocity dis-

tributions over the surface are obtained in this way Then the boundary layer characteristics can be determined in terms of the nonviscous flow properties. A primary feature of the boundary layer concept is the result that the pressure does not vary along surface-normals within the boundary layer. This permits the determination of forces other than shear forces by neglecting the presence of the boundary layer.

Exceptions to this procedure of negligible viscous displacement are of 3 main types:

(1) Very slow "creeping motions" with Reynolds numbers on the order of 10 or less. In this case a boundary layer does not form. However, this situation is not of practical importance for missile flight.

(2) Hypersonic flows with simultaneous high Mach numbers and low Reynolds number, where the low Reynolds numbers stem from low densities and proximity to sharp leading edges and tips. This leads to pronounced boundary layer growth and displacement of the outer flow. After first neglecting this interaction, the displacement effect can be estimated and the changed inviscid properties calculated by a second iteration. It is important to note that the constancy of the pressure along surface normals still holds in this case. A rough criterion for neglecting this interaction effect is that the quantity $M_e^3 R_e^{-1/2}$ be much smaller than one. This criterion is based on the pressure change induced by the viscous flow deflection. This change is proportional to M_e times the induced flow deflection. The flow deflection being proportional to the boundary layer growth-rate which varies like $M_e^2 R_e^{-1/2}$.

(3) Under conditions of rising pressure, the boundary layer may lose its energy and become separated from the surface causing a wake to form in the separated region, and causing a major change in the inviscid flow pattern, especially in the wake region. An estimate of the separation point can be made in a first approximation by assuming that separation does not occur and thus deriving the inviscid and boundary-layer properties. These will indicate the incipient separation point by producing a point of zero shear stress. The shape and flow characteristics of the separated flow pattern are not readily amenable to purely theoretical analysis but can be treated empirically.

REFERENCES

1. E. A. Bonney, "Aerodynamics," Monograph in *Principles of Guided Missile Design*, G. Merrill, Ed., D. Van Nostrand, N. Y., 1956.

2. S. S. Chin, *Missile Configuration Design*, McGraw-Hill, Inc., N. Y., 1961.

3. S. Feldman, "Numerical Comparison Between Exact and Approximate Theories of Hypersonic Inviscid Flow Past Slender Blunt-Nosed Bodies," ARS Journ. **30**, 463 (1960).

4. R. Vaglio-Laurin and M. Trella, "A Study of Flow Fields about Some Typical Blunt-Nosed Slender Bodies," Aerospace Eng. **20**, 20 (1961).

5. V. Van Hise, *Analytic Study of Induced Pressure on Long Bodies of Revolution with Varying Nose Bluntness at Hypersonic Speeds*, National Aeronautics and Space Administration Technical Report 78, 1961.

6. R. Vaglio-Laurin and M. H. Bloom, *Chemical Effects in External Hypersonic Flows*, ARS Preprint 61-1976, 1961.

7. R. W. Truitt, *Hypersonic Aerodynamics*, Ronald Press, Inc., N. Y., 1959.

8. M. H. Bertram and A. Henderson, Jr., *Effects of Boundary-Layer Displacement . . .* , National Advisory Committee for Aeronautics Technical Note 4301, 1958.

9. M. H. Bertram and T. A. Blackstock, *Some Simple Solutions to the Problem of Predicting Boundary Layer Self-Induced Pressures*, National Aeronautics and Space Administration Technical Note D-798, 1961.

10. W. D. Hayes and R. F. Probstein, *Hypersonic Flow Theory*, Academic Press, N. Y., 1959.

11. G. G. Chernyi, *Introduction to Hypersonic Flow*, Academic Press, N. Y., 1961.

12. R. R. Dickey, *Forces and Moments on Sphere-Cone Bodies in Newtonian Flow*, National Aeronautics and Space Administration Technical Note D-1203, Ames Research Center, California, October 1961.

13. R. W. Rainey, *Working Charts for Rapid Prediction of Force and Pressure Coefficients on Arbitrary Bodies of Revolution by Use of Newtonian Concepts*, National Aeronautics and Space Administration Technical Note D-176, 1959.

CHAPTER 8

AERODYNAMIC TESTING

8-1 INTRODUCTION

The experimental simulation of high speed thermal conditions encountered in hypersonic ballistic flight requires the use of a variety of complementary devices. Whereas the measurement of forces, heat transfer and surface friction have dominated aerodynamic testing in the past, additional factors of current importance are flow details which bear on the chemical and electrical properties of the high energy air surrounding the vehicle and in its wake. The latter properties are significant in relation to communications, detection and discrimination problems, and for some purposes require relatively new testing techniques.

The need for tests on a basis other than full-scale is clear from a financial, design and scientific standpoint. The economy of model tests has been well proven although accepted design practice requires the acquisition of all available theoretical and experimental data on a vehicle in parameter ranges as close to full-scale as possible. Moreover, detailed testing of a type only possible with models, leads to improved performance which, in the full scale ballistic missiles, may involve faster re-entry with increased payloads, and improved stability and launching behavior.

Finally, the scientific aspect of the information gathered in experiments gives rise to new ideas and technical advancement.

The variety and severity of ballistic flight conditions, as well as the aforementioned multiple objectives of testing, make it clear that no single facility will suffice for all purposes. Rather a set of coordinated experimental facilities is required to provide maximum flexibility and research capability.

The experimental aerodynamics connected with ballistic vehicles may be divided into three categories:

(1) The first is essentially of a fluid-mechanical nature, and involves the pressure distribution and frictional resistance of the vehicle which give rise to the aerodynamic forces. These aspects may be considered to be influenced indirectly by the thermodynamics of the air at high speed and high temperature. In most ballistic missiles, the friction drag is a relatively small fraction of the total drag, being on the order of 0.1 or 0.01 of the total. Hence, it does not require very accurate evaluation, and is not given prominence in testing programs. The remaining forces require rather accurate determination but do not necessarily require the simulation of the full-scale thermodynamic effects.

(2) The second involves the heat transfer to the vehicle. Even this type of information, which at first appears to be so intimately connected with the thermodynamic behavior of the air, may be largely uncoupled from the explicit thermodynamic and chemical effects and thus may be dealt with by the use of various types of partial simulation.

Also in this category may be placed the study of cooling methods, and the behavior of materials such as heat sinks and ablators under various types of thermal loading.

(3) The third category involves the explicit investigation of the chemical state of the gas sheath around the vehicle and in the wake. Moreover, it concerns the chemical behavior of the flow in various parts of the test facilities which utilize high energy gases in their operations, i.e., the chemical nature of the flow in shock-tubes and in hypersonic nozzles supplied by high energy air sources is of importance.

Fortunately the problem of dealing with chemical effects in flows around vehicles can be simplified in some cases by the expedient of uncoupling the fluid-mechanical behavior from the chemical behavior. For example, in many hypersonic flows the general flow-field configuration, including pressure distributions, are not affected strongly by the details of the chemical processes. Thus, the shock pattern, streamline shapes and pressures can be determined to a first order, theoretically or experimentally, by taking into account simplified chemical and thermodynamic effects. On the other hand the chemistry may be strongly influenced by the pressure distribution in the field and in particular along streamlines. Thus, as a second step, the pressure variation along streamlines may be prescribed and the chemistry determined by one-dimensional analysis along the streamlines. Experimentally this means that simple

nozzle flows may be used to simulate the chemical behavior of the flow along the streamline. It is true that this procedure does not provide a full chemical configuration; however, it is an important step in the simulation of a very complicated and difficult flow property. Other aspects of this problem will be discussed later.

8-2 TYPES OF TEST FACILITIES

Listed below are various types of aerodynamics test facilities with brief statements on the features of each type. Most require heat-supply systems for their operation. Sources of heat for these facilities are outlined separately in Paragraph 8-3. A more detailed description of several of these testing systems is given in Paragraph 8-4. Considered are:

(1) Free flight-testing of prototypes or models[44]
(2) Ballistic firing ranges.[2-8]
(3) Wind tunnels, continuous or intermittent, with preheating systems to prevent test section condensation of the expanded gas or to achieve increased stagnation temperatures.[10-17]
(4) Shock tunnels.[18-22]
(5) Electrical discharge methods to generate a stream of high temperature fluid (plasma jets and "hot-shot")[10,23-26]
(6) Low-density tunnels.[27-29]

Free flight-testing usually is the most expensive method. Unmanned rocket vehicles are expensive and are usually considered to be expendable. Their use presents problems in the collection of data which must be recoverable or accurately telemetered to the ground. Furthermore, accurate knowledge and control of the flight plan and altitude of the vehicle is required but is often difficult to acquire in practice. This method, however, can supply test conditions close to those in actual flight.

A "ballistic range" is generally a long tube which may be pressurized or filled with gases other than air and through which models are fired from guns. It is a relatively economical device and can supply excellent material for visual study by various photographic means. Electrical, radiative and chemical effects of the flow around the body and in the wake can be made with the use of microwaves, photosensors, and spectrometers, respectively. At present, miniature recording and telemetering devices are being developed to permit certain detailed measurements to be made. Size is still a restricting factor, however, and in this sense range testing has some of the disadvantages of flight-testing.

The firing of a projectile upstream in a wind tunnel augments the relative velocity and hence the stagnation temperature.[3,9] Certain aspects of actual trajectories can also be duplicated by this means.

In "wind tunnels," models are usually held fixed with respect to the ground. This facilitates the making of controlled and accurate measurements. Wind tunnels are usually found to be economical when the cost is compared to the amount of data obtained. The intermittent or blow-down type of tunnel is less expensive than its continuously operating counterpart. Duration of the test run can vary from several seconds to minutes depending upon the test conditions and the reservoir capacity. There are many areas in which the desired information can be obtained in a relatively short test run, thus justifying this type of tunnel. In certain applications, continuous operation may be desirable, but the cost and power requirements may be prohibitive.

In wind tunnels using air, Mach numbers of 4 or 5 can be achieved without preheating the air supply to avoid condensation in the test section.[10,30] Otherwise some form of preheating is required. A number of these preheating systems are discussed separately in the next paragraph.

High Mach number wind tunnels using certain gases other than air, particularly helium, do not require preheating to prevent condensation phenomena. However, with these devices it is necessary to relate the flow phenomena occurring in helium to those in air.

"Shock tubes" have been used to produce relatively low speed flows, on the order of Mach 2, at temperatures as high as 15,000°R. Flow durations on the order of 1 msec are typical and the entire measurement problem under these circumstances is a difficult one. To overcome these difficulties it has been proposed that a series of shock tubes can be used successively to supply their air to a collection chamber which could act as a settling or supply chamber for a supersonic nozzle.[19,33] This device may modify the shock tubes disadvantage of short running times.

Mach numbers above 2 may be obtained by expanding the high energy gas sample provided by the shock tube through a nozzle attached to the end of the shock tube. The augmented shock tube is termed a "shock tunnel."

It is important to note that "shock tubes," which form the driving portions of shock tunnels, also have an extremely important use as tools for the study of the high-temperature properties of gas samples, i.e., as tools for physical-chemical studies of gas properties. The shocked gas samples may be

examined for composition, reaction rates and radiative properties under high energy conditions. Such information relative to the properties of air and possible gaseous contaminants clearly is important for hypersonic flow studies.

Electrical discharges from arcs have been used to generate streams of high-temperature fluid. The temperatures are reported to be in the order of 15,000°R, but the properties of the so-called *"plasma"* fluid are not well-known. This method appears to be useful for materials testing. Gas stabilized plasma jets and fluid transpiration arcs have been developed which supply cleaner high energy streams at low density.

Low density phenomena of importance at high altitudes are studied by means of special wind tunnels whose dominant components are the vacuum exhaust systems.

8-3 TYPES OF HEATERS

Among the various types of heating systems available for aerodynamic test facilities, the following are perhaps the most widely used:

(1) Conventional tubular or electric heaters for air.[13]
(2) Ceramic storage heaters heated electrically or with combustion products.[34]
(3) Compression heaters.[10,14]

Heating devices such as induction heaters and radiation heaters are not considered here inasmuch as fluid is not involved.

Relatively large tubular or electric heaters are currently available for raising wind tunnel stagnation temperatures. These are now mainly in the 1500°R range, but an increase to the 2500°R range is quite likely in the near future.

A ceramic heater intermittenly operated and electrically powered has provided air at 3000°R and 600 psi with flow rates up to 12 lb/sec. This temperture can be raised to 4000°R or 5000°R if combustion firing is used.

By operating these heaters with gases other than air, the heat transfer rates can be increased for the same conditions of supply temperature and pressure. The use of gases other than air has been investigated from the standpoint of power-saving. Some wind tunnels have been operated directly with the products of chemical reactions such as the usual combustion exhaust gases or special reaction products.

Adiabatic compression heaters may also be used to achieve high supply temperatures and pressures.

Such a heater is exemplified by the light gas free-piston gun tunnel described in Paragraph 8-4.6.

8-4 DESCRIPTION OF SELECTED TESTING FACILITIES

In the following description of test facilities, emphasis is placed on the blow-down wind tunnel with combustion-fired ceramic storage heater for fluid mechanical information in all ranges of rarefaction and on the shock tunnel for real-gas information.

8-4.1. Blowdown Hypersonic Wind Tunnel with Storage Heater[10,34]

Perhaps the most generally useful and versatile single device for fluid mechanical information and testing is the intermittent hypersonic blow-down wind tunnel, using axially symmetric nozzles with air supplied through a ceramic storage heater (Figure 8-1).[34] This facility is a ground test device and has the evident advantages of fixed models and instrumentation.

Up to the present time, the maximum stagnation temperatures achieved in conjunction with consistent operation have been in the 3000°R range. It appears possible to increase this maximum capability of ceramic storage heaters to 4000°R or 5000°R if the elevated temperature characteristics of the ceramic (e.g., zirconium oxide) would be improved. Improved performance can also be achieved if the scarcer refractories such as beryllium oxide could be produced in pebble form at a nonprohibitive cost.

Even supply temperatures as high as 5000°R, however, are not sufficient to produce actual physical chemical effects, such as molecular dissociation of air which is encountered in hypersonic flight. The elevated temperatures and the corresponding enthalpies in this range have had the following main purposes:

(a) to prevent component condensation at Mach numbers above 4;
(b) to provide temperature or enthalpy differences sufficient to yield well-defined heat transfer measurements;
(c) to establish a temperature or enthalpy ratio, particularly a ratio of stagnation-to-surface enthalpy, which is an important similarity parameter for determining boundary layer and heat transfer characteristics;
(d) to establish an enthalpy flux of sufficient magnitude and duration to permit meaningful

mass transfer cooling tests and tests of thermal effects in structures;

(e) to permit the study of interactions between gas molecules and solid surfaces, for example, free molecular accommodation coefficients at high temperatures.

Mach number limits above which air component condensation is possible under equilibrium conditions at a given stagnation temperature T_s are shown in Figure 8-2.[10] In this figure, the abscissa is the static temperature T_t corresponding to a given Mach number M. It is important to remember that whereas condensation is a rate process, the above limits are based upon an infinitely rapid condensation rate, i.e., equilibrium condensation, and therefore represent conservative estimates. These limiting values could therefore be exceeded with currently available supply temperatures, particularly at low density levels.
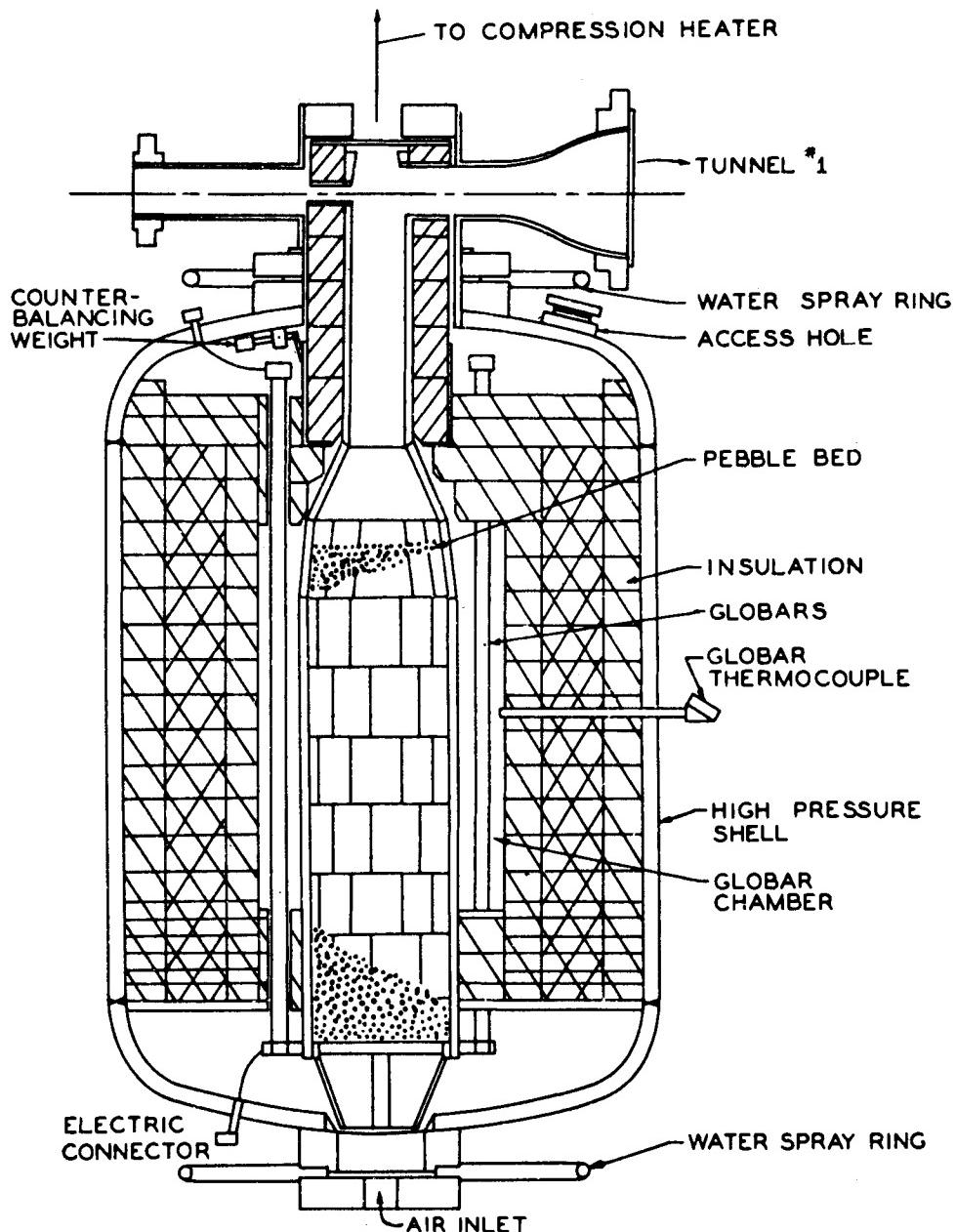

Figure 8-1. Schematic Cross-Sectional View of Convection Heater and Inlet Section, Polytechnic Institute of Brooklyn Aerodynamics Laboratory[34]
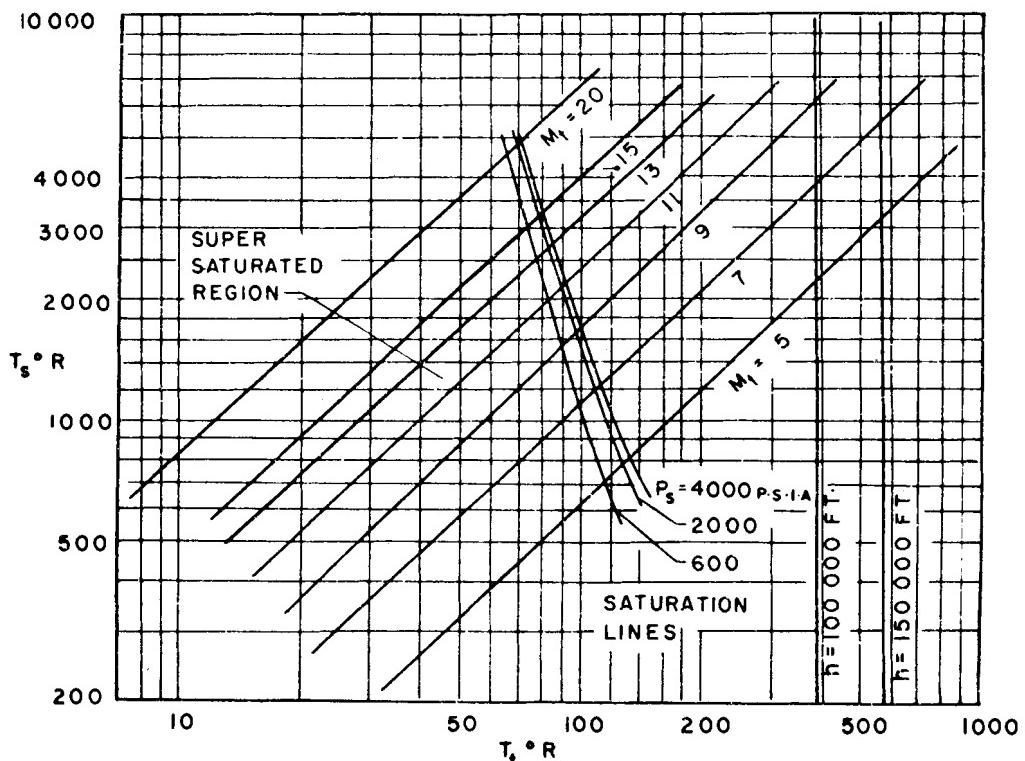
Figure 8-2. Limit of Mach Number for Component Saturation Lines[10]

With the blow-down system, stagnation pressures as high as 3000 psia are considered quite feasible. There appears to be no limit in principle on the extent to which the stagnation pressure can be decreased for low density testing; the capability of the vacuum system being the determining factor in this connection.

Supply pressures p_s required for equal Reynolds numbers in the test section and in flight are shown in Figures 8-3(A) and 8-3(B)[10] for $T_s = 3000°R$ and $5000°R$ and for the following ratios of prototype to model characteristic lengths: $L_p/L_m = 0.1$ and 1.0. Altitudes of 100,000 and 200,000 feet have been considered. It is seen that Reynolds numbers at altitudes around 200,000 feet and above may be readily achieved with reasonable stagnation pressures.

Mass flows achievable in a blow-down hypersonic facility may be as high as 100 lbs/sec. In general, much lower mass flows are required for low density hypersonic operation than for high density operation. For example, with $p_s = 100$ psia, $T_s = 3000°R$ and a mass flow of 2.5 lbs/sec, a Mach 14 tunnel 8.8 feet in diameter can be operated. This yields full scale flight Reynolds number simulation at 200,000 feet when $L_p/L_m = 1$ (see Figure 8-3(A)). It should be noted, however, that large test section

dimensions result in long nozzles—for the case cited above, the nozzle length would be about 100 feet long.

Running times for facilities of this type can vary from several seconds to several hours depending upon the particular type of test or nozzle size. For low density, low mass flow operation, runs may be virtually continuous, being limited primarily by the air supply and exhaust system capabilities.

Worthy of mention in connection with the blow-down tunnel is the shrouded model technique which has been developed primarily for high Reynolds number testing. Sketches of the system as applied in forebody studies, and in base and wake flow studies, are presented in Figures 8-4 and 8-5. For forebody flows, the shroud forms a channel around the body and thus impresses on it a prescribed pressure distribution which may correspond to that of actual flight, if desired. Boundary layer and heat transfer characteristics are thus produced at stagnation pressures which exist in the settling chamber ahead of the shroud. Large models may, therefore, be utilized with relatively small amounts of fluid.

In connection with afterbodies and wakes, the shroud is utilized to duplicate a streamtube in the inviscid region where shape may be deduced from

8-5
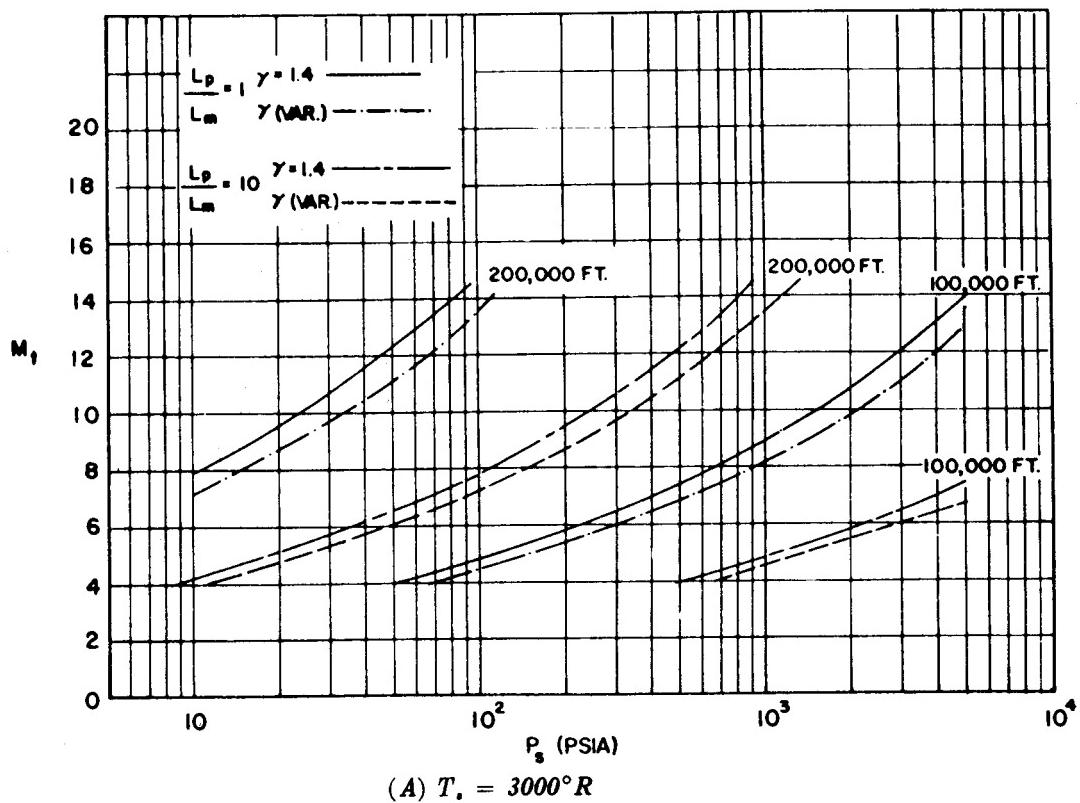
(A) $T_s = 3000°R$
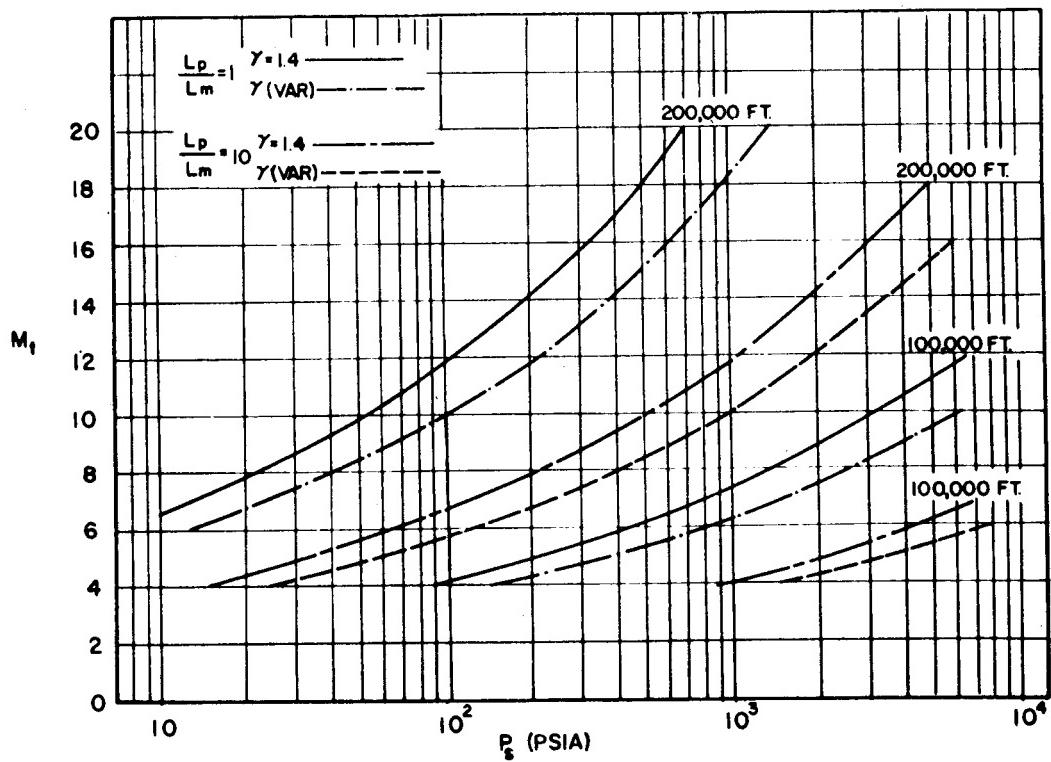
(B) $T_s = 5000°R$

Figure 8-3. Requirements for Reynolds Number Simulation[10]
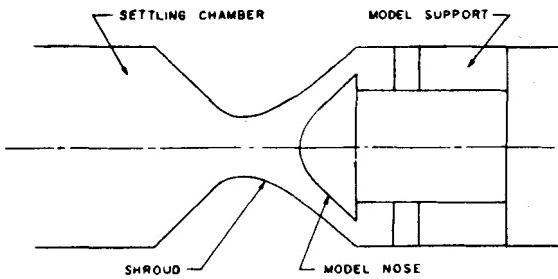
Figure 8-4. Schematic Diagram of Shrouded Model Technique for Forebodies (Reference 31 of Chapter 6)

calculations or small body tests. Proper flow conditions prior to the afterbody are regulated within the settling chamber of the shroud.

Gases other than air may be employed as a test media in the blow-down system but they would not be used in conjunction with a ceramic pebble bed heater. A simple gas such as helium may be used to avoid condensation or to produce high heat fluxes.

The direct use of other combustion reactions to produce gas mixtures resembling air has received some attention. It appears possible to produce relatively large mass flows of test gas which can be supplied continuously and conveniently. Their supply temperatures, however, are in the range 3000°–5000°R and do not produce the dissociation phenomena of hypersonic flight. Up to the present time, combustion products have been used primarily as a source of high temperature gas for structural testing rather than as a medium for the study of flow field properties. A schematic diagram of a rig utilizing a heater of this type recently put into operation at the Polytechnic Institute of Brooklyn is shown in Figure 8-6.

It is important to note that under certain conditions there may not be the necessity to test at extremely high Mach numbers. For a body enveloped in a shock which is everywhere strong, the flow between the body and the shock depends only on the free stream speed and density and is independent of all other free-stream conditions, including the free-stream Mach number. This "Mach number independence" principle includes all real gas, transport, relaxation, and rarefied gas effects. Thus it is seen that for these studies around bodies enveloped in strong shocks, the full-scale Mach number need not be duplicated. It is emphasized, however, that the principle applies to flows around the same body and that further reasoning is involved in comparing two bodies of different scale.

The Mach number independence principle can also be applied to hypersonic boundary layers. It has been demonstrated that if the fluid composition, pressure distribution, surface temperature distribution, and the virtually constant external speed are given, the flow in major portions of the boundary layer is independent of the external Mach number.

An interesting application of the blow-down wind tunnel with axially symmetric nozzle arises in connection with the firing of a free flight model upstream through the tunnel.[3,10] The relative velocity between the model and stream creates stagnation enthalpies and Reynolds numbers close to those encountered in free flight. This method can be applied to duplicate some features of the time-dependent changes occurring during the course of a trajectory, e.g., the heat flux history.

It can be concluded that there appears to be very few high speed phenomena whose dominant characteristics are fluid mechanical (including heat transfer) rather than physio-chemical which cannot be investigated or tested for by means of the blow-down tunnel. The similarity parameters or model laws are quite well understood for these types of flows, and are the same for both high and low densities, e.g., Mach number, Reynolds number, Nusselt number and other similarity parameters.
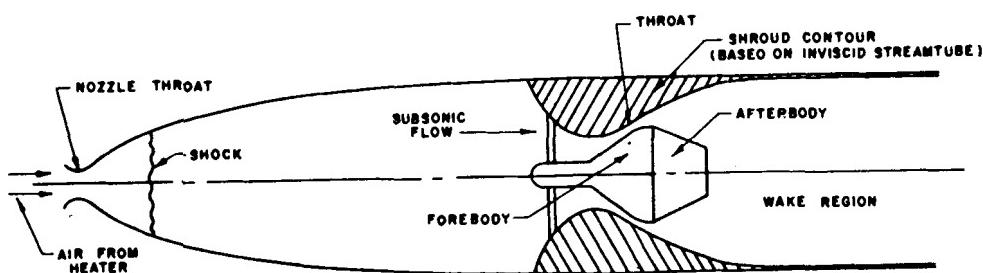

Figure 8-5. Schematic Diagram of Shrouded Model Technique for Afterbodies and Wakes (Reference 31 of Chapter 6)

COMBUSTION HEATER

SETTLING CHAMBER

SHROUD **MODEL**

AIR
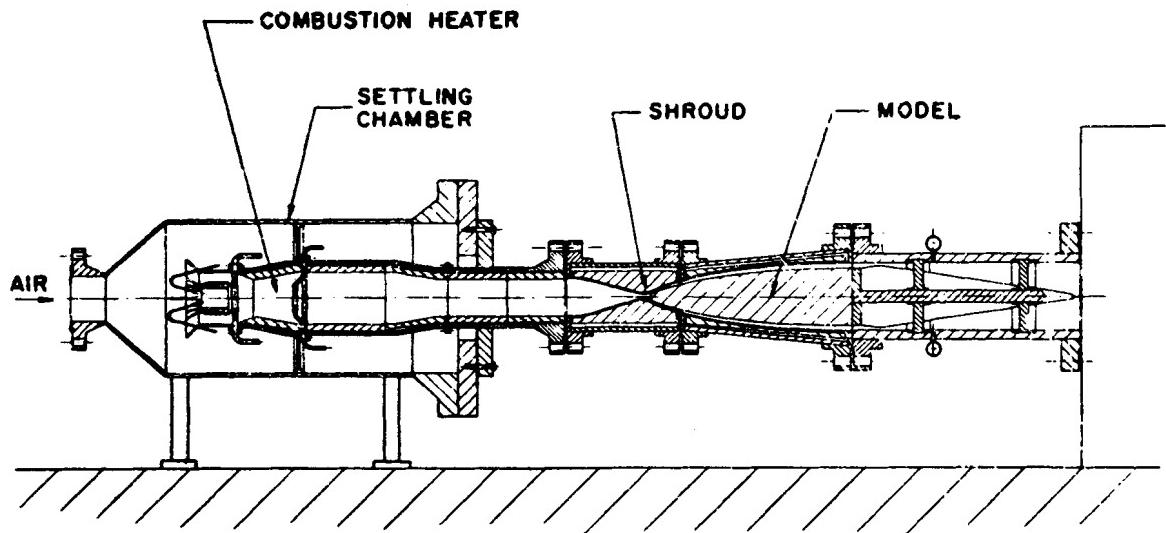
Figure 8-6. Schematic Diagram of Combustion Type Wind Tunnel with Shroud Rig, Polytechnic Institute of Brooklyn Aerodynamics Laboratory[12]

This permits test data to be readily interpreted in terms of free flight conditions.

In the full use of this facility, ingenuity is a factor not to be disregarded. A set of test configurations employing high energy gas sources is shown in Figure 8-7.[27]

8-4.2. Shock Tunnel

At air temperatures in the 4000° to 5000°R range and higher, the effects of molecular dissociation, ionization and radiation become important. The blow-down system, just discussed is incapable of developing supply energies sufficiently high to produce these "real gas" effects. In order to obtain air energies of proper order in ground test facilities, it has been found feasible to use systems which produce high energy bursts for very short periods of time—on the order of milliseconds.

The most highly developed and versatile of these systems at present is the shock-tube wind tunnel, sometimes simply referred to as the *shock tunnel*. (Figure 8-8(D)).

Basically the shock tunnel consists of a shock tube which provides a small amount of high-enthalpy high pressure gas, which is then expanded to high velocity through a nozzle. The shock tube itself consists of a duct separated by a diaphragm into regions of high pressure (driver gas) and low pressure (driven or test gas). When the diaphragm is ruptured, artificially or by a further increase in driver pressure, the driver gas expands into the low pressure section, sending before it a shock which compresses the driven gas. The interface between

the driver and driven gases follows the shock, and in practice the usable test gas is contained between the shock and the interface. As the shock passes through the driven gas, it sets the compressed gas in motion at a Mach number which varies roughly between 1.8 and 3.0 depending upon the real gas effects. A model may be placed in this high enthalpy, high pressure, low supersonic Mach number gas in one method of using the shock tube, this being referred to as the "straight through" method (Figure 8-8(A)).

In a second method, the shock may be permitted to impinge upon the downstream face of the shock tube and then be reflected back, further compressing the gas in its wake. A nozzle may be placed in the downstream face of the shock tube for further expansion of the small amount of test gas in both the straight-through and reflected shock methods. In still another arrangement, the shock tube may be left open at the downstream end so that the test gas is expelled in a free jet from the open end.

One of the most significant difficulties in the use of the shock tube is the attenuation of the shock as it travels down the tube. This attenuation is due to the viscous effects in a tube of high length-to-diameter ratio, the latter being required to achieve practical durations of run in the test gas.

In an important development, this problem has been greatly diminished by the use of the "tailored-interface" modification of the reflected shock method (Figure 8-8(D)). This permits the reflected shock to pass through the driver interface without further reflection, and thus allows all the air processed by

the reflected shock to be used as supply gas for an expansion nozzle. The increased utilization of such procedures has allowed significant reductions in the required shock tube lengths and accompanying reduced effects of attenuation. Testing times on the order of 10 times that obtainable with the simple reflected shock are possible by this means.

The many technological and engineering factors involved in the effective use of shock tunnels are discussed in detail in the literature. Significant advances in the art have evolved since its inception. Measurements of heat transfer and pressure distributions over models; visual observations of waves, and some wake studies have been made. Reliable measurements in the wake or base region of bodies are most difficult to achieve in the shock tunnel because of the relatively long times required to produce steady flow in these regions. Force balances
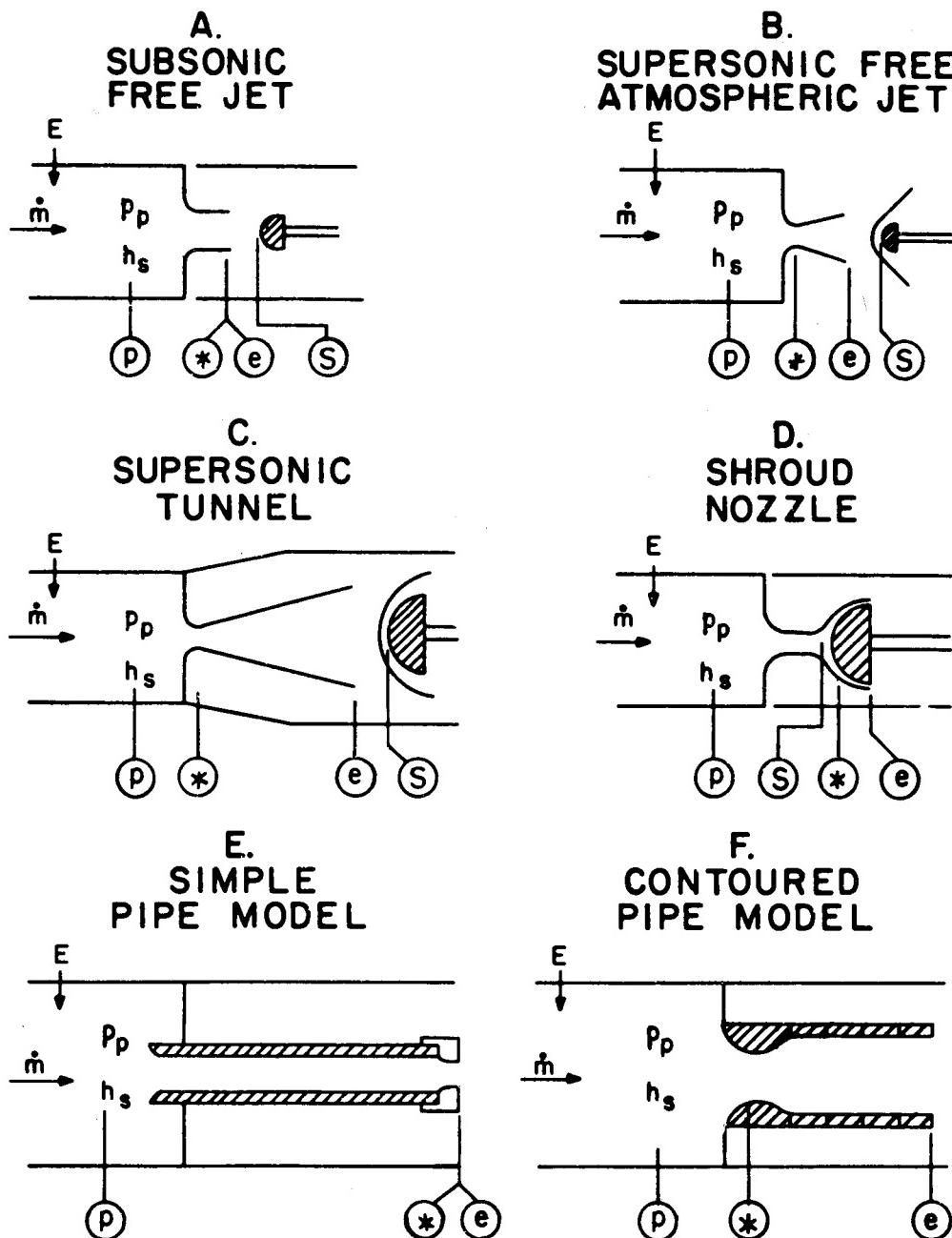

Figure 8-7. Test Configurations for Use with High Energy Gas Sources[27]

for test runs of 5 to 10 milliseconds duration appear to be feasible. In addition several types of testing configurations can be utilized in connection with a shock tube gas generator, (Figure 8-7), in which a wide range of high altitude test conditions are attainable.

An advantage of the shock tunnel lies in the fact that the test gas is virtually free of impurities, which may not be the case in systems such as the *plasma jet* and *hot-shot*. This is because the test gas is not contaminated by the driver, although particles from the ruptured diaphragm may pass down-stream and strike a model mechanically. Nevertheless, the gas remains chemically pure, and diaphragm particles can be removed mechanically by means of a turning passage prior to the nozzle.
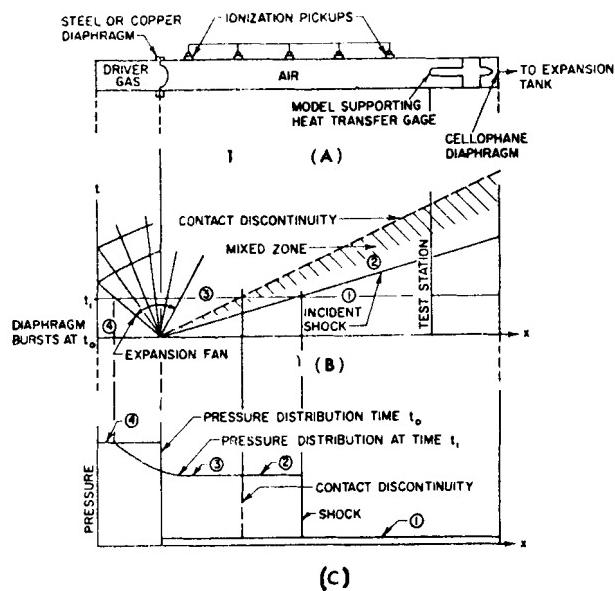
(*A*) *Schematic Diagram of Shock Tube*

(*B*) *X−T Diagram Showing the Progress of the Shock Wave and the Expansion Wave Following the Diaphragm Burst (The gases which were originally separated by the diaphragm are separated by the contact discontinuity (interface).)*

(*C*) *Pressure Distribution at Several Typical Times in the Shock Tube (Time t_0 and t_1 from (B).)*
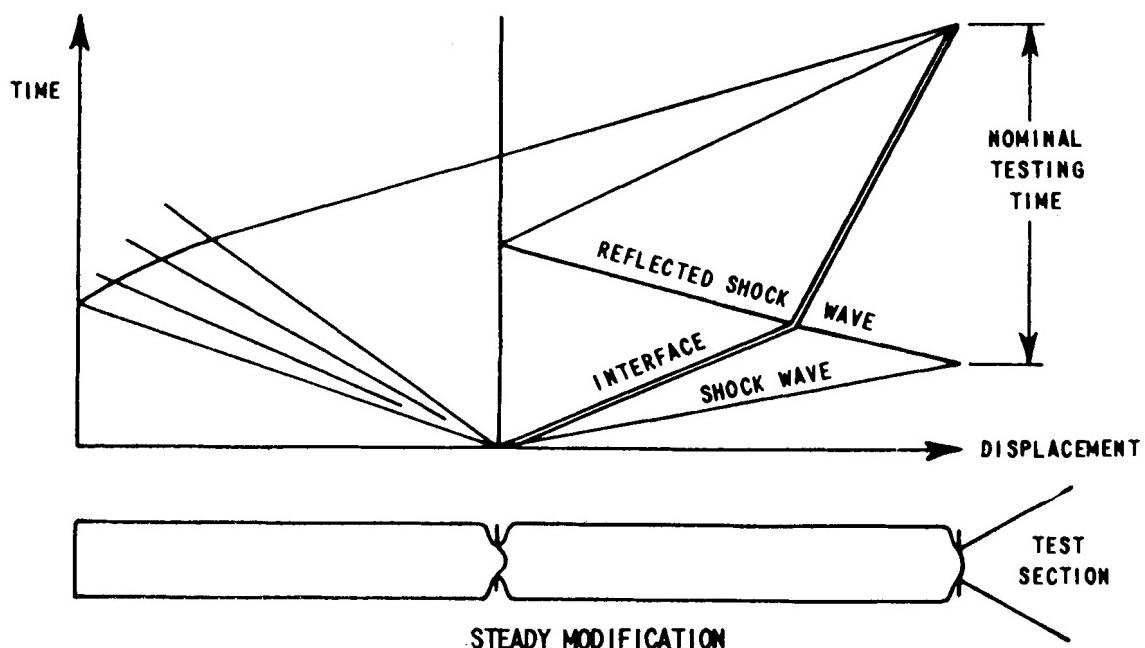

(*D*) *Tailored Interface*

Figure 8-8. Nomenclature for Shock Tube[18]

In the hot-shot system,[11] on the other hand, the gas in the stagnation chamber is heated and compressed directly by means of an arc discharge immersed within the gas. This gas is actually the test gas, which is expanded through the nozzle. It, therefore, has the possibility of being contaminated by electrode material or of possessing extraneous ionized components. The same is true of the plasma jets, although these jets my operate for time periods on the order of seconds. Moreover, the hot-shot may produce erosion of the nozzle throat which also may increase the flow contamination.

An advanced and complex type of gas heating system developed at the Cornell Aeronautical Laboratory, Inc. consists of a rotating bank of shock tubes which discharge into a collector to provide a steady flow of shock-heated air for an interval on the order of tens of seconds.[19,33] This device is termed the "wave superheater." Its aim is to overcome the disadvantage of short running times in the shock tube and to provide real-gas test media for mass transfer studies, tests of thermal effects in structures and materials, pressure distribution and force studies, and other conditions in which extended testing times are required or are convenient.

8-4.3. Combined Wind Tunnel and Shock Tunnel

A new variation of test facilities is obtained by the use of the shock tunnel combined with a blow-down hypersonic wind tunnel or, alternatively, by the combination of two shock tunnels, in a manner under development at the Polytechnic Institute of Brooklyn Aerodynamics Laboratory.[22] The objective is to add energy to a hypersonic stream (the primary flow) which has already been expanded to low static temperature. This is accomplished by sending a shock downstream along the primary flow. The shock is provided by a secondary shock tube whose downstream end is attached obliquely to the test section of the primary nozzle through which its shock discharges into the primary stream. It is important to note that the stagnation temperature of the primary flow may be kept sufficiently low (e.g., less than 3000°R) to avoid the introduction of real gas effects. Thus the stagnation enthalpy and limiting velocity of the basic flow are increased by the secondary shock, while the resultant test gas is not significantly influenced by chemical history, since its static temperature is always maintained at a relatively low level.

This method is of importance since it appears that under low density conditions it will not be possible to maintain thermodynamic equilibrium

hypersonic nozzle flows which expand their test media from a high energy source in the real gas range, regardless of whether the source is a shock tube, hot-shot, or plasma jet. It is believed that the nonequilibrium state in the nozzle will not be of extreme importance for fluid mechanical or heat transfer effects, provided that the actual state and velocity conditions in the nonequilibrium flow in the test section are known and used to explain the data. For chemical and physical problems in the shock layer and wake, however, it may be important to approach the precise thermodynamic state of a prototype in a model test. For this purpose, a method of creating flows simulating the equilibrium conditions of flight in a ground test facility becomes extremely useful. This problem may also be partially overcome by the use of high velocity guns and firing ranges, which form useful adjuncts to the fixed model techniques.

Another use of this method lies in the fact that the stagnation enthalpy level of a basic flow can be increased by the action of the superimposed shock. In principle, the effect of several shocks may be superimposed in this way to provide a flow with extremely high stagnation enthalpy or limiting velocity. The difficulty lies in the effective running time which is diminished with each superimposed shock.

8-4.4. Hot-Shot Tunnel

In this system, electrical energy stored in capacitor bank (which may have a capacity of a million joules or more) is released in an arc chamber, and, through a constant-volume process, produces a high pressure, high energy air mass. For example, the power supply in use at AEDC[11] consists of twin 47-ton flywheels driven by a pair of 1000 hp motors, which operate a 1.28×10^8 joule induction coil. A plastic diaphragm upstream of the nozzle throat is ruptured and expansion into the nozzle takes place.

Among the advantages of this type of test facility is the relatively long duration of the test run compared to that of the shock tunnel. This permits sufficient time for the measurement of heat transfer, pressures, forces, and moments. The hot-shot tunnel also provides a wide operating range and convenience of operation.

A critical feature, previously mentioned, is the impurity of the test gas caused by the arc in the explosion chamber and by throat erosion. However, substantial improvements in the purity of the test gas have resulted from recent work. In this method, expansion of the test gas from a constant-volume stagnation chamber causes an unsteadiness in the

stagnation conditions. This unsteadiness can be diminished by increasing the chamber volume for a given length of run but at the expense of an increase in the power required for operation.

8-4.5. Plasma-Jet

The arc-powered jet is a device in which a high intensity arc formed between an anode and cathode, stabilized by a gas which is passed over, around or through the arc (Figure 8-9), results in a high enthalpy ionized gas jet consisting of the heated stabilizer plus residue from the electrodes. Some modern arc techniques utilize wall-cooling methods for stabilization; these do not require the addition of a foreign fluid to the jet.

At present, the power input requirements are high for relatively small mass flows. For example, in one jet, 700 kw of AC power are required to produce 0.080 lb/sec of "air" at a stagnation temperature of about 11,000°R and a stagnation pressure of 150 psia. A 2000 kw version is cited as yielding 0.30 lb/sec of test fluid at a stagnation pressure of 2000 psia and temperature of 13,000°R. Running times on the order of seconds or even minutes may be achieved.

The plasma jet provides an interesting high enthalpy ionized medium for testing materials and structures. It is particularly useful for ablating systems which are primarily sensitive to the enthalpy absorbed per pound of material rather than to the fluid mechanical and other detailed parameters of the jet. One of the difficulties in the operation of plasmas for aerodynamic testing has been minimizing contamination of the stabilizing gas which forms the test medium. This contamination stems primarily from the anode, usually carbon, rather than the cathode, which may be water-cooled copper. Decreasing the power input, and the arc chamber pressure (stagnation pressure) serves to diminish anode material loss. In addition, anode cooling methods have been utilized to advantage to deter material loss. Thus clean plasma jets become more practical in aerodynamic testing under low density conditions.

The plasma jet has the same problem, with regard to non-equilibrium conditions within the hypersonic expansion nozzle, as has been mentioned in connection with the shock and hot-shot tunnels. Under low density conditions the nozzle flows may be expected to be frozen. Moreover, a problem of unsteadiness (small scale) exists under many conditions. The use of settling chambers between the arc and expansion nozzle, to minimize non-uniformity and unsteadiness, results in substantial heat loss.

Plasmas have also provided a useful medium for the study of the behavior of ionized media and for magnetohydrodynamic investigation.

8-4.6. Light Gas Free-Piston Gun Tunnel

An interesting device for generating a short burst of high temperature, high pressure air is a compression heater superficially resembling a shock tunnel. In this device, termed a gun tunnel,[14] a free piston is interposed between the driver and driven gas, as shown in Fig. 8-10. High thermal energy on the downstream end of the piston is achieved if a light gas such as helium or hydrogen is used
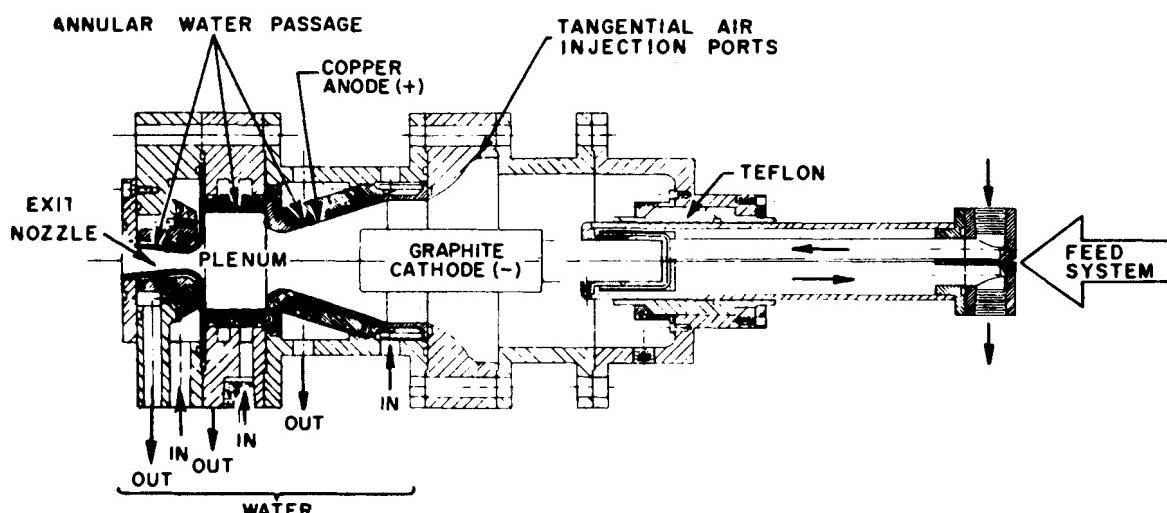

Figure 8-9. Plasma Generator[26]
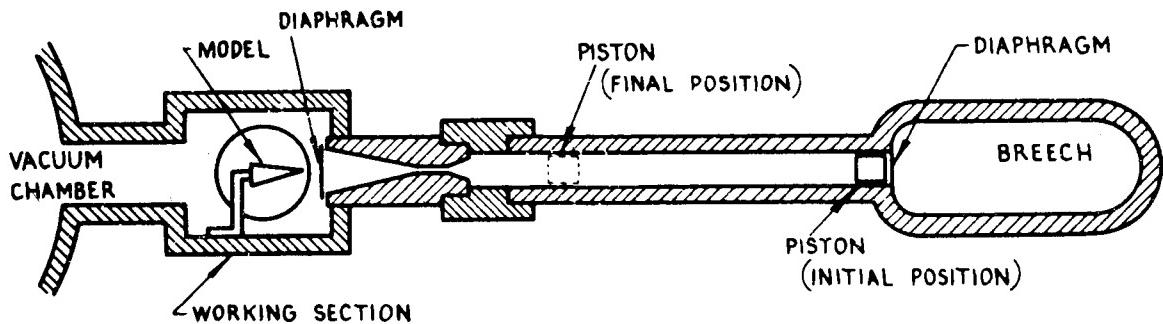
Figure 8-10. Schematic Diagram of Light Gas-Free Piston Gun Tunnel[14]

in the breech as a driver, since the high temperature results from multiple shock reflections which take place between the moving piston and the downstream end of the barrel. The temperatures attainable are higher than those corresponding to isentropic compression. In principle, temperatures as high as 10,000°K can be achieved after 3 shock reflections with initial pressure ratios on the order of 600 across the piston. Running times on the order of hundreds of milliseconds can be obtained. However, the erosion of the nozzle throat restricts the running time during high stagnation pressure runs.

This device appears to be quite attractive for hypersonic testing, at least on the pilot scale for which information is available. Factors such as reliability and steadiness will influence final evaluations of this device.

8-4.7. Firing Ranges

A wide variety of techniques for studying models fired in free flight has been accumulated in ballistic studies over the years.

The possibilities for flight simulation are excellent in firing ranges. However, a disadvantage is the difficulty in obtaining data on the flow near the model, or effects on the model without the use of fixed instrumentation. In wake studies this factor is not as important.

Past observation methods have been primarily photographic. More recently, small telemetering devices have also been developed for making rudimentary heat transfer and pressure measure-

ments on the model. These devices must withstand accelerations as high as 200,000 g in some cases. A simple resistance, inductance, capacitance circuit developed at the U.S. Naval Ordnance Laboratory responds to an intermittent radar pulse by reemitting a decaying signal. The circuit resistance, a measure of temperature or pressure, can be estimated from the decay rate of the signal. This system is inexpensive, rugged, and can be applied to multiple channels.

Projectile studies have become even more important with the advent of aerophysical problems connected with the communication through and detection and diagnosis of high energy flows in the shock layer and in the wake of hypersonic vehicles. These problems have been studies with the use of optical techniques such as the schlieren and shadowgraph systems, electro-magnetic wave diagnostics (usually in the microwave range), molecular beams, spectroscopy, radiation sensors and other methods of experimental physics. Wake measurements can be made at points fixed in laboratory space over a period of time after the model has passed.

The modern development of light gas guns[2-6,9] has led to projectile velocities on the order of 30,000 fps with certain types of models. Problems arise in connection with the launching of light delicate models without injury to the model and in connection with the stabilization of slender projectiles. A typical modern flight range for purposes of aerophysical measurements may consist of a gun section on the order of 50 ft in length, a measurement section about 50 ft long and an enlarged terminal section for radar measurements.

REFERENCES AND BIBIOGRAPHY

1. M. H. Bloom and M. H. Steiger, "Inviscid Flow With Nonequilibrium Molecular Dissociation for Pressure Distributions Encountered in Hypersonic Flight," J. Aerospace Sci. 27 (1960).

2. A. C. Charters, B. P. Denardo and V. J. Rossow, *Development of a Piston-Compressor Type Light-Gas Gun for the Launching*, National Advisory Committee for Aeronautics Technical Note 4143, 1957.

3. A. Seiff, *The Use of Gun-Launched Models for Experimental Research at Hypersonic Speeds*, Advisory Group for Aeronautical Research and Development Report 138, 1957.

4. J. S. Curtis, *An Accelerated Reservoir Light-Gas Gun*, National Aeronautics and Space Administration Technical Note D-1144, 1962.

5. A. C. Charters and J. S. Curtis, *High Velocity Guns for Free-Flight Ranges*. Paper presented to AGARD Fluid Dynamics Panel Specialists' Meeting, Brussels, Belgium, 1962.

6. P. A. Thurston, *Research in the U. S. Naval Ordnance Lab. Ballistic Ranges*, Advisory Group for Aeronautical Research and Development Report 137, 1957.

7. W. K. Rogers, *The Transonic Free Flight Range*, BRL Report 1044, Aberdeen Proving Ground, Md., June 1958.

8. W. F. Braun, *The Free Flight Aerodynamics Range*, BRL Report 1048, Aberdeen Proving Ground, Md., July 1958.

9. A. J. Eggers, Jr., *A Method for Simulating the Atmospheric Entry of Long-Range Ballistic Missiles*, National Advisory Committee for Aeronautics Report 1378, 1958.

10. A. Ferri and P. A. Libby, *The Hypersonic Facility of Polytechnic Institute of Brooklyn and Its Application to Problems of Hypersonic Flight*, Advisory Group for Aeronautical Research and Development Report 136, 1957.

11. J. Lukasiewicz, "Experimental Investigation of Hypervelocity Flight," *Advances in Aeronautical Sciences*, Vol. 1, Pergamon Press, London, 1959.

12. M. Visich, Jr., *The Use of Small Blowdown Supersonic Wind Tunnels for University Research*, Polytechnic Institute of Brooklyn. Paper presented at the Joint STA-AGARD Meeting, Marseilles, France, 1959.

13. R. Smelt and J. C. Sivells, *Design and Operation of Hypersonic Wind Tunnels*. Advisory Group for Aeronautical Research and Development Report 135, 1957.

14. R. N. Cox and D. F. T. Winter, *The Light Gas Hypersonic Gun Tunnel at A. R. D. E. Fort Halstead, Kent*, Advisory Group for Aeronautical Research and Development Report 139, 1957.

15. E. Bluestone, *The Design and Construction of The Ballistic Research Laboratories Hypersonic Wind Tunnel*, Aberdeen Proving Ground, Md., September 1959.

16. J. Sternberg, *Ballistic Research Laboratories' New Hypersonic Tunnel*, BRL Report 1076, Aberdeen Proving Ground, Md., January 1960.

17. J. C. McMullen, *Wind Tunnel Testing Facilities at the Ballistic Research Laboratories*, BRL Memorandum Report 1292, Aberdeen Proving Ground, Md., July 1960.

18. A. Hertzberg, *The Shock Tunnel and its Applications to Hypersonic Flight*, Advisory Group for Aeronautical Research and Development Report 144, 1957.

19. R. C. Weatherston, A. L. Russo, W. E. Smith, and P. V. Marrone, *Gasdynamics of a Wave Superheater Facility for Hypersonic Research and Development*, Cornell Aeronautical Laboratory Report, Air Force Office of Scientific Research Technical Note 59-107, 1959, AD 1118-A-1.

20. C. E. Witliff, M. E. Wilson and A. Hertzberg, "The Tailored-Interface Hypersonic Shock Tunnel," J. Aerospace Sci. 26, 219 (1959).

21. P. H. Rose, *Physical Gas Dynamics Research at the AVCO Research Laboratory*, Advisory Group for Aeronautical Research and Development Report 145, 1957.

22. A. Ferri, *Preliminary Description of a New Scheme for a Low Density Hypersonic Shock Wind Tunnel*, Polytechnic Institute of Brooklyn, PIBAL Report No. 519, 1959, Nonr 839(25).

23. T. R. Brogan, "The Electric Arc Wind Tunnel," ARS Journ. 29, 648 (1959).

24. W. N. MacDermott, "Preliminary Test Results with an Arc-Heated, Hypersonic Wind Tunnel at Mach Numbers of 10 to 20," *Fifth Midwestern Conference on Fluid Mechanics*, University of Michigan, 1957.

25. P. H. Rose and E. Offenhartz, *Ablation Measurements in Turbulent Flow*, AVCO Research Laboratory, Everett, Mass., Research Report 114, 1959.

26. P. H. Rose, W. E. Powers and D. Hritzay, *The Large High Pressure Arc Plasma Generator*, AVCO Research Laboratory, Everett, Mass., Research Report 56, 1959.

27. W. R. Warren and N. S. Diaconis, *Air Arc Simulation of Hypersonic Environments*. Presented at the International Hypersonics Conference, sponsored by the American Rocket Society and Air Force Office of Scientific Research, at the Massachusetts Institute of Technology, August 16–18, 1961.

28. R. R. Heldenfels and J. N. Kotanchik, *Electric Arc-Powered Air Jets for Materials and Structures Testing at Temperatures to 10,000°R*. National Advisory Committee for Aeronautics Paper presented at Institute of Aerospace Sciences Summer Meeting, July 1958.

29. S. A. Schaaf, "Recent Progress in Rarefied Gas Dynamics Research," *Sixth Midwestern Conference on Fluid Mechanics*, University of Texas, September 1959.

30. A. Ferri and V. Zakkay, *Measurements of Stagnation Point Heat Transfer at Low Reynolds Number*, Polytechnic Institute of Brooklyn PIBAL Report No. 644, Aerospace Research Lab. 38, 1961.

31. J. T. Frasier, *A Small Light-Gas Gun Range*, BRL Memorandum Report 1290, Aberdeen Proving Ground, Md., July 1960.

32. G. H. Stever, *Condensation Phenomena in High Speed Flows*, Vol. III, Princeton Series on High Speed Aerodynamics, Princeton University Press, 1958.

33. W. E. Smith and R. C. Weatherston, *Studies of a Prototype Wave Superheater Facility for Hypersonic Research*, Cornell Aeronautical Laboratory Report HF-1056-A-1, Air Force Office of Scientific Research Technical Report 58-158, 1958.

34. M. H. Bloom, *A High-Temperature-Pressure Air Heater*, Wright Air Development Center Technical Note 55-694, 1956. (Also ASME Paper 59-A-233, 1959.)

Additional Bibliography

35. V. D. Agosta, *A Theoretical Investigation on the Use of Combustion Products for the Simulation of Hypersonic Flow*, Polytechnic Institute of Brooklyn, Wright Air Development Center Technical Note 59-81, 1959, AD 211916.

36. J. M. Allen, J. F. Quirk, J. J. Ward and D. R. Bussman, *Determination of Preferred Method of Producing Air Temperatures Encountered in Flight by Hypersonic Aircraft and Missiles*, U.S. Air Force, Arnold Engineering Development Center Technical Report 57-11, 1957, AD 131407.

37. A. Ferri and M. H. Bloom, "Achievement of High Heat Fluxes in a Wind Tunnel," J. Aeronaut. Sci. **24** (1957).

38. A. Ferri and P. A. Libby, "A New Technique for Investigating Heat Transfer and Surface Phenomena under Hypersonic Flow Conditions," J. Aeronaut. Sci. **24** (1957).

39. J. G. Hall and A. L. Russo, *Studies of Chemical Non-equilibrium in Hypersonic Nozzle Flows*, Cornell Aeronautical Laboratory. Presented at Combustion Institute Meeting, Los Angeles, California, Noverber 2–5, 1959.

40. E. S. Love, A. Henderson and M. H. Bertram, *Some Aspects of Air-Helium Simulation and Hypersonic Approximations*, National Aeronautics and Space Administration Technical Note D-49, 1959.

41. H. T. Nagamatsu, R. E. Geiger and R. E. Sheer, Jr., "Hypersonic Shock Tunnel," ARS Journ. **29**, 332(1959).

42. R. W. Perry and W. N. MacDermott, *Development of the Spark-Heated, Hypervelocity, Blowdown Tunnel—Hotshot*, Arnold Engineering Development Center Technical Report 58-6, 1958.

43. A. P. Sabol and J. S. Evans, *Investigation of the Use of the Thermal Decomposition of Nitrous Oxide to Produce Hypersonic Flow of a Gas Closely Resembling Air*, National Advisory Committee for Aeronautics Technical Note 3624, 1956.

44. K. E. Tempelmeyer, *High Temperature Gas Mixtures for Simulating Air and Other Planetary Atmospheres*, 1959 Heat Transfer and Fluid Mechanics Institute, Stanford University Press, 1959. (Also U.S. Air Force Arnold Engineering Development Center Technical Note 59-8, 1959.)

45. Clyde W. Winters, *Heat Transfer Rates and Ablation on a Blunted Cylinder-Flare Configuration in Free Flight Up to a Mach Number of 8.98*, National Aeronautics and Space Administration Technical Note D-2383, 1964.